eman ta zabal zazu

Universidad del País Vasco

Euskal Herriko Unibertsitatea

Ultrashort-pulsed laser ablation of poly-L-lactide (PLLA) for cell and tissue engineering applications

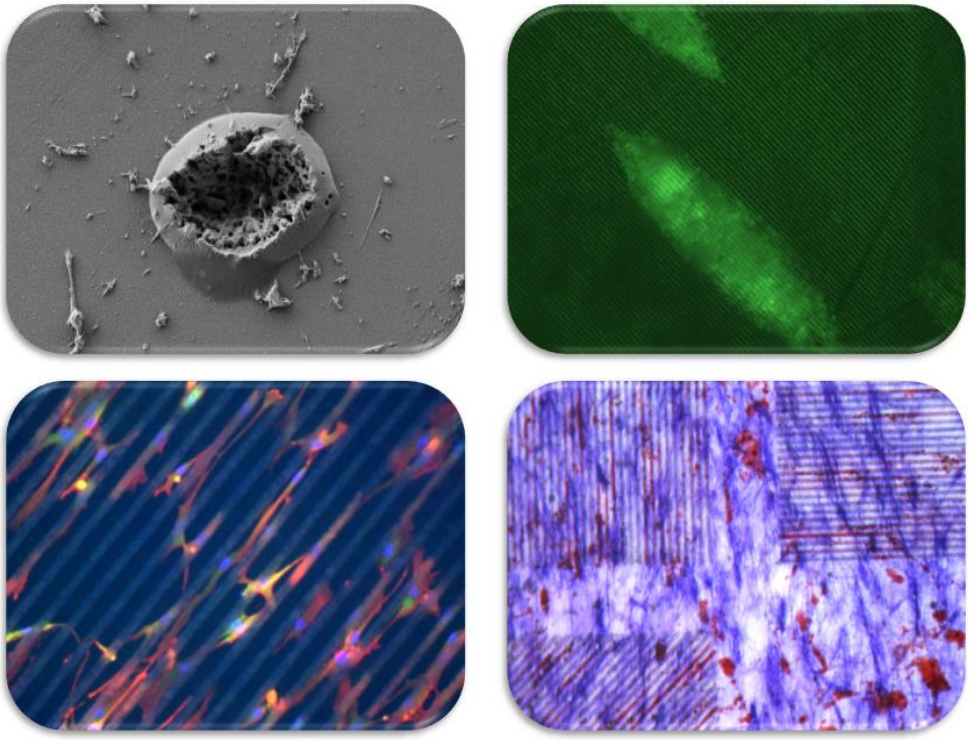

Dissertation presented to the department of Mining and Metallurgy Engineering & Materials Science (UPV/EHU) by

Rocío Ortiz Márquez

for the degree of Doctor of Philosophy

Thesis advisors: Dr. Iban Quintana Fernández; Dr. Jose Ramon Sarasua Oiz

Acknowledgments

En primer lugar, agradecer a la Universidad del País Vasco, en particular a Jose Ramón Sarasua miembro del Departamento de Ingeniería Minero-metalúrgica y Ciencia de los Materiales, y a IK4-TEKNIKER por la oportunidad de realizar el doctorado con la colaboración de las dos entidades y poder contar con sus recursos y conocimiento. En este punto, agradecer sobre todo a Iban Quintana, por la confianza depositada en mí al seleccionarme para llevar a cabo la investigación en este campo multidisciplinar, en el que he tenido la oportunidad de trabajar en distintos entornos buscando la convergencia entre los mismos. Gracias también por tu paciencia, tu apoyo, tu capacidad de motivación, tu claridad para ver las cosas, por estar siempre dispuesto a ayudar, y a la vez dejarme libertad para poder aprender a tener criterio y dirigir un proyecto de investigación por mí misma. No me puedo olvidar de Susana Moreno-Flores que ha sido parte fundamental en la dirección científica de este trabajo de tesis, y mi maestra en el arte del cultivo celular. Tanto a Iban como a Susana les debo el haber aprendido a trabajar de forma honesta, a mantener la calidad científica, y a ver siempre más allá, buscando las causas detrás de todo lo observado. Me considero más que afortunada por haber podido trabajar (y espero que poder seguir trabajando) con vosotros. También quiero agradecer a Jose Luis Toca y a María del Mar Vivanco por estar siempre dispuestos a echar una mano, permitirme el acceso a sus laboratorios de cultivo celular para poder desarrollar toda la parte “bio” de la tesis, y hacer siempre las cosas tan fáciles. Gracias por vuestra ayuda y vuestros consejos durante la realización de esta tesis. Thanks to Sandra Pacharra and Jochen Salber for their contribution to this thesis, and to all the colleagues of the ReBioStent project, in which I could developed part of this work in the best atmosphere.

Son muchos los compañeros que me han acompañado y ayudado de alguna forma durante estos años, en TEKNIKER, en la Universidad, en CICbiomaGUNE, en CICbioGUNE, y en el BOKU, contribuyendo a que el trabajo fuera mejor y más fácil, y a todos os agradezco el apoyo y la compañía; pero tengo que agradecer de forma especial a Jon Etxarri (el trisca) por hacer mi entrada en el mundo de la ingeniería mucho más fácil y enseñarme cómo hay que tratar a las máquinas, pero, sobre todo, por aguantarme y por todo el tiempo compartido a pie de máquina.

Por último, pero más importante, a toda mi familia y amigos, por estar siempre ahí y aportarle alegría a mi vida. Y muy especialmente a Octavio, que me aguanta sin descanso y hace que todo en mi vida sea mejor.

Table of contents

Summary

La tesis está organizada en 4 secciones principales: alcance y objetivos, introducción, resultados y discusión (la cual está dividida a su vez en 4 capítulos), y conclusiones generales. El objetivo principal de este trabajo de tesis es el de evaluar la tecnología de ablación mediante láser pulsado de picosegundos como método de fabricación de componentes poliméricos micro-estructurados para su aplicación como soportes (*scaffolds*) en el campo de la regeneración de tejidos, y más concretamente, en la estrategia de la ingeniería de tejidos. Además, el estudio llevado a cabo en este trabajo permitirá determinar el efecto de la topografía superficial en el comportamiento de distintos tipos celulares, en ausencia de una funcionalización bioquímica del substrato. De esta manera, los resultados obtenidos en este trabajo abren la puerta al diseño y fabricación directa de topografías superficiales *ad hoc*, que cumplan con las especificaciones o requerimientos marcados por distintas aplicaciones en la ingeniería de tejidos.

En la introducción, se recoge una breve revisión del estado del arte referente a la fabricación de soportes para su utilización en la ingeniería de tejidos, incluyendo materiales típicos, técnicas de micro- y nano-fabricación, y conceptos básicos sobre la interacción entre células y superficies. La ingeniería de tejidos consiste en fabricar un repuesto tisular para su implantación en una zona dañada del cuerpo y reforzar la capacidad del cuerpo para curar la lesión por sí mismo, reparando la función de las células presentes en la zona dañada para que actúen sobre la misma. Esta estrategia de regeneración necesita conocer y controlar el comportamiento de las células del tejido que se necesita reparar, y un soporte o andamio para sostener y promover el crecimiento de las células en la zona de lesión durante el proceso de regeneración del tejido. El soporte debe estar compuesto por un material biocompatible (biomaterial) de forma que no se produzcan reacciones adversas en el cuerpo, y debe de cumplir una serie de requerimientos, en cuanto a propiedades, según la función y características del tejido que remplazará. En muchos casos es deseable además que el soporte se disuelva y sea absorbido por el cuerpo una vez finalizado el proceso de regeneración del nuevo tejido. La degradación del material debe ser progresiva y dar lugar a productos no tóxicos que puedan ser metabolizados por el cuerpo. De entre el amplio rango de biomateriales que se usan e investigan para la fabricación de soportes, los polímeros tienen una presencia destacada debida a la variedad de propiedades, tanto mecánicas como químicas, con las que pueden ser sintetizados, y su flexibilidad en términos de procesado y fabricación. En concreto, el ácido poliláctico (PLA) ha despertado un gran interés, ya que además

se degrada dentro del cuerpo humano sin dar lugar a productos dañinos, y la velocidad de degradación puede ser controlada. Además del material que formará el soporte, la geometría y las características superficiales del mismo juegan un papel fundamental en la biocompatibilidad del implante y su funcionalidad para reparar el tejido. El soporte debe tener una estructura que permita la adhesión de células y la conexión entre las mismas, así como la transferencia de nutrientes a través del mismo y la formación de vasos sanguíneos para mantener vivo el tejido. Este tipo de estructuras se consiguen generalmente por medio de soportes porosos creados por distintas técnicas. Sin embargo, la interacción de las células con el material ocurre a través de la superficie del mismo, lo que supone que las propiedades superficiales del biomaterial tengan una gran influencia en el comportamiento de las células adherentes. Las propiedades físicas y químicas de la superficie determinan varios aspectos del comportamiento celular como son la adhesión, la proliferación, la migración e incluso la función o fenotipo celular. Por lo tanto, para poder inducir un determinado comportamiento de las células sobre el soporte, de forma que promueva la regeneración del tejido, es necesario controlar las propiedades superficiales del mismo. Estas propiedades están altamente relacionadas con la topografía superficial, y esta se puede modificar con estructuras en el rango de las dimensiones celulares mediante técnicas de nano- y microfabricación. Las técnicas de nano-fabricación son la tendencia actual para la generación de superficies biocompatibles, ya sea con patrones físicos o químicos, debido a su demostrada influencia en el comportamiento celular por medio de la creación de motivos con una alta precisión, sin embargo, se caracterizan por costes elevados, se encuentran limitadas a un número restrictivo de biomateriales y no son válidas para el tratamiento de superficies no planas o amplias con formas complejas. Las técnicas de microfabricación, sin embargo, a pesar de alcanzar una menor precisión en las dimensiones de los motivos generados, presentan un potencial mucho mayor para la fabricación de componentes tridimensionales con superficies extensas y no planas, que las convierte en la herramienta idónea para su adaptación al tratamiento de cualquier tipo de implante. En este aspecto, consideramos de gran importancia la realización de una investigación extensa sobre los efectos de los micropatrones en el comportamiento celular, aplicando para su fabricación tecnologías capaces de procesar el amplio rango de biomateriales considerados para su utilización como soportes en la ingeniería de tejidos

y que puedan ser integradas en procesos de fabricación de componentes 3D sin restricciones en la forma o área de la superficie a tratar.

La tecnología de ablación láser es una herramienta bien establecida para la modificación superficial de materiales de distinta naturaleza (metales, polímeros, cerámicas, vidrio…). La ablación de material mediante láseres de pulso ultracorto (menor que 10 picosegundos) es capaz de generar motivos topográficos micrométricos con una alta precisión debido a un proceso de ablación "frío" minimizando los efectos térmicos en el material sin producir cambios químicos en el mismo. Es por tanto una tecnología versátil para la fabricación de superficies microestructuradas en un proceso directo y sin contacto y aplicable a una gran variedad de materiales para generar motivos con distintas geometrías sobre superficies no planas. En este trabajo de tesis se aplica la tecnología de ablación mediante láser pulsado de picosegundos para la creación de micro-patrones topográficos en planchas de ácido poli-L-láctico (PLLA), para investigar el mecanismo de ablación del mismo y el efecto de los micro-patrones en el comportamiento de varios tipos de células mediante ensayos *in vitro*, con el objetivo final de elucidar el alcance de la influencia de estos micro-patrones en el comportamiento celular y evaluar la tecnología como método de fabricación rápido y versátil de soportes para su utilización en la ingeniería de tejidos.

En el primer capítulo de resultados de la tesis, se investiga la respuesta del PLLA a la irradiación láser. Para ello, se analiza el fenómeno de ablación mediante láser pulsado de picosegundos en films de PLLA con distinto grado de cristalinidad, en función de la energía depositada por el láser en el material. Se analizan los parámetros de la ablación y la modificación superficial generada para distintas condiciones de irradiación aplicando dos longitudes de onda distintas (ultravioleta y visible). En el caso del PLLA amorfo, tanto el valor de energía umbral necesario para causar ablación en el material como la topografía varían considerablemente para las dos longitudes de onda aplicadas. Se observa que la energía umbral de ablación por láser disminuye a medida que el grado de cristalinidad del PLLA aumenta. Esto está relacionado probablemente con los efectos fotomecánicos que se producen en el material durante la ablación láser con pulso ultracorto, y la baja acomodación de tensiones que presentan los polímeros semicristalinos: un mayor grado de cristalinidad restringe y obstaculiza los movimientos cooperativos de cadenas, lo que reduce la disipación de energía en el material y da lugar a un comportamiento mecánico más frágil. Los

resultados experimentales obtenidos en cuanto a la tasa de ablación alcanzada en función de la energía depositada por el láser permiten deducir que la ablación láser con longitud de onda ultravioleta sobre PLLA semicristalino es más eficiente que la correspondiente a la longitud de onda visible: esto es, la longitud de onda ultravioleta presenta mayores tasas de ablación para un amplio rango de energías por pulso. Estos resultados se pueden interpretar en términos de los mecanismos de ablación fototérmica y fotoquímica por los que se produce la ablación de polímeros en función de la microestructura superficial generada y la longitud de onda incidente. En el PLLA amorfo, se generaron además una serie de micro-canales con alta calidad superficial, en los que se observa, a su vez, una alta densidad de poros que podrían ofrecer ventajas en la integración del mismo en las aplicaciones de regeneración de tejidos consideradas. De esta manera, en este capítulo se pone de manifiesto el potencial de la técnica de procesado con láseres de pulso ultracorto para la fabricación de micropatrones en polímeros biocompatibles y biodegradables para su aplicación en el campo biomédico.

En el segundo capítulo, se aborda la aplicación de la tecnología láser de pulso ultracorto para el micromecanizado de sustratos de PLLA y posterior uso de los mismos como soportes para el cultivo de células *in vitro*, y de esta forma estudiar el efecto de los micropatrones creados en el comportamiento celular. Para este estudio se consideraron células de cáncer de mama, analizando el efecto de la topografía en el crecimiento y morfología de las mismas. El estudio se extendió al tratamiento de superficies de poliestireno (PS), siendo este material uno de los más empleados (junto con el vidrio) en material de cultivo celular. Los micropatrones generados incluyen líneas o canales paralelos de anchura similar al tamaño de una célula (que en el caso de las células consideradas es aproximadamente de 20 micrómetros), así como compartimentos cuadrados con área mucho mayor al tamaño de la célula (250000 μm^2). Los ensayos *in vitro* realizados muestran que a pesar de que la irradiación láser altera y aumenta la rugosidad superficial, esta no afecta de forma notable a la adhesión y el crecimiento de las células de cáncer de mama sobre los micropatrones. Sin embargo, la dirección de los patrones basados en canales afecta de forma directa al crecimiento celular, guiando a los grupos celulares (*clusters*) que forman este tipo de células a crecer preferentemente en la dirección de los canales. Por otro lado, los compartimentos cuadrados fabricados en la superficie del PS, permiten confinar las células dentro de los mismos por un periodo de hasta 11 días en cultivo. Estos resultados

demuestran el potencial del micromecanizado con tecnología láser como método directo para modificar el microentorno celular y de esta forma inducir un comportamiento celular concreto, pudiendo facilitar el estudio del efecto del microentorno físico en el crecimiento celular.

El tercer capítulo se centra en el ámbito de la regeneración de tejidos, y para ello se estudió el efecto de la topografía del sustrato en el comportamiento de células madre mesenquimales (MSCs), antes y después de inducir la co-diferenciación de las mismas a células de grasa (adipocitos) y células de hueso (osteoblastos). Se aplica de nuevo el micromecanizado láser para generar distintos micropatrones, basados en microcanales y microcavidades con distintas formas, en planchas de PLLA e investigar el crecimiento, la forma y la diferenciación de las MSCs sobre los mismos. En los microcanales, y bajo ciertas condiciones topográficas, se observa que las células modifican su forma para anclarse a aquellos puntos más prominentes de los canales. Tras la diferenciación, los adipocitos son capaces de responder a los cambios de profundidad y altura de los patrones, adaptando la distribución intracelular de vacuolas lipídicas a las restricciones físicas impuestas por el patrón. Estos resultados muestran de nuevo la aplicabilidad de la tecnología de micromecanizado láser para la fabricación de estructuras tridimensionales con capacidad de guiar la forma y el crecimiento celular y la morfología de los adipocitos sin necesidad de aplicar una funcionalización bioquímica específica.

A partir de los resultados obtenidos en los capítulos anteriores y dirigiendo la investigación hacia una aplicación concreta, el cuarto y último capítulo de resultados de la tesis, se centra en el desarrollo del micromecanizado láser como tecnología de fabricación óptima en la obtención de superficies que mejoren la funcionalidad regenerativa de implantes vasculares bio-absorbibles (stents microvasculares). Para ello, se considera un sustrato de PLLA modificado con polietilenglicol (PEG), desarrollado exclusivamente para adaptar la velocidad de degradación del material a los requerimientos establecidos para la aplicación mencionada. El objetivo de los micropatrones generados es el de promover y acelerar la adhesión y el crecimiento de las células endoteliales que forman la monocapa que cubre la pared de las venas y arterias tras la implantación del stent. Este proceso de regeneración se conoce como endotelialización. Los micropatrones generados se basan en canales con distinta geometría y densidad, pudiendo alcanzar un criterio en la determinación de la configuración más adecuada para promover la endotelialización en la superficie. Los micropatrones se realizan variando la anchura y

profundidad de los mismos, así como la distancia entre canales. En análisis *in vitro* se inicia con un estudio de citocompatibilidad usando una línea celular de fibroblastos (L929). Después se analiza la adhesión y el crecimiento de células endoteliales microvasculares cardíacas (HCMECs), y por último se aplican ensayos de hemocompatibilidad con sangre humana. Los resultados obtenidos de este estudio *in vitro* muestran que todas las superficies evaluadas (con y sin patrón) son citocompatibles y no tóxicas. Los patrones generados por láser mejoran notablemente la adhesión y viabilidad de las células endoteliales con respecto al sustrato sin patrón, así como su crecimiento orientado, lo cual se relaciona con una aceleración del proceso de endotelialización. Los ensayos de hemocompatibilidad muestran, sin embargo, que los patrones también favorecen la adhesión de plaquetas y la activación de leucocitos en la superficie. En este aspecto, se necesita una investigación más extensa para elucidar la adhesión de células endoteliales y plaquetas sobre los patrones cuando ambas se encuentran en el medio y sometidas a flujo sanguíneo, ya que la adhesión de las primeras evita el de las segundas.

El conjunto de resultados obtenido en cuanto a la ablación láser del polímero considerado, y el efecto de las microestructuras o micropatrones creados con el láser sobre el crecimiento de distintos tipos de células, permiten concluir que la técnica de micromecanizado láser con fuente pulsada de picosegundos es un método de fabricación adecuado y con gran versatilidad y potencial para el desarrollo de soportes en la ingeniería de tejidos, caracterizados por una topografía superficial *ad-hoc* que cumpla con los requerimientos marcados por dicha aplicación. Esta conclusión se apoya, en primer lugar, en la calidad superficial alcanzada en el microestructurado de un polímero transparente, biocompatible, y biodegradable, sin afectación significativa de las propiedades químicas y estructurales del mismo. En segundo lugar, en la notable influencia ejercida por los micropatrones creados con el láser sobre distintos aspectos del comportamiento de varios tipos de células, muy diferentes entre ellas, tales como: a) elongación y confinamiento de células de cáncer de mama, tanto de perfil invasivo bajo como alto; b) organización y adhesión de células madre mesenquimales; c) organización de las vacuolas lipídicas en los adipocitos y adaptación morfológica de las mismas a la topografía superficial; d) elongación y adhesión de células endoteliales. Es importante destacar que el control demostrado por los micropatrones sobre el comportamiento celular es debido

exclusivamente a los cambios topográficos generados por el láser en la superficie, sin considerar el empleo de una funcionalización superficial en términos bioquímicos.

El trabajo desarrollado durante esta tesis ha dado lugar a publicaciones en revistas científicas y participaciones en congresos internacionales mediante presentaciones orales, las cuáles se detallan a continuación.

Publicaciones:

- Ortiz R, Quintana I, Etxarri J, Lejardi A, and Sarasua JR. Picosecond laser ablation of poly-L-lactide: Effect of crystallinity on the material response. J Appl Phys 2011; 110: 094902.
- Ortiz R, Moreno-Flores S, Quintana I, Vivanco MdM, Sarasua JR and Toca-Herrera JL. Ultra-fast laser microprocessing of medical polymers for cell engineering applications. Mater Sci Eng C 2014; 37: 241-250.
- Ortiz R, Moreno-Flores S, Quintana I, Vivanco MdM, Sarasua JR, and Toca-Herrera JL. Topological cues to anchor stem cells, control adipocyte morphology, and improve cell adherence. Surf Coat Technol 2017. En preparación.
- Pacharra S, Ortiz R, McMahon S, Wang W, Salber J, and Quintana I. Surface patterning of a novel PEG-functionalised Poly-L-lactide polymer to improve its biocompatibility: Applications to Bioresorbable Vascular Stents (BVS). J Biomed Mat Res A 2017. En preparación.

Presentaciones orales en congresos internacionales:

- Ortiz R, Quintana I, Moreno-Flores S, Toca-Herrera JL, Etxarri J, Lejardi A, Sarasua JR, and Vivanco MdM. Ultra-fast laser microprocessing of medical polymers for cell engineering applications. European Symposium on Biomaterials and Related Areas. April 13-14, 2011. Jena, Germany.
- Ortiz R, Moreno-Flores S, Quintana I, and Toca-Herrera JL. Surface modification of poly-L-lactide by picosecond laser irradiation: Effect of substrate topography on morphology and differentiation of human Mesenchymal Stem Cells. World Conference on Regenerative Medicine. October 23-25, 2013. Leipzig, Germany.

- Quintana I. Bioresorbable Systems: The role of surface functionalization. 27th European Conference on Biomaterials. August 31-September 3, 2015. Cracow, Poland.

Además de las mencionadas publicaciones, el trabajo desarrollado en la tesis ha permitido participar en el siguiente proyecto europeo:

Reinforced Bioresorbable Biomaterials for Therapeutic Drug Eluting Stents (ReBioStent, https://rebiostent.eu/) financiado por la Unión Europea dentro del marco del *Seventh Framework Programme* (FP7/2007-2013) bajo el acuerdo de subvención nº604251.

Scope and Objectives

The fundamental aim of this work, which arises from the collaboration between the University of the Basque Country (UPV/EHU), and the technological research centre IK4-TEKNIKER, is the evaluation of the picosecond pulsed laser ablation technology as a reliable fabrication method for manufacturing polymeric scaffolds containing 2D and 3D surface microstructures, which geometry can be easily tuned to modulate cell response. This work also pursues the analysis of the effect of surface patterns and topological cues on cell behaviour without the interplay of chemical factors, which will allow us to isolate the effect of the surface physical constraints on the mechanobiology of cell adhesion, growth and differentiation.

For this purpose, it is necessary to achieve the next partial objectives:

- Selection and characterization of a synthetic biocompatible and biodegradable polymer suitable for scaffold fabrication. The selected polymer should be synthesised with tuned mechanical properties and degradation rates, so it can be adapted for manufacturing of scaffolds for different tissue engineering applications.
- Preparation of polymeric films and sheets with controlled crystallinity by casting from solution and application of thermal treatments, and thermoplastic processing.
- Characterization and optimization of the laser ablation process by picosecond pulses on the polymeric films to create surface microfeatures. Surface quality and precision of the generated microstructures should be good enough to not affect the material bulk properties.
- Analysis of cell behaviour on laser-ablated microstructures for different pattern and feature designs, as well as cell types and tissue engineering applications. In this respect, the surface quality and precision of the generated microstructures should be good enough to not avoid or reduce cell proliferation and adhesion on the surface, and influence cell response for three different cell types: breast cancer cells (cancer therapies), human mesenchymal stem cells (regeneration therapies), and endothelial cells (vascular diseases therapies). This activity required the collaboration with other centres with a wide experience on biomaterials and biomedical applications: the Centre for cooperative research in biomaterials (CICbiomaGUNE, San Sebastián), the University of natural resources and life sciences of Vienna (BOKU, Vienna), the Centre for cooperative

research in biosciences (CICbioGUNE, Derio) and the Zentrum für klinische Forschung (Ruhr-Universität Bochum, Bochum) and Universitätsklinikum Knappschaftskrakenhaus (Bochum).

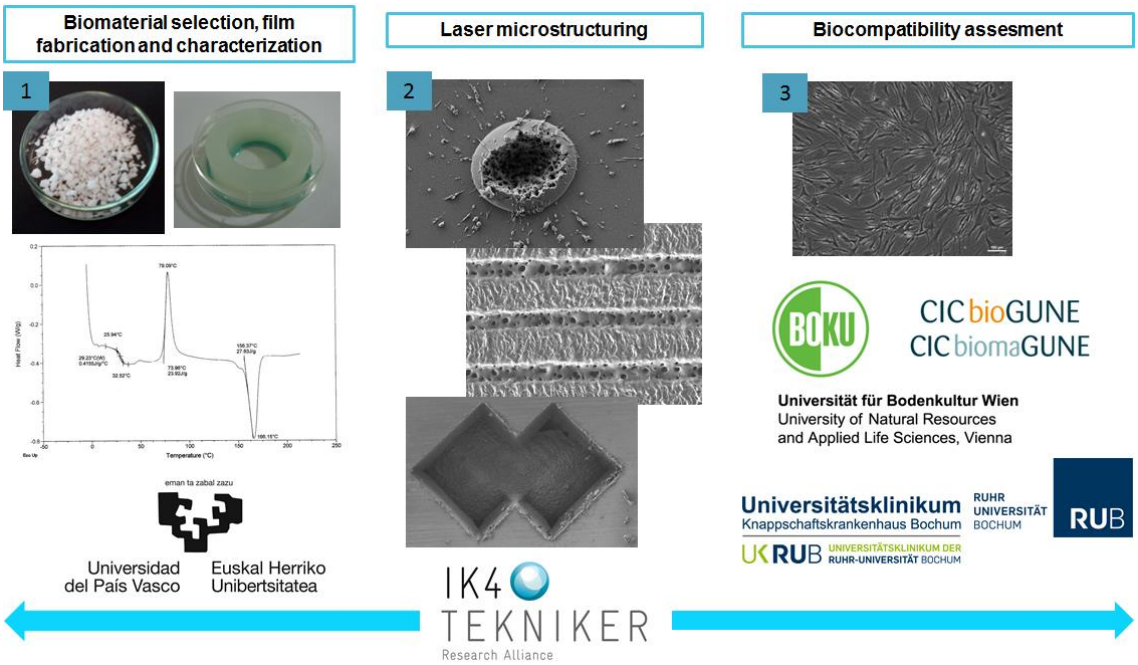

Figure 1. Diagram of the partial objectives that must be accomplished to achieve the main goal of this thesis.

Introduction

1. Background

1.1. Regenerative medicine and tissue engineering

The aim of the regenerative medicine is not only repairing a certain lesion in the body, but in addition to this, the actual aim is that the body may be able to heal the wounded tissue or area by itself. The body can be able to treat a certain lesion by itself if the function of the surrounding cells to the damaged area is repaired or stimulated to act on the wound. There are three different strategies to achieve this objective: cell therapy, genetic therapy, and tissue engineering. In the cell therapy a cluster of cells is directly injected in the damaged area without any manipulation of them (treatment of peripheral arterial disease, for example [1]). In the genetic therapy, the cluster of cells that is injected in the wound is previously manipulated *in vitro* to develop any type of tissue or a DNA implant is done (treatment of Leber's congenital amaurosis, for example [2]). The tissue engineering strategy is different to the cell and genetic therapy: in this case, a tissue replacement is created by implantation of cells and materials in the damaged area in order to restore the tissue function. Tissue reconstruction is needed when tissue dysfunctions occur by congenital defects or when the tissue is not able to total repair itself after a lesion (myocardial infarction, for example [3]); since, in this regard, autologous transplantation or autografts are limited. Out of the regenerative medicine, permanent implants are applied with high success to replace tissue function, but they involve also a lot of problems derivate from the immune response of the body to the implant [4], bacterial colonization [5], or the need of a second surgery to remove the implant from the body when it fails by occurrence of any of these phenomena [6].

Tissues are organized in three-dimensional structures [7]. According to this and in order to perform tissue engineering, in addition to the cluster of cells to be implanted, a support or scaffold is needed to promote cell growth and organization into a specific architecture. Biodegradable temporary scaffolds are those that remain in the body while the injured tissue is regenerating and are absorbed by the body once the injure is healed. These temporary scaffolds are generally made by natural or synthetic polymers due to their biodegradation capacity. Tissue engineering with bio-resorbable polymeric scaffolds would be an ideal solution to the problems shown by permanent implants since it would get to restore tissue function by the incorporation of live components and materials that can be integrated in the body and be resorbed. In order to choose

the appropriate support or scaffold for each application within the tissue engineering field, there are three main aspects to consider: first, material selection according to the functional requirements of the final scaffold for a certain application, in terms of mechanical properties and biodegradability, for example; second, the development of appropriate 2D and 3D micro-fabrication technologies that enable the manufacturing of functional scaffolds with controlled surface properties that induce a specific response of the surrounding cells; the investigation of the interaction processes between cells and surfaces is essential to reach a greater understanding about the role of the cell microenvironment on the cellular processes. Therefore, collaborative efforts from multiple disciplines are needed to perform the tissue engineering strategy, such as material science, manufacturing issues at the micro- and nano-scale (size-scale characteristic of cells and biological entities), and cell biology [8] (Figure 0.1). The current trends in the scaffold fabrication field will be briefly described in the following sections.

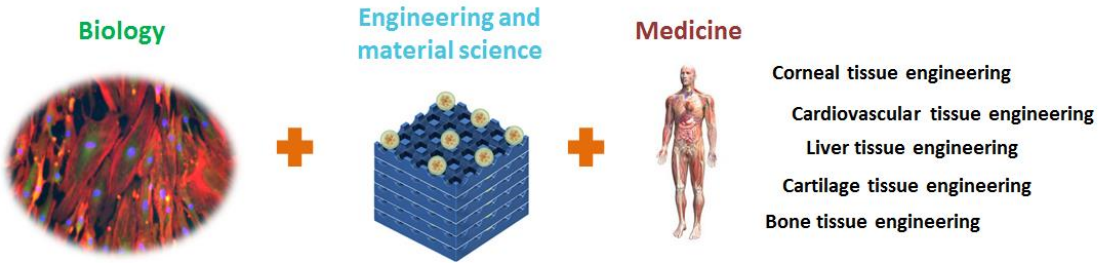

Figure 0.1. Disciplines involved in the development of tissue engineering strategies.

1.2. Materials for scaffold fabrication

Tissue engineering, initiated in the nineties, involves the manufacturing of a scaffold made of an artificial biomaterial, which is seeded by cells to colonize the component (this can be done *in vitro* or *in vivo*) and be implanted in the body to restore tissue function after a lesion. A widely-accepted definition of biomaterials was proposed by David F. Williams in 2009 [9] as “a substance that has been engineered to take a form which, alone or as a part of a complex system, is used to direct, by control of interactions with components of living systems, the course of any therapeutic or diagnostic procedure, in human or veterinary medicine”. Therefore, this definition includes classic implants made by natural (collagen, silk, cellulose, chitosan) and synthetic materials such as metals (stainless steel, cobalt-chromium alloys, titanium and their alloys with niobium and

tantalum), ceramics (zirconium, alumina, bioglasses, hydroxyapatite) and polymers both either non-biodegradable (polymethylmethacrylate, teflon, ultra-high molecular weight polyethylene) and biodegradable (polylactides PLAs, polyglycolides PGAs, polycaprolactones PCLs), which were the only existing medical devices until the nineties [10], but also new developed systems as composites (poly-L-lactic acid/apatite), biomineral components (calcium carbonate, calcium phosphate, bioglass [11]), self-assembled systems [12], nanoparticles [13], carbon-nanotubes [14], quantum dots and nanotechnology based imaging and diagnostic systems [15, 16], drug and gene delivery systems [17,18], or microelectronic devices [19].

A biomaterial used as scaffold for tissue engineering must meet some requirements to be implanted in the body and show a good performance when the tissue engineering strategy is applied, such as biocompatibility (no inflammatory or toxic reactions in the body), corrosion resistance, mechanical and physical properties consistent with the specific function it will have in the body (ductility and durability), and biodegradability [20]. Biodegradability implies the control on the biodegradation time, the mechanical resistance of the material during this degradation and the nature of the degradation products that will be metabolized by the body.

Metals show a great conformability, due to their high ductility and toughness, and suitable fracture strength to support the mechanical stresses sustained by the organic structures in the body. These characteristics make it imperative the use of metals in load-bearing implants. However, biocompatibility is always a challenge when using these materials because of the corrosion phenomena that metals may undergo in the body, leading to the delivery of electrons and ions to the environment. Although metal alloys can be passivated, corrosion phenomena produced by wearing (fretting corrosion) or cracking (crevice corrosion) still remain [21].

Bioceramics show a good biocompatibility due to their low reactivity, and this biocompatibility is encouraged by their similar composition to biominerals, which gives them a great osteointegration capacity. However, bioceramics are stiff and brittle, and, consequently, their applications are reduced to scaffolds not subjected to high loads, such as filling of bone defects, or dental implants and metal joints coating [22].

Polymers can be designed and synthesized with a big variety of mechanical and chemical properties by controlling the synthesis and processing [23]. Polymer mechanical properties can

be tuned by selecting appropriate monomer, chemical initiator, additives and process conditions. The biodegradability is certainly influenced by the polymer properties, but also by the environment (temperature, moisture, pH), and the existing microorganisms. Biodegradable polymers are used for manufacturing of temporary barriers (artificial skin, surgical sutures), drug delivery systems and temporary scaffolds (orthopaedic devices, vascular grafts) [24]. Synthetic polymers show a great potential for scaffold fabrication in the tissue engineering field: their thermoplastic behaviour enables an easy scaffold fabrication with tuned and reproducible properties by conventional hot melting processing techniques. These characteristics make them the ideal material to assist in the current investigation on biomaterial manufacturing with the aims of mimicking the properties of the existing natural materials and finding cheap but high biocompatible medical devices made by easy-to-process biomaterials, which improves the patient´s quality of life.

1.3. Micro- and nano-fabrication techniques for polymeric scaffold fabrication.

As mentioned before, biomaterials and temporary scaffolds must meet some requirements in order to be implanted in the body without producing inflammatory and toxic reactions and in order to properly perform the function of the replaced tissue. In addition to the biomaterial bulk properties (mechanical properties or biodegradation rate), surface properties have also a great influence on the acceptation of the scaffold by the organism and on the tissue regeneration process, since the first contact between the biomaterial and the host organism is produced via the biomaterial surface [25]. Surface physical and chemical properties can be tuned by modifying the surface topography without changing the bulk properties needed to fulfil the requirements of the application [26]. Micro- and nano-scaled surface patterns (either chemical and/or topographical) have a great influence on cell behaviour in terms of cell morphology, migration and proliferation, and on protein synthesis and gene expression [27-30]. In this regard, the investigation on micro and nano-fabrication and patterning technologies play a key role in the manufacturing of advanced polymeric scaffolds with surfaces able to control or influence cell behaviour to improve the implant performance. Many techniques are being investigated for the fabrication of micro- and nano-patterned surfaces or components with a double function: firstly, act as scaffold for cell attachment and growth, and secondly, be able to influence on cell

proliferation and function to control the cell behaviour. The main techniques that are being investigated for micro- and nano-structured/patterned polymeric scaffold fabrication can be classified in two groups: techniques to produce scaffolds or surfaces with random features or patterns with none or low control on their periodicity and dimensions; and techniques able to produce scaffolds or surfaces with features or patterns with controlled dimensions and periodicity. These techniques are described below.

1.3.1. Fabrication of micro- or nano-structured scaffolds with random features.

Porous scaffolds are needed to enable cell ingrowth, vascularization, and transport of nutrients and waste through the 3D structure. Porous scaffolds are typically produced by porogen leaching or gas foaming [31, 32] and by electrospinning [33]. In the first case, micropores are simply created by leaching out solid particles, such as salt, from the polymer matrix (melt or dissolved in a solvent) leaving pores of the same dimensions as the solid particles. Pore sizes can be highly controlled by means of a proper selection and preparation of the porogen, but their orientation is not easy to control in most cases. The porogen density must be that one to enable particle leaching and interconnectivity between the created pores, without significantly reducing the mechanical properties of the polymer. One of the major disadvantages of this technique is the possible presence of residual solvent in the scaffold. In the second case (gas foaming), instead of solid particles, liquid or gaseous phase are removed from the polymer matrix to create foams, emulsions and TIPS (thermally induced phase separation). This method enable to create scaffolds with very high porosities (>90%) but the control over the pore size and distribution is lower than in the case of the porogen leaching technique. Another major disadvantage of this technique is that requires an organic solvent, leading to possible toxicity of the scaffold. Electrospinning is a process in which a charged polymer jet, formed by applying an electrostatic charge to overcome the surface tension of a polymeric solution, is collected on a grounded collector to produce fibres. Rapidly rotating collectors result in aligned nanofibers, while stationary collectors result in randomly oriented fibre mesh. The quality of the created nanofibers is defined in terms of their alignment and morphology and it depends on the length, thickness, consistency and movement of the polymer jet. The characteristics of the jet can be optimized by adjusting the composition of the solution and the configuration of the electrospinning equipment, to control the alignment and morphology of the fibres being produced. Although this technique enables tuning

of the porosity and composition of the nanofibers, it offers a low versatility in terms of feature geometry.

1.3.2. Fabrication of micro- or nano-structured/patterned scaffolds with control on feature shape and size.

Photolithography-based methods [34], such as nanoimprint lithography (NIL), are based on transferring geometric patterns from a mask to a substrate coated by a photoresist (light sensitive organic polymers) by UV light, to use the substrate as a master for patterning a certain material. The photoresist is then lifted off to expose the remaining areas. Although these methods enable to obtain a wide range of pattern geometries with high accuracy in size (in the nano-scale), the process is expensive since several steps must be applied and clean room facilities are required. In addition, the chemicals used in these processes, such as resistant and developer solutions, can show biotoxicity. Another major disadvantage of this technique is that it cannot be applied for micro-and nano-structuring of 3D components.

Soft-lithography-based methods, such as microcontact printing (μCP) [35], use elastomeric polymers (such as PDMS) as stamps for manufacturing of chemical nano- and micropatterns by embossing, moulding and printing methods. The μCP is widely used for patterning self-assembled monolayers, proteins, cells and DNA. These techniques are low-cost since once the polymeric mould is created under clean room conditions, the rest of the process can be done under regular lab conditions and the mould can be used repeatedly. However, the transfer efficiency of the patterns depends on energetic consideration of stamp and substrate, and, therefore, only a fraction of chemicals can presently be patterned by this technology. μCP also shows some limitations when producing complex geometries and 3D micro - structures.

Rapid prototyping techniques (RP) are applied for the fabrication of 3D components by material deposition [36]. Most of these processes use a layered manufacturing approach whereby a 3-D CAD model is first decomposed into thin cross-sectional layer representations which are typically 0.01 to 0.7 mm thick. Then, to build the physical shape, each layer is selectively added or deposited and fused to the previous layer. Some of these processes are frequently employed for the fabrication of complex shaped scaffolds for tissue engineering: Stereolithography (STL) and fused deposition modelling (FDM) can be used for printing of polymers, ceramics, composites,

hydrogels and even cells; Selective Laser Sintering (SLS) is applied for printing of polymers, ceramics and composites by powder sintering. The major advantage of these techniques is the high controlled scaffold manufacturing; however, these processes are time consuming and typically involve heat or toxic chemicals to remove the support structures and these chemicals would kill living cells. Photo-polymerisation-based techniques [37], such as STL (more conventional technology) and two-photon polymerization (2PP, more novel technology), apply laser irradiation to cure conventional photosensitive materials by solidification of liquid photo resins (due to high intensities focused on small volumes) and can create 3D microstructures with sizes ranging from less than 100 nm to hundreds of micrometres in a single step [38]. The major disadvantage of these techniques lies on the limited materials that can be processed (photosensitive polymers), since the solidification process depends on the solubility of a suitable photo initiator present in the polymer solution and the density of polymerizable vinyl groups.

Direct laser ablation is well established as a universal tool for surface modification of polymers. Material ablation via ultrashort laser pulses enable to generate high precision 2D and 3D microstructural features, taking advantage of the “cold” ablation process, which turns solid into plasma, minimizing the thermal effects on the substrate and without changing the chemical properties of the material. This technology represents a very versatile method for direct micro-structuring of non-flat substrates, covering a wide variety of materials and geometries, in a direct, contactless and single step process, and without the requirement of expensive vacuum equipment.

In summary, technologies with nano-scaled precision provide high accuracy in the created feature sizes, but they are generally expensive, restricted to a short variety of materials and difficult to adapt for structuring or patterning non-flat and large 3D components. In the opposite, micromanufacturing technologies show lower accuracy in the feature scale, but higher potential for the fabrication of patterned/structured scaffolds with 3D complex shapes. Although nanopatterns are typically applied to influence on cell behaviour [39], cell sizes are in the micrometre range, and they also respond to micropatterns [40, 41]. In this regard, great efforts must be made in order to deeply investigate the effects of micropatterns on cell behaviour, applying technologies that can be used for processing the wide range of biomaterials investigated

for tissue engineering and can be scaled up for the fabrication of 3D components without restrictions in the patterned area or form.

1.4. Cell-biomaterial interaction.

1.4.1. Cell-surface interaction

Cells interact with their environment via biorecognition processes, which occur between the receptors inside the cell membrane (integrins) and the biomaterial surface. Cells *in vivo* are attached to a collection of protein layers produced by the cells that are known as the extracellular matrix (ECM). This ECM acts as a mechanical support for the cells and constitutes a microenvironment for cell growth and development, since it contains growth factors that control the cell behaviour, and leads to deposition of extracellular signal molecules and adhesion proteins, such as fibronectin, vitronectin, laminin, and collagen. When considering cell cultured *in vitro* on a material surface, the first step before cell adhesion is the protein adsorption on the surface, and cell-material or cell-surface interaction occurs via this layer of adhered proteins. Among the surface properties of the biomaterial, mechanical properties, which act via the ECM, have a great influence on cell phenotype [42]. After a mechanical stimulation, cells become the mechanical signals in biochemical responses by means of a mechanism known as mechanotransduction. Animal cells do not grow isolated but in close contact with other cells or forming tissues, where they undergo stretching and compression forces during their growth process which will be transferred to tensional changes in their cytoskeleton and will affect their behaviour. Every type of tissue show certain elasticity or stiffness. These are represented by the Young elastic modulus, and different tissues grow under different Young modulus. The influence of external mechanical forces on the development of a tissue is essential when stem cells (SCs) are considered [43]. SCs have two key characteristics which become these cells into a useful tool for cell therapies, drugs and tissue engineering strategies: the capability to reproduce and renew themselves for long periods (self-replication) and the ability to differentiate into any type of specialized cells or tissues (potentiality). Kilian et al. [44] observed that SCs differentiate preferentially to osteoblasts (bone cells) when they were attached to a chemical pattern with a geometry that leads to cell contractility (a vital property of muscular fibre cells), as concave zones;

while they differentiated to adipocytes (fat cells) when they grow on chemical-patterned-geometries that promotes cell extension, as convex zones. Spatial dimensions can play also a key role in cell differentiation. Most of the studies that investigate on stem cells differentiation are done in flat dishes coated with different types of biomaterials, but these conditions are different from those found during grow tissue in vivo (3D), and cell differentiation can be deficient. A 3D culture promotes cell interactions, enclose the ECM, keep cell spherical morphology and provide with a structural support for a high order tissue. Lee et al. [45] reported on 3D-culture of mammalian endothelial cells, which recapitulate the structural organization and the multicellular complexity of the mammalian epithelia. These models have proved to be physiological relevant and useful for studying some aspects of normal and tumour physiology of the mama [46].

1.4.2. Biocompatibility

Biocompatibility defines the degree of tolerance shown by the live tissue towards the material surface. The biomaterial and the physiological medium must co-exist without producing adverse effects. According to David F. Williams [47] “the biocompatibility of a long term implantable medical device refers to the ability of the device to perform its intended function, with the desired degree of incorporation in the host, without eliciting any undesirable local or systemic effects in that host”. This is applied to the biomaterial selection, but when we consider a scaffold for tissue engineering, “the biocompatibility refers to the ability to perform as a substrate that will support the appropriate cellular activity, including the facilitation of molecular and mechanical signalling systems, in order to optimize tissue regeneration, without eliciting any undesirable local or systemic responses in the eventual host”.

The response and behaviour of the cells on a surface depends strongly on the surface properties of the material, which can improve or diminish the compatibility of the surface with respect to cell adhesion, proliferation, viability and differentiation. Basic biocompatibility essays via cell seeding *in vitro* involve the observation of some main cell aspects when cells are cultured on the material, such as cell proliferation, adhesion, morphology, migration and function. Cell proliferation and adhesion are typically measured by counting the number of cells that detach from the surface after applying trypsin, an enzyme to break protein connections. Colorimetric methods, mostly based on testing cell metabolic viability (MTT assay), are generally applied to react with cells

producing coloured substances easy to monitor and quantify by optical absorption. One disadvantage of this method lay on the differences in the metabolic viability between cells, causing that the cell number is not necessarily proportional to the metabolic viability. Cell morphology, which is often related to cell function, is evaluated by fluorescence and confocal microscopy to observe cell shape and distribution on the material using dyes and fluorophores to stain different cells components (i.e. cytoplasm, nuclei, focal adhesions). A most advanced technique to observe cell morphology and function is the immunofluorescence, which enables to observe cell dynamic processes: this technique is based in the affinity between two molecules (i.e. an antibody and an antigen), so that a component that recognize a cell molecule binds to a fluorescent dye. Cell function can be determined evaluating the gene expression. The quantitative polymerase chain reaction (qPCR) is a laboratory technique for gene expression analysis, in which fluorescent dyes are used to label PCR products during a thermal cycling. More advanced biocompatibility essays will depend on the studied cell type and the intended function of the scaffold: in the case of vascular implants, for example, *in vitro* essays should involve investigation on blood contacting properties, platelet adhesion and activation, and competitive growth and adhesion between cells present in the environment of the tissue *in vivo* (i.e. endothelial cells, smooth muscle cells). The materials and devices classified as biocompatible by *in vitro* assays must be evaluated subsequently via *in vivo* assays.

2. Synthetic biopolymers: Polylactides

Biodegradable polymers, and among them polylactides (PLA), have generated a great interest in the tissue engineering field due to the wide variety of properties with which they can be synthesized, and their degradability capacity in natural conditions inside the human body without harmful products. The PLA is one of the most used biodegradable polymers, since, in addition to the aforementioned biodegradable properties, it can be obtained from renewable sources (from starch and sugar), and their mechanical properties can be suited to the application requests. Moreover, the thermoplastic nature of the PLA gives them other advantageous properties such as light weight, low processing temperature (respect to metal and glass), and easy to process [48].

PLA is an aliphatic polyester with lactic acid as the starting monomer. The lactic acid is composed of an asymmetric carbon with all their substituents different from each other, which gives chirality to the repetitive unities of the polymer structure. Both resulting isomers are enantiomers and most of their physical properties are identical (boiling temperature, melting temperature, density, dissolution, polarity…). The enantiomers are optically active, which means that they rotate the plane of polarization of the light that passes through them; both make this in the same magnitude but against each other: one of isomers rotate the plane of polarization to the left (levogyre) and the other one to the right (dextrogyre). Poly-L-lactide (PLLA) and poly-D-lactide (PDLA) are obtained from these monomers, respectively (Figure 0.2). Material properties will be different depending on the enantiomer proportion in the polymer. This enables to produce a wide spectrum of polylactides, both semicrystalline (PLLA) and amorphous (PDLLA), to meet the requirements for different applications.

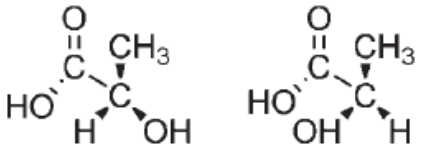

Figure 0.2. Chemical structure of L and D-lactic acid [49].

2.1. Polymerization

The lactic acid can be obtained from fermentation of the carbohydrates, that produces the L-acid lactic, or by chemical synthesis, which produces D-lactic acid. The major proportion of the acid lactic production is obtained by fermentation. There are several techniques to obtain PLA of high molecular weight (over 100000 r.u.) such as condensation by dehydration, polymerization by direct condensation, polymerization from solid state, and polymerization via formation of the lactide dimer by ring opening polymerization (ROP) (Figure 0.3) [49, 50].

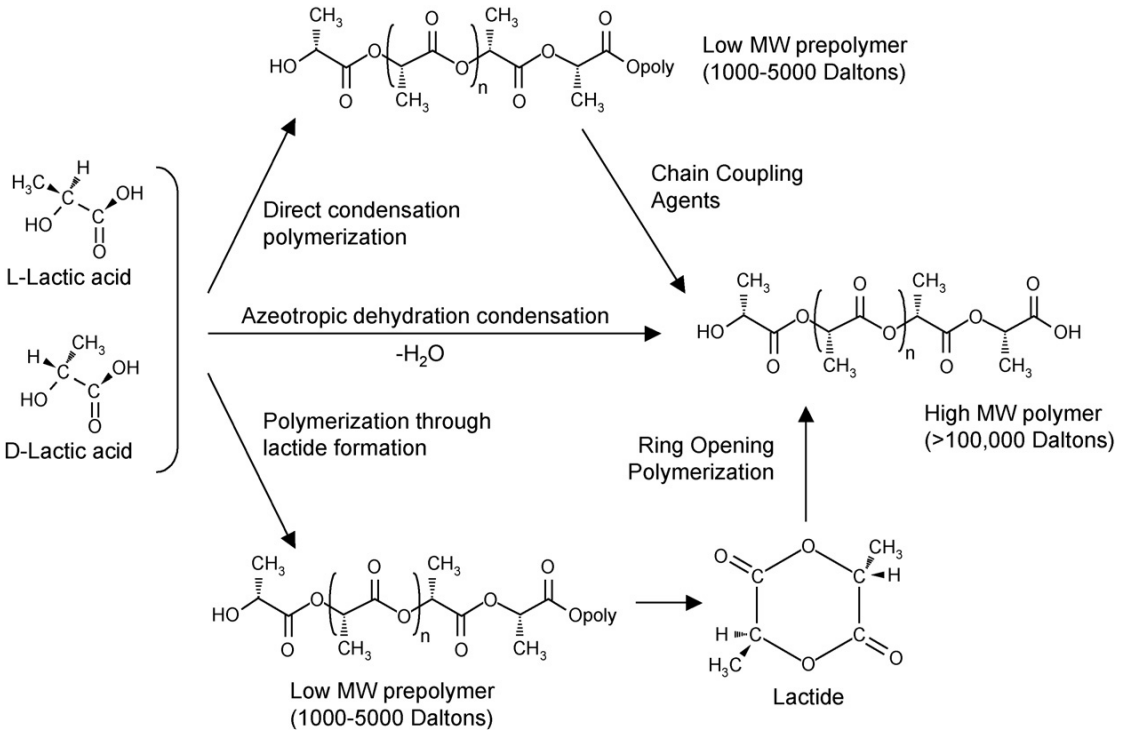

Figure 0.3. PLA polymerization [49,50].

In the case of polymerization by direct condensation, the lactic acid is polymerized in presence of a catalyst under reduced pressure conditions. The resulting polymer has a low molecular weight, since it is difficult to remove water from the high viscous reaction products. The PLA obtained by this technique shows low mechanical properties in comparison to the PLA synthetized by other manufacturing routes.

In the case of polymerization by condensation with dehydration or azeotropic condensation, the challenge regarding water removing from the reaction products is solved manipulating the balance between the monomer and the polymer in an organic solvent, and the lactic acid is directly poly-condensed in a high molecular weight polymer.

In the case of polymerization from solid state, a solid semi-crystalline prepolymer, with a relatively low molecular weight, in form of power, chips or fibre is heated up to a temperature below the melting point, while as the residual products are removed from the material surface by volatilization under reduced pressure conditions, or by a carrier (i.e. injecting an inert gas). This reaction occurs in the polymer amorphous fraction where the reactive terminal groups are located, therefore, it must be developed over the glass transition temperature. The PLA resulting from this polymerization process shows high molecular weight and good physical properties.

ROP from the dimmer lactide is the most used and studied PLA production method, since it enables to control in a precise way the chemistry of the reaction and, therefore, the resulting polymer properties, increasing the fields of application. This method is used to synthesize PLA of high molecular weight with a high degree of stereo-regularity. The PLLA used in this work has been synthetized by ROP.

2.2. Structure and crystallinity

The L-isomer constitutes the major fraction of the PLA obtained from renewable sources, since most of the lactic acid present in biological sources shows this form. The PLLA can exhibit three different types of crystalline structures: α, β, or γ. The most common PLLA crystallization form is the α-structure, since the PLLA crystallize sooner like α-homocrystals from melt material [51-53]. The crystallization kinetics of this isomer is low, enabling to vary the degree of crystallinity of the polymer by different thermal treatments. This parameter determines many of the material physical properties and can affect the compatibility of the polymer with biological components (i.e. cell cultures). The degree of crystallinity, which can be determined by differential scanning calorimetry (DSC), is evaluated by the next expression:

$$x_C(\%) = \frac{\Delta H_m - \Delta H_C}{\Delta H_m^0} \cdot 100 \qquad (0.1)$$

In this expression, ΔH_m and ΔH_C represents the enthalpy of the melting and crystallization processes, respectively. ΔH_m^0 is the theoretical value of the enthalpy at the melting point for a fully crystallized polymer, and in the case of PLLA with α crystallization, this value is 106 J/g [53]. The maximum degree of crystallinity of the PLLA is typically about 60% [54].

Depending on the heat treatment applied, the resulting polymer will have different degree of crystallization and different morphology. The PLLA crystallize from the melt forming birefringent spherical polycrystalline entities (spherulites) originated by chain folding. At high heating rates, a small material fraction is crystallized forming a big number of small spherulites, while as at low heating rates, most of the material crystallizes and, although there are a minor number of crystallization nucleus, the formed spherulites are bigger.

2.3. *Thermal properties*

Semi-crystalline polymers are characterized by three characteristic temperatures which allow their identification. The glass transition temperature (T_g) involves a temperature range from which the material starts softening (weakening of the chain secondary bonds is produced and the movement capacity of the chains is increased) until the polymer shows and elastomeric behaviour first, and finally, with further heating, a viscous liquid appearance. The crystallization temperature (T_c) is the temperature at which energy is released as a consequence of a chain arrangement in the polymer. The melting temperature (T_m) corresponds to the polymer crystalline fraction. The characteristic temperatures of the PLLA are the following: T_g at 60-65 ˚C, T_c at around 110 ˚C, and T_m at about 170-190 ˚C [55, 56]. These values can vary depending on the degree of crystallinity of the material.

2.4. *Mechanical properties*

PLLA (semicrystalline) show a neater and compact structure than PDLLA (amorphous), and that is why their mechanical properties are better (in terms of stiffness) for a given molecular weight and its service life is longer. The stiffness of the PLLA can be further improved by increasing the degree of crystallinity via application of a certain thermal treatment [56]. However, semicrystalline systems with higher degree of crystallinity are characterized by a decrease in ductility. This means that you need to reach a compromise about the optimal value of the degree of crystallinity for obtaining certain technological properties.

The PLLA shows the typical linear stress-strain curve at low strains with a Young's modulus of 3GPa (quite high), followed by a non-linear behaviour before reaching the breaking point, with a high tensile strength around 67 MPa for a high crystalline PLLA. The Young's modulus increases with the degree of crystallinity. An increase in the polymer crystallinity is characterized by a reduction in the width of the size distribution relative to the material free volume (which can be evaluated by positron annihilation technique, for example). This reduction results in a decrease of the chain motility, and therefore it could be related to the increase of the stiffness. As mentioned above, a high increase in polymer crystallinity would lead to a decrease of its ductility. In PLLA,

the high tensile strength increases with the degree of crystallinity until reaching a maximum value, and then suffers a slight reduction at higher crystallinities.

2.5. Dynamic properties

Restrictions on polymer chain movements caused by entanglements or by crystallization affect the different secondary relaxations present in the polymer as well as its glass transition. In semi-crystalline polymers, the macromolecules are bigger than the crystalline lamellae thickness and they can pass through the phase borders leading to formation of entanglements with different degree. If chain coupling is weak, non-crystalline chain segment dynamics shows a widening of the glass transition region, whereas if there is a strong chain coupling, the non-crystalline polymer portion can show the glass transition at higher temperature than the glass transition related to the amorphous phase, due to formation of a stiffer amorphous phase. The glass transition is related to the cooperative movements of chain segments, and the entanglement constraints this type of movements.

There are several reports focused on the study of molecular dynamics of PLLA [55, 57] in different ranges of temperature. They are usually characterized by solid state nuclear magnetic resonance (NMR) and techniques based on neutron scattering. Nozirov et al. [58] have observed two main chain movements in PLLA: the first one is a rearrangement of the tri-fold formed by the methyl groups; and the second one is a rearrangement of the double-fold formed by the hydroxyl groups. Methyl group rotation predominates at low temperatures (90K) (similar to that observed in other polymers), whereas at temperatures over the glass transition temperature (323K) the main movement is the hydroxyl group rearrangement. At temperatures from 200 to 325 K both rearrangements are present, with a major influence of the methyl group rotation.

2.6. Degradation properties

PLLA is a biodegradable polymer, so that the material is subjected to structural changes and loss of properties in a natural environment [59]. Polyesters degrade generally by water absorption, and loss of molecular weight, mass and mechanical properties. At the first stage of the degradation process, PLLA loses molecular weight to form oligomers. Opposite to the PLLA with high molecular weight, the oligomer is water-soluble. Water infiltrates into the polymeric matrix leading to ester group hydrolysis, weakening the chemical bonds in the amorphous phase, and converting the large polymer chains into short segments to obtain water-soluble oligomers and monomers. Degradation increases the number of carboxyl chain-ends that auto-catalyse ester hydrolysis. The nearest oligomers to the surface escape before the total polymer degradation occurs whereas the remained oligomers in the polymeric matrix continue contributing to the autocatalytic process. Polymer degradation depends on many factors such as molar mass, macromolecular conformation, stiffness, chemical structure, molecular weight, chain motility and crystallinity. In semicrystalline PLLA, crystalline regions are more resistant to degradation than amorphous regions, and the degradation rate decreases with an increase in the degree of crystallinity [60]. The biodegradation of the polymer depends also on the environment to which is exposed: in human or animal bodies, it is believed that PLAs degrade first by hydrolysis and the soluble oligomers formed are then metabolized by cells [61].

3. Ultrashort-laser ablation of polymers

3.1. Fundamentals of laser-material interaction: focus on polymers.

Laser ablation is the removal of material from a solid surface by direct absorption of laser energy. The ablated volume is determined by the penetration depth (l) and the spot diameter (Figure 0.4).

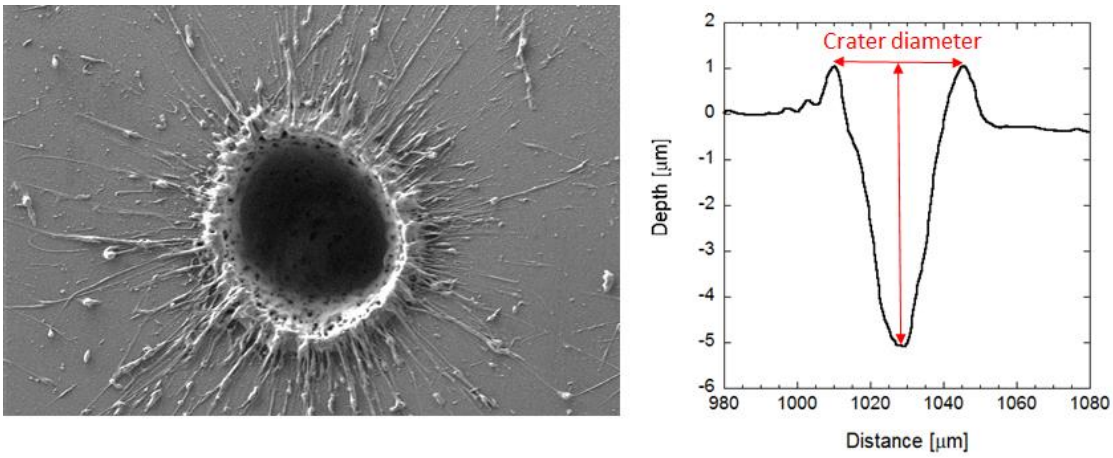

Figure 0.4. SEM and profilometry images of a crater generated by pulsed laser ablation on a polymeric film.

The penetration depth at which a laser pulse interacts with a material is determined by the optical (l_α) and thermal penetration (l_{th}):

$$l = l_\alpha + l_{th} \qquad (0.2)$$

In the case of considering polymeric substrates, optical penetration depth dominates over the thermal one, and it is defined as the depth at which the intensity of the transmitted light drops to 1/e of its initial value at the interface. The optical penetration depth is inversely proportional to the material's absorption coefficient (α) and this is heavily dependent on the incident wavelength. Considering a constant wavelength, the incident beam intensity at surface (I_0) decays exponentially with depth (d) according to the Beer-Lambert law [62]:

$$I(d) = I_0 e^{-\alpha d} \qquad (0.3)$$

The penetration depths are typically short relative to bulk material dimensions and the energy absorption is approximately confined within the penetration depth. Wavelengths with shorter penetration depths enable the local modification of the surface without affecting the material bulk properties. The absorption coefficient determines the absorption of the laser beam on the material but the specific mechanisms by which the absorption occurs will depend on the material. The absorption of the laser beam in insulators and semiconductors mainly occurs through resonant excitations, such as transitions of valence band electrons to the conduction band (interband transitions) or within bands (intersubband transitions). These excited electronic states can then

transfer energy to lattice phonons. Laser photons with energy high enough to overcome the material ionization potential or bandgap will be absorbed, and “single photon absorption” will be the main mechanism for excitation; On the contrary, if the material bandgap is higher than the laser photon energy, the “multiphoton absorption” mechanism will lead the excitation. Such energies typically correspond to laser beam frequencies below vacuum ultraviolet for insulators and below the visible to infrared spectrum for semiconductors. The time it takes for the excited electronic states to transfer the absorbed energy to phonons and thermalize depends on the material and the mechanism within the material. For non-metals, the absorption mechanism and the thermalization time (τ_{th}) can be quite different from one material to another, reaching values as long as 10^{-6} seconds [63]. Polymers are typically on the slower end of this range, since defects and quantum confined electronic states can play a significant role in slowing down this thermalization time. When the incident laser pulse is longer than the thermalization time, the absorbed laser energy is directly transformed into heat and leads to thermal bond breaking. These processes are known as photothermal and predominate when long laser pulses (typically longer than 10 picoseconds (ps)) are applied. On the contrary, when the laser pulse is shorter or in the order of the thermalization time, the excitation energies can be high enough to directly break bonds (photo-decomposition), which is known as ablation by photochemical processes.

Photothermal processes (associated to laser **pulse duration (τ_p) longer than 10 ps**) involved material evaporation and sublimation at low fluences (energy per surface), and heterogeneous nucleation of vapor bubbles that leads to boiling. If material heating is sufficiently rapid to approach the material thermodynamic critical temperature, it is overheated and a phase explosion is produced (also known as explosive evaporation) leading to an inhomogeneous decomposition of the material in a mixture of liquid drops and molecules in gaseous phase. The laser energy is absorbed by a large volume of material which is heated and melted, and the ablation is accomplished through melt expulsion driven by the vapor pressure and the recoil of the beam pressure. This decomposition process leads to a fast material cooling that produces recast material around the ablation zone (Figure 0.5 (a)). In this scenario, the threshold ablation energy is defined as the critical energy density required to produce an overheating on the surface of the material beyond its thermodynamical stability.

Photochemical processes (associated to laser **pulse duration (τ_p) shorter than 10 ps**) are characterized by direct ionization and formation of dense electron-hole plasmas that can lead to athermal phase transformations, direct bond-breaking, and explosive disintegration of the lattice through electronic repulsion (Coulomb explosion). When pure photochemical ablation occurs, the temperature of the material remains relatively unchanged. In this scenario (ultrashort pulsed ablation) the deposited laser energy is limited in a small volume causing the material to past very quickly from the liquid phase to the vapor phase with high kinetic energy (way above the vaporization temperature). The material removal occurs by direct vaporization away from the surface (into vacuum or air) consuming a large amount of the absorbed laser energy. This reduced the heat diffusion on the material and, although this still occurs after the end of the laser pulse duration, the resulting melt thickness is small, because of the rapid cooling generated by the steep temperature gradient [64]. Hence, laser ablation by ultrashort pulses is known as “cold ablation”, due to the minimization of thermal effects on the substrate (Figure 0.5 (b)). In particular laser ablation of polymers with short wavelengths and ultrashort laser pulses has been considered as an example of a photochemical ablation process.

Ultrashort laser pulses (**from femtoseconds to 10 picoseconds**) can enable photochemical processes even in metals and semiconductors, but it is important to remark that most of the materials (including polymers) exhibit both thermal and photo-chemical mechanisms during the laser ablation process [65]. When both thermal and non-thermal processes are involved, two independent channels of bond breaking or different bond breaking energies for ground-state and electronically excited-state chromophores (light absorbing functional groups of a molecule) are considered. This model is known as photo physical [66]. Additionally, for ultras-short pulses, the heating process induced by the laser irradiation occurs under constant volume conditions, and leads to the generation of a high thermoelastic pressure wave in the material. In this case, the onset of ablation occurs at lower laser energies than in the case of pure photothermal processes. This is attributed to photomechanical effects caused by the relaxation of the pressure wave induced by the laser in the material [67]. These phenomena cause that the laser-crated vapor ejected plume containing solid or liquid clusters of material is larger and faster in this case than those produced under the pure photothermal processes. At high intensities, a significant fraction of the species may become ionized, producing a high-absorbing plasma, which affects the ablated

surface due to scattering effects. These effects, which are known as nonlinear processes and involve avalanche and multiphoton ionization, increase with the energy density and the number of pulses and are more influent for times below 5 ps. Specially the multiphoton ionization process play a key role on laser ablation at ultrashort pulse durations and is behind the laser ablation phenomenon on transparent materials [64, 68].

The edges of the laser beam with an energy density below the threshold for material removal may have unwanted effects on the substrate surface, causing thermal damage around the ablated zone (known as heat affected zone: HAZ, Figure 0.5 (a)). In addition, recoil from the plume can generate shockwaves in the material and further expulsion of any remaining molten material. Because of all these effects, the burr observed at the edges of the ablated structures is produced by the accumulation of thin layers of melt material accelerated by vapor pressure to the structure sides. This acceleration can be reduced decreasing the fluence to values slightly above the ablation threshold, but this reduction must be compensated (in terms of ablated volume) by an increase of the laser pulses frequency. In general, for shorter pulse durations the energy is deposited faster into the material causing a faster material ejection. Since the volume of material excited by the laser has less time to transfer energy to the surrounding material the ablated volume is more precisely defined by the laser's spatial profile and optical penetration depth, and there is less residual energy and, therefore, less HAZ.

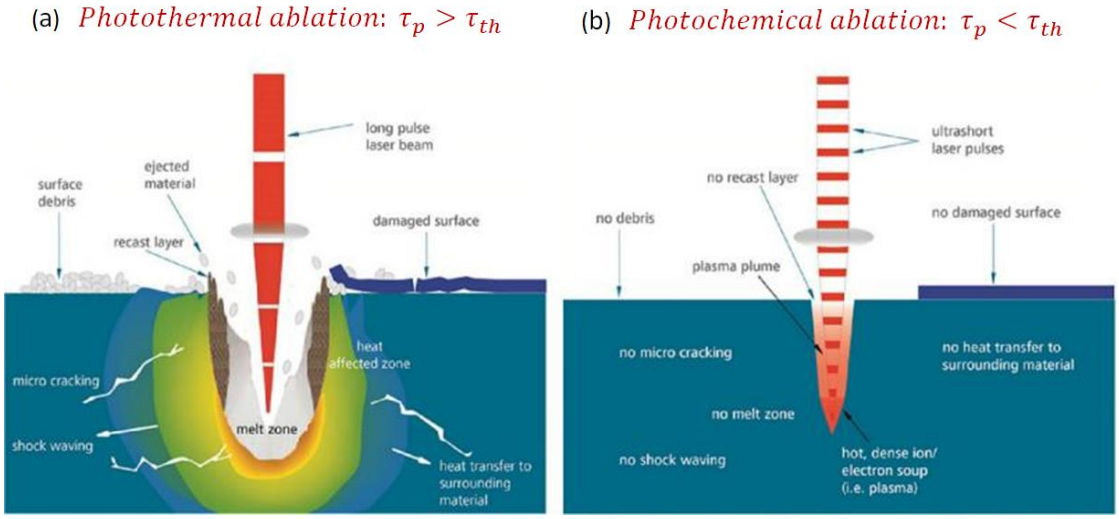

Figure 0.5. Typical phenomena occurred on materials under short ($\tau_p > \tau_{th}$) and ultrashort ($\tau_p < \tau_{th}$) pulsed laser ablation (image slightly modified from [69]).

Laser ablation of polymers was first reported by Srinivasan and Mayne-Banton [70], and, since then, numerous studies reporting laser ablation of a wide variety of polymers have considered different ablation mechanism and models, to elucidate the contribution between photothermal and photochemical processes in the ablation process [66, 71-80]. Regarding surface microstructuring of polymers, and in terms of surface quality and precision of the structuring, photochemical ablation is generally most desirable to occur due to two main characteristics of this ablation mechanism: the minimization of thermal damage into the adjacent zones, and the conversion of polymer into gaseous products, diminishing the deposition of ablation products (known as debris) on the structured surface (leading to clean microstructured surfaces with no need of post-processing steps). The decomposition mechanisms of polymers under laser irradiation depend heavily on their synthesis method [65]: the polymers produced by radical polymerization from monomers, which contains double bonds, depolymerize generally into monomers; on the contrary, polymers obtained by reactions like polycondensation, such as PLA (Figure 0.3), decomposed into different fragments.

3.2. Laser Micromachining: Key process parameters.

The laser considered in this work is a pico-second pulse Nd: YVO_4 laser (RAPID: Lumera Laser). The laser source delivers 10 ps pulses at 1064nm wavelength with a maximum average power of 12W and an energy of 18 µJ operating at a maximum repetition rate of 1 MHz. In addition to the fundamental mode, the laser emits at second and third harmonic wavelengths of 532 and 355 nm with maximum energies of 2.5 and 1.5 µJ respectively at the same repetition rate (1 MHz). The laser frequency can be tuned from 4 to 1000 kHz. The laser beam was focused over the sample by focusing lens placed in air with a 100-mm focal length for 532 and 1064 nm wavelengths, and a 103mm focal length for the 355nm wavelength. Spot sizes (beam radius at $1/e^2$) of 30 µm and 20.5 µm were obtained for wavelengths of 532 nm and 355 nm at energy of 0.2 µJ by selecting optional fixed beam expanders.

The average power emitted by the picosecond pulsed laser considered in this work is shown in Figure 0.6 for the range of wavelengths and frequencies available. The average power achieved at the surface of the work piece is compared to the average power emitted by the laser source

(measured out of the laser resonator). The first one is lower than the second one because of the losses caused by absorption or scattering of the beam through the optical components that guide the beam from the source to the work piece.

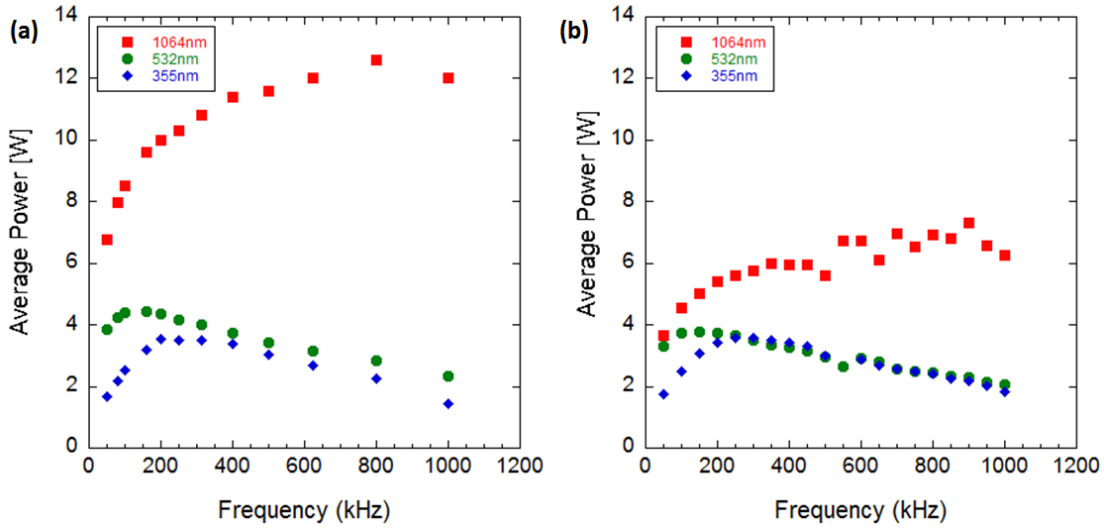

Figure 0.6. Average power of the picosecond pulsed laser considered, measured out of the laser resonator (a) and at the work stage (b) for the range of wavelengths and frequencies available.

The peak power of a laser pulse is defined by the average power of the pulsed laser beam (P_{av}), the pulse length (τ) and the frequency of pulse emission (f) according to the next equation:

$$P_{peak} = \frac{P_{av}}{\tau \cdot f} \qquad (0.5)$$

According to this equation, high peak powers are reached when short pulse lengths and low frequencies are applied. However, the processing time increases for low frequencies; this means that to address the processing of a certain material, a commitment between the power required to ablate the material and the processing time should be reached to optimize the ablation process. The pulse energy can be calculated from the average power and the frequency. The energy per pulse, as in the case of the peak power, increases when low frequencies are applied.

$$E_{pulse} = \frac{P_{av}}{f} \qquad (0.6)$$

The peak fluence (F_{peak}) is defined by the energy per pulse and the radius of the laser beam in 1/e^2 of the maximum irradiance (ω_0), which is the beam waist radius in focus:

$$F_{peak} = \frac{2E_{pulse}}{\pi\omega_0^2} \qquad (0.7)$$

The theoretical beam waist is defined by the beam quality (M^2), the focal length of the lens (f_L), and the collimated beam diameter (D_{beam}):

$$\omega_0 = \frac{4M^2 f_L \lambda}{\pi D_{beam}} \qquad (0.8)$$

The average beam fluence (F_{av}) is defined by the following expression:

$$F_{av} = \frac{F_{peak}}{2} \qquad (0.9)$$

The onset of ablation occurs above a threshold energy or fluence, which depends, as mentioned before, on the absorption mechanism, material properties, microstructure, morphology, the presence of defects, and on laser parameters such as wavelength and pulse duration. Typical threshold fluences for organic materials are between 0.1 and 1 J/cm^2 [73, 74, 78, 81]. If we define the ablation rate as the depth of the ablated crater after one pulse (d) at a given energy, the effective absorption coefficient (α_{eff}) and the energy ablation threshold (E_{th}) can be estimated by applying the Beer-Lambert law valid when single-photon absorption processes occur and considering sufficiently small energies above the ablation threshold [82]:

$$d = \frac{1}{\alpha_{eff}} \ln\left(\frac{E}{E_{th}}\right) \qquad (0.10)$$

Only in rare cases the beam radius measured at 1/e^2 coincides coincidentally with the diameter of the ablated crater (D), which in the case of a Gaussian beam is determined by the incident energy and the energy ablation threshold [83]:

$$D^2 = 2\omega_0^2 \ln\left(\frac{E}{E_{th}}\right) \qquad (0.11)$$

These equations imply that by measuring the dimensions of the craters (diameter and depth) generated by a laser beam with a certain incident wavelength on a material, and the incident laser energies applied to create these craters, the characteristic parameters of the laser-material interaction (energy ablation threshold and effective absorption coefficient) can be estimated.

When considering material ablation by pulse overlapping, it must be considered that the energy deposited on the material also depends on the pulse distance (d_p) (Figure 0.7), which is defined by the frequency of emission of the pulses and the speed of the scanner to move over the substrate (v):

$$d_p = \frac{v}{f} \qquad (0.12)$$

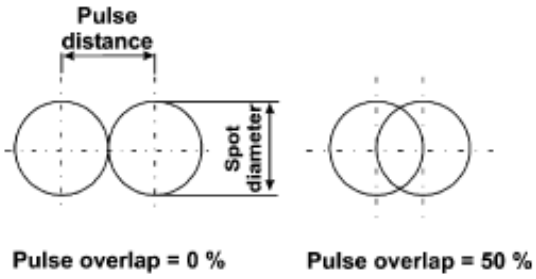

Figure 0.7. Drawing representing the pulse distance and overlapping.

When shorter is the pulse distance, higher is the overlapping between two consecutive pulses, and, therefore, the energy deposited on the material and the ablation rate. The percentage of overlapping between pulses (U_d) can be calculated by the next equation:

$$U_d = \left(1 - \frac{v}{(f \cdot D)}\right) \cdot 100\% \qquad (0.13)$$

A high percentage of overlapping between pulses can be reached by diminishing the speed of the laser beam over the surface, or increasing the laser frequency (Figure 0.8). In order to maintain an optimal pulse overlap of 85%, low speed must be applied for working at low laser frequencies which show high pulse energies and high ablation rates; in this scenario, the process time increases due to the low speed. The process time can be shorter by applying a high speed, but the ablation rate is reduced, since higher frequencies must be applied to maintain the optimal pulse overlap and lower pulse energies are reached. A commitment between processing time and

ablation rates must be established to optimise the laser ablation process for each application case.

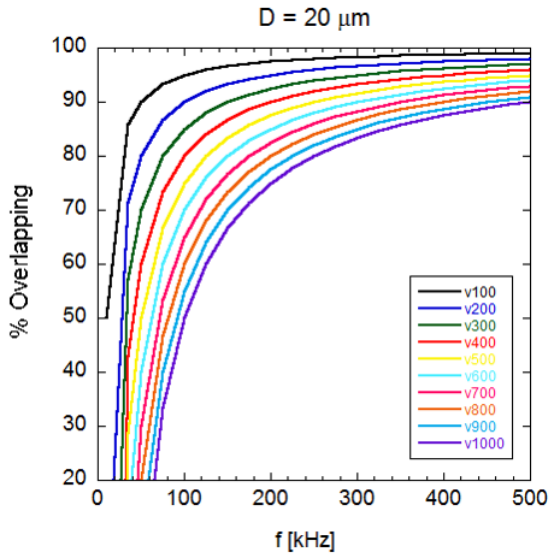

Figure 0.8. Representation of the percentage of overlapping between laser pulses like a function of frequency and speed, considering a spot diameter of 20 micrometres.

4. Structure and organization

In the following chapters of this thesis we are going to consider the picosecond pulsed laser ablation technology for manufacturing of surface micropatterns on films and sheets of PLLA, to investigate the ablation mechanism on this polymer, and the effect of laser-created micropatterns on the response of several cell types via *in vitro* essays; this investigation is made with the overall goal to elucidate the influence of these topological micropatterns on cell response and asses the laser technology as a method for scaffold manufacturing and surface functionalisation in the tissue engineering field.

In the first chapter, the picosecond laser ablation of PLLA as a function of laser energy and degree of crystallinity is examined. The ablation parameters and the surface modifications are analysed under various irradiation conditions using laser wavelengths ranging from the ultraviolet through the visible. These results are interpreted in terms of photothermal and photochemical response of polymers as a function of material micro-structure and incident laser wavelength. In the second chapter, different micropatterns are laser-generated on polystyrene (PS) and PLLA and employed

to study cellular proliferation and morphology of breast cancer cells. The laser-induced microstructures included parallel lines of comparable width to that of a single cell and the fabrication of square-like compartments of a much larger area than a single cell. In the third chapter, the effect of the laser micropatterns on the behaviour of human mesenchymal stem cells (MSCs) before and after co-differentiation into adipocytes and osteoblasts is evaluated. Laser ablation is applied in this case to generate microgrooves and microcavities on PLLA, where orientation, cell shape and MSCs co-differentiation are investigated. In the fourth and last chapter, laser ablation technology is applied on modified PLLA to generate patterns with different geometry and density and find a pattern configuration able to promote endothelialisation on the surface. The patterns generated include parallel micro-grooves with different width, depth and inter-groove spacing. These patterns are evaluated by cytocompatibility tests using a L929 cell line, endothelial cell adhesion and hemocompatibility tests. Finally, the set of outcomes obtained from the aforementioned studies, about laser ablation of the considered polymer and effects of the laser-generated micropatterns on the behaviour of three different cell types, are reviewed to reach a conclusion about the suitability of the laser technology considered for manufacturing and surface functionalisation of scaffolds for tissue engineering applications.

References

[1] Lawall H, Bramlage P, and Amann B. Treatment of peripheral arterial disease using stem and progenitor cell therapy. Journal of Vascular Surgery, 2011; 53(2): 445-453.

[2] Cideciyan AV, Hauswirth WW, Aleman TS, Kaushal S, Schwarts S, Boye SL, Windsor EAM, Conlon TJ, Sumaroka A, Roman AJ, Byrne BJ, and Jacobson SG. Vision 1 year after gene therapy for Leber's congenital amaurosis. N Engl J Med 2009; 361(7): 725-727.

[3] Kolettis TM, Vilaeti A, Dimos K, Tsitou N, and Agathopoulos S. Tissue engineering for post-myocardial infarction ventricular remodeling. Mini Rev Med Chem 2011; 11(3): 263-270.

[4] Franz S, Rammelt S, Scharnweber D, and Simon JC. Immune responses to implants – A review of the implications for the design of immunomodulatory biomaterials. Biomaterials 2011; 32: 6692-6709.

[5] Campoccia D, Montanaro L, and Arciola CR. A review of the clinical implications of anti-infective biomaterials and infection-resistant surfaces. Biomater 2013; 34: 8018-8029.

[6] Brown RM, Wheelwright EF, Chalmers J. Removal of metal implants after fracture surgery—indications and complications. J R Coll of Surg of Edinb 1993; 38(2): 96-100.

[7] Albretch DR, Underhill GH, Wassermann TB, Sah RL, and Bhatia SN. Probing the role of multicellular organization in three-dimensional microenvironments. Nature Methods 2006; 3(5): 369-375.

[8] Kaplan D L, Moon R T and Vunjak-Novakovic G. It takes a village to grow a tissue Nature Biotechnol. 2005; 23: 1237–1239.

[9] Williams DF. On the nature of biomaterials 2009; Biomaterials 30: 5897–5909.

[10] Burny F, Donkerwolcke M, and Muster D. Biomaterials education: a challenge for medicine and industry in the late 1990s. Mater Sci Eng A 1995; 199: 53-59.

[11] Larrañaga A, Ramos D, Amestoy H, Zuza E, and Sarasua JR. Coating of bioactive glass particles with mussel-inspired polydopamine as a strategy to improve the thermal stability of poly (L- lactide) / bioactive glass composites. RSC Advances 2015; 5(80): 65618-65626.

[12] Zhou M, Smith AM, Das AK, Hodson NW, Collins RF, Ulijn RV, and Gough JE. Self-assembled peptide-based hydrogels as scaffolds for anchorage dependent cells. Biomater 2009; 30: 2523-2530.

[13] Zhang L, Gu FX, Chan JM, Wang AZ, Langer RS, and Farokhzad OC. Nanoparticles in medicine: Therapeutic applications and developments. Clin Pharmacol Ther 2008; 83(5): 761-769.

[14] Kostarelos K, Bianco A, Prato M. Promises, facts and challenges for carbon nanotubes in imaging and therapeutics. Nat Nanotech 2009; 4: 627-633.

[15] Bailey RE, Smith AM, Nie S. Quantum dots in biology and medicine. Physica E Low Dimens Syst Nanostruct 2004; 25: 1-12.

[16] Jamieson TJ, Bakhshi R, Petrova D, Pocock RI, Imani M and Seifalian AM. Biological applications of quantum dots, Biomaterials 28 (31) (2007), pp. 4717–4732.

[17] Vemula PK, Cruikshank GA, Karp JM and John G. Self-assembled prodrugs: an enzymatically triggered drug-delivery platform. Biomaterials 30 (3) (2009), pp. 383–393.

[18] Kamimura K, Suda T, Zhang G, and Liu D. Advances in gene delivery systems. Pharmaceut Med 2011; 25(5): 293-306.

[19] Wu ZS, Zheng F, Shen GL and Yu RQ. A hairpin aptamer-based electrochemical biosensing platform for the sensitive detection of proteins. Biomaterials 30 (15) (2009), pp. 2950–2955.

[20] O'Brien FJ. Biomaterials & scaffolds for tissue engineering. Mater Today 2011; 14(3): 88-95.

[21] Balamurugan A, Rajeswari S, Balossier G, Rebelo AHS and Ferreira JMF. Corrosion aspects of metallic implants – An overview. Mater Corrosion 2008; 59(11): 855-869.

[22] Best SM, Porter AE, Thian ES, and Huang J. Bioceramics: Past, present and for the future. J Eur Ceram Soc 2008; 28: 1319-1327.

[23] Fernández J, Etxeberria A, and Sarasua JR. Synthesis, structure and properties of poly(L-lactide-co-ε-caprolactone) statistical copolymers. J Mech Behav Biomed Mater 2012; 9: 100-112.

[24] Nair LS and Laurencin CT. Polymers as biomaterials for tissue engineering and controlled drug delivery. Adv Biochem Engin/Biotechnol 2006; 102: 47-90.

[25] Ramsden JJ, Allen DM, Stephenson DJ, Alcock JR, Peggs GN, Fuller G and Goch G. The design and manufacture of biomedical surfaces. CIRPS Ann Manuf Techn 2007; 56(2): 687-711.

[26] Grewal HS, Cho IJ and Yoon ES. The role of bio-inspired hierarchical structures in wetting. Bioinspir Biomim 2015; 10: 026009.

[27] Lim JY and Donahue HJ. Cell sensing and response to micro- and nanostructured surfaces produced by chemical and topographic patterning. Tissue Eng 2007; 13(8): 1879-1891.

[28] Green AC, Washburn CM, Bachand GD and James CD. Combined chemical and topographical guidance cues for directing cytoarchitectural polarization in primary neurons. Biomaterials 2011; 32: 8860-8869.

[29] Nikkhah M, Edalat F, Manoucheri S and Khademhosseini A. Engineering microscale topographies to control the cell-substrate interface. Biomater 2012; 33: 5230-5246.

[30] Dolatshahi-Pirouz A, Nikkhah M, Kolind K, Dokmeci M, and Khademhosseini A. Micro- and nanoengineering approaches to control stem cell-biomaterial interactions. J Funct Biomater 2011; 2(3): 88-106.

[31] Chen G, Ushida T, and Tateishi T. Development of biodegradable porous scaffolds for tissue engineering. Mater Sci Eng C 2001; 17: 63-69.

[32] Salermo A, Oliviero M, Di Maio E, Iannace A and Netti PA. Design of porous polymeric scaffolds by gas foaming of heterogeneous blends. J Mater Sci: Mater Med 2009; 20: 2043-2051.

[33] Sill TJ, and von Recum HA. Electrospinning: Applications in drug delivery and tissue engineering. Biomater 2008; 29: 1989-2006.

[34] Liu WW, Chen ZL, and Jiang XY. Methods for cell micropatterning on two-dimensional surfaces and their applications in biology. Chin J Anal Chem 2009; 37(7): 943-949.

[35] Ruiz SA and Chen CS. Microcontact printing: A tool to pattern. Soft Matter 2007; 3: 1-11.

[36] Upcraft S and Fletcher R. The rapid prototyping technologies. Assembly Automat 2003; 23(4): 318-330.

[37] Skoog SA, Goering PL and Narayan RJ. Stereolithography in tissue engineering. J Mater Sci: Mater Med 2014; 25: 845-856.

[38] Burmeister F, Steenhusen S, Houbertz R, Zeitner UD, Nolte S and Tünnermann A. Materials and technologies for fabrication of three-dimensional microstructures with sub-100 nm feature sizes by two-photon polymerization. J Laser Appl 2012; 24(4): 042014.

[39] Bettinger CJ, Langer R and Borenstein J. Engineering substrate topography at the micro- and nanoscale to control cell function. Angew Chem Int 2009; 48: 5406-5415.

[40] Ruiz SA and Chen CS. Emergence of patterned stem cell differentiation within multicellular structures. Stem Cells 2008; 26(11): 2921-2927.

[41] Seo CH, Furukawa K, Suzuki Y, Kasagi N, Ichiri T, and Ushida T. A topographically optimized substrate with well-ordered lattice micropatterns for enhancing the osteogenic differentiation of murine mesenchymal stem cells. Macromol Biosci 2011; 11: 938-945.

[42] Melzak K, Moreno S, Vivanco MdM and Toca-Herrera JL. “Mechanical cues for cell culture”. Handbook of biofunctional surfaces”, Chapter 25. W. Knoll Ed. 2012, Taylor & Francis Group.

[43] Hwang NS, Varghese S, and Elisseeff J. Controlled differentiation of stem cells. Adv Drug Deliver Rev 2008; 60: 199-214.

[44] Kilian KA, Bugarija B, Lahn BT and Mrksich M. Geometric cues for directing the differentiation of mesenchymal stem cells. PNAS 2010; 107(11): 4872-4877.

[45] Lee GY, Kenny PA, Lee EH and Bissell MJ. Three-dimensional culture models of normal and malignant breast epithelial cells. Nature Methods 2007; 4: 359-365.

[46] Schmeichel KL and Bissell MJ. Modeling tissue-specific signaling and organ function in three dimensions. J Cell Sci 2003; 116: 2377-2388.

[47] Williams DF. On the mechanisms of biocompatibility. Biomater 2008; 29: 2941-2953.

[48] Lim LT, Auras R and Rubino M. Processing technologies for poly (lactic acid). Prog Polym Sci 33 2008; 33(8): 820-852.

[49] Auras R, Harte B and Selke S. An overview of polylactides as packaging materials. Macromol Biosci 2004; 4: 835-864.

[50] Gupta AP, Kumar V. New emerging trends in synthetic biodegradable polymers – Polylactide: A critique. Eur Polym J 2007; 43: 4053-4074.

[51] Zhang J, Tashiro K, Domb AJ, Tsuji H. Confirmation of disorder form of poly(L-lactic acid) by the X-ray fiber pattern and polarized IR/Raman spectra measured for uniaxially-oriented samples. Macromol Symp 2006; 242: 274-278.

[52] Gazzano M, Focarete ML, Riekel C and Scandola M. Structural study of Poly (L-lactic acid) spherulites. Biomacromol 2004; 5: 553-558.

[53] Sarasua JR, Prud'homme RE, Wisniewski M, Le Borgne A and Spassky N. Crystallization and melting behavior of polylactides. Macromol 1998; 31(12): 3895-3905.

[54] Tsuji H and Ikada Y. Properties and morphologies of poly (L-lactide): 1. Annealing condition effects on properties and morphologies of poly (L-lactide). Polym 1995; 36(14): 2709-2716.

[55] Mano JF, Gómez Ribelles JL, Alves NM, Salmerón Sánchez M. Glass transition dynamics and structural relaxation of PLLA studied by DSC: Influence of crystallinity. Polym 2005; 46: 8258-8265.

[56] Sarasua JR, López Arraiza A, Balerdi P and Maiza I. Crystallinity and mechanical properties of optically pure polylactides and their blends. Polym Eng & Sci 2005; 45 745-753.

[57] Zuza Z, Ugartemendia JM, Lopez A, Meaurio E, Lejardi A, Sarasua JR. Glass transition behavior and dynamic fragility in polylactides containing mobile and rigid amorphous fractions. Polym 2008; 49: 4427-4432.

[58] Nozirov F, Nazirov A, Jurga S, Fu R. Molecular dynamics of poly(L-lactide) biopolymer studied by wide-line solid-state ^{1}H and ^{2}H NMR spectroscopy. Solid State Nucl Mag (2005) 258-266.

[59] Auras R, Lim LT, Selke SE and Tsuji H. Poly (Lactic Acid): Synthesis, structures, properties, processing, and applications. John Wiley & Sons, Inc. 2010; 25: 423-430.

[60] Tsuji H, Miyauchi S. Effects of crystallinity on enzymatic hydrolysis of poly(L-lactide) without free amorphous region. Polym Degrad Stab 2001; 71:415–424.

[61] Tokiwa Y, and Calabia BP. Biodegradability and biodegradation of poly(lactide). Appl Microbiol Biotechnol 2006; 72:244-251.

[62] Brown MS and Arnold CB. Fundamentals of laser-material interaction and application to multiscale surface modification. Laser Precision Microfabrication. Springer Series in Materials Science 135. Springer-Verlag Berlin Heidelberg. 2010; 4: 91-120.

[63] Bäuerle DW. Thermal, Photophysical, and Photochemical Processes. Laser Processing and Chemistry. Springer-Verlag Berlin Heidelberg. 2011; 1: 13-38.

[64] Liu X, Du D and Mourou G. Laser ablation and micromachining with ultrashort laser pulses. J Quant Elec 1997; 33(10): 1706-1716.

[65] Urech L and Lippert T. Photoablation of polymer materials. Photochemistry and Photophysics of Polymer Materials. Ed. Norman S Allen, John Willey & Sons, Inc. 2010; 14: 541-568.

[66] Luk'yanchuk B, Bityurin N, Anisimov S, Malyshev A, Arnold N and Bäuerle D. Photophysical ablation of organic polymers: the influence of stresses. Appl Surf Sci 1996; 106: 120-125.

[67] Zhigilei LV and Garrison BJ. Microscopic mechanisms of laser ablation of organic solids in the thermal and stress confinement irradiation regimes. J Appl Phys 2000; 88: 1281-1298.

[68] Tien AC, Backus S, Kapteyn H, Murnane M and Mourou G. Short-pulse laser damage in transparent materials as a function of pulse duration. Phys Rev Lett 1999; 82(19): 3883-3886.

[69] Machining with Long Pulse Lasers, Machining with Ultrafast Laser Pulses. 2011. Available from: http://www.cmxr.com/Education/Short.html, http://www.cmxr.com/Education/Long.html

[70] Srinivasan R and Mayne-Banton V. Self-developing photoetching of poly (ethylene terephthalate) films by far-ultraviolet excimer laser radiation. Appl Phys Lett 1982; 41(6): 576-578.

[71] Garrison BJ and Srinivasan R. Laser ablation of organic polymers: Microscopic models for photochemical and thermal processes. J Appl Phys 1985; 57(8): 2909-2914.

[72] Srinivasan R, Braren B and Casey KG. Ultraviolet laser ablation and decomposition of organic materials. Pure & Appl Chem 1990; 62(8): 1581-1584.

[73] Serafetinides AA; Skordoulis CD, Makropoulou MI and Kar AK. Picosecond and subpicosecond visible laser ablation of optically transparent polymers. Appl Surf Sci 1998; 135: 276-284.

[74] Serafetinides AA, Makropoulou MI, Skordoulis CD and Kar AK. Ultrashort pulsed laser ablation of polymers. Appl Surf Sci 2001; 180: 42-56.

[75] Castex MC and Bityurin N. is the VUV laser ablation of polymers a pure photochemical process? Appl Surf Sci 2002; 197-198: 805-807.

[76] Bityurin N and Malyshev A. Bulk photothermal model for laser ablation of polymers by nanosecond and subpicosecond pulses. J Appl Phys 2002; 92(1): 605-613.

[77] Yingling YG and Garrison BJ. Photochemical ablation of organic solids. Nucl Instrum Methods 2003; B202: 188-194.

[78] Gordon P, Balogh B and Sinkovics B. Thermal simulation of UV laser ablation of polyimide. Microelectron Reliab 2007; 47: 347-353.

[79] Conforti PF, Prasad M and Garrison BJ. Elucidating the thermal, chemical and mechanical mechanisms of ultraviolet ablation in poly (methyl methacrylate) via molecular dynamics simulations. Accounts Chem Res 2008; 41(8): 915-924.

[80] Prasad M, Conforti PF and Garrison BJ. Interplay between chemical, thermal, and mechanical processes occurring upon laser excitation of poly (methyl methacrylate) and its role in ablation. J Phys Chem C 2009; 113: 11491-11506.

[81] Baudach S, Bonse J, Krüger J and Kautek W. Ultrashort pulse laser ablation of polycarbonate and polymethylmethacrylate. Appl Surf Sci 2000; 154-155: 555-560.

[82] Pettit GH and Sauerbrey R. Pulsed ultraviolet laser ablation. Appl Phys A 1993; 53(1): 51-63.

[83] Liu JM. Simple technique for measurements of pulsed Gaussian-beam spot sizes. Opt Lett 1982; 7(5): 196-198.

Chapter 1. Laser ablation of a biodegradable synthetic polymer: effect of crystallinity of poly-L-lactide films on the material response.

1. Introduction

In the past few years, significant advances have been made in the development of biocompatible and biodegradable polymers for biomedical applications like tissue engineering [1], cell therapy [2], or clinical diagnostic [3]. Polylactides (PLA) have attracted considerable interest in biomedicine owing to their biodegradable nature and their versatility in terms of specific mechanical and thermal properties performance. Particularly, poly–L–lactide (PLLA) with different degrees of crystallinity has been investigated as scaffolds for nerve, vascular and cartilage tissue engineering [4-8]. The bulk mechanical and degradation properties of these materials may influence biological response and can be tuned by a proper choice of heat treatment conditions, leading to a change in their crystallization behaviour [9-11].

Several studies in cell biology reveal that most animal cells need to attach to a surface to survive, grow and proliferate [12]. In this context, specially designed biomaterials can act like temporal scaffolds inside the human body that mimic extracellular matrix structures and promote cell growth and organization into a specific architecture. Recent reports have shown that cell behaviour is strongly connected to the surface properties of the substrate material. This way, by changing the physicochemical properties of the substrate, it was possible to improve cell-material interactions such cell adhesion and proliferation. Moreover, these changes may affect the direction and accumulation of cells at a proper site or even may influence on cell phenotype [13-15]. This control over cells fate is especially important in case of stem cells, which research holds enormous potential for the treatment of human diseases. The design of biomaterials systems that mimic some aspects of natural cells microenvironments may be a powerful tool to better understand and manipulate cell function as a basis for future cell-based therapeutics. In this field, surface micro-structuring and micromachining techniques play an important role in the fabrication of three-dimensional scaffolds designed to mimic the *in vivo* microenvironment, such as cellular networks and structural organization that promotes tissue formation [16, 17].

As mentioned in the previous section, surface micro- and nano-patterning of polymers can be achieved through different techniques by chemical or physical methods. The most common techniques used for surface micropatterning are lithography based fabrication technologies and micro-contact printing (μCP) [18-21]. Soft lithography technology is frequently used to create a

surface pattern on a silicon wafer that can be easily replicated onto a polymeric material surface to form regular physical topographies like ridges, grooves, pillars and dots, but the average height of these features usually does not exceed 10 microns. Moreover, the versatility of this technique in terms of materials to pattern and application on 3D components is still limited, being generally restricted to patterning of flat substrates and small areas.

As mentioned before, pulsed laser ablation is well established as a universal tool for surface modification of polymers. Ultra-short laser pulses enable to obtain high precision 3-D microstructures, taking advantage of the “cold” ablation process. Ultrashort pulse laser irradiation can bring material into a highly non-equilibrium state and provides unique insights into material behaviour under extreme conditions that can hardly be achieved by any other method. This technology represents a very versatile method for 3D direct micro-structuring, covering a wide variety of substrates and geometries. Laser ablation is defined as the massive removal of material that results from photon absorption. This regime is characterised by the observation of large clusters of substrate in the plume, followed by crater formation. Melting mechanism depends on some other factors such as laser fluence and wavelength and this contribution does not completely vanish even at pulse duration lower than 10 ps [22, 23]. In the case of polymeric materials, the absorption of laser photon leads to electronic excitation, followed by intra- and intermolecular conversion of energy to heat and bond scission. Comparisons between experiments and molecular dynamics simulations suggest that this phenomenon occurs as a combination of two main mechanisms: photo-thermal and photo-chemical ablation [24, 25]. In the photo-thermal regime, the photon absorption is followed by rapid thermalisation, and ablation occurs due to explosive vaporisation of the substrate when a critical number of bonds are broken. In the photo-chemical ablation regime, however, energy deposition causes the electronic excitation leading to direct bond breaking. It is important to remark that high pressure/mechanical stresses may also play an important role on laser ablation, especially for pulse widths down to 15 ps. Hence, mechanical properties and material microstructure may play an important role on the onset of ablation. Other significant factors that affect the ablation process are laser parameters (wavelength, pulse duration, pulse energy) and material properties such as optical absorption and surface microstructure.

During the last decade, ablation of different polymers by means of laser irradiation of different characteristics has been reported [26-29]. Studies made by Serafetinides et al. [27] showed that picosecond laser is more efficient for laser ablation of transparent polymers than femtosecond and nanosecond laser. Laser irradiation effects on biopolymers (polyethylene glycol diacrylate, polystyrene, PLLA) have been extensively studied by means of excimer and pulsed lasers (femto- and nanosecond pulse duration) [30-35]. However, these studies were specifically focused on polymer surface modification and photo-polymerisation by laser irradiation. To the best of our knowledge, no previous study has examined the impact of crystallisation on biopolymer response when irradiated with picosecond lasers. Additionally, it is worth to note that laser ablation and microstructuring of PLLA with picosecond pulses and high repetition rates has not been previously reported.

The focus of the research reported in this chapter was on investigating the micromachining response of PLLA when performing structuring with ps pulsed laser operating at wavelength of 355 nm and 532nm. The effect of laser wavelength, pulse energy and material microstructure (crystallinity) were extensively analysed in order to identify the different factors affecting ablation efficiency and surface integrity. Single and multiple pulses ps – laser ablation was performed on PLLA with different degree of crystallinity. As in the case of other amorphous systems, it was expected a higher surface integrity to be achieved on the amorphous PLLA, because no crystalline structural features were present to facilitate the formation of micro – cracks during the laser ablation process.

2. Materials and Methods

2.1 Materials

Poly-L-lactide (PLLA) was supplied by Purac Biochem [36] (The Netherlands). PLLA pellets were previously dried at 40˚C for 24 h. PLLA films (degree of crystallinity X_c = 4%) of 50 microns thick were prepared by casting PLLA solution in Chloroform at a concentration of 2 wt %. After preparation, the films were dried at least 24h at 60˚C to ensure complete evaporation of the solvent. Crystalline PLLA films were obtained by annealing (1h at 120˚C) amorphous films. We

fabricated smooth, clear PLLA films of 33% and 49% degree of crystallinity. The characterisation of the films was done by Differential Scanning Calorimetry (Mettler Toledo DSC 1 Star^{e} System).

2.2 Laser ablation technique

For surface modification of the polymer samples we used the ps-laser system described in the previous section, integrated in a micromachining workstation (microSTRUCT^{vario}, 3D-Micromac AG, Germany). Sample position can be selected with lateral resolution in µm-range and a depth control of roughly 10 µm through a machining table with X/Y axes and Z positioning system.

It is important to point out that Polylactides show high transparency in the UV and visible range [37]. Laser ablation experiments were carried out on PLLA by changing laser parameter, such as speed, frequency and pulse energy. Craters were produced by single pulses, considering a frequency of 10 KHz (highest pulse energy) and scanning speed of 1000 mm/s. Energy ablation threshold is specific for each type of polymer, and its value may be linked with their microstructure properties, such as cohesive energy, absorption coefficient, degree of crystallinity, etc. In this chapter, we studied the effect of laser wavelength and material crystallinity on laser ablation threshold and surface integrity of PLLA films. Additionally, ablation rate for micromachined grooves was analysed in terms of pulse energy.

The material response on laser – machined regions was assessed using scanning electron microscopy SEM (Karl Zeiss XB1540), Focused Ion Beam processing (FIB, FEI Helios 600 Nanolab dual beam focused ion beam system), X-ray photoelectron spectroscopy (XPS, hemispherical analyser PHOIBOS 150 SPECS with 2D-DLD detector), and Fourier transform infrared (FTIR) spectroscopy (Vertex 70 with Hyperion IR microscope, Bruker). The information depths of these techniques are 10 nanometres (XPS) and 1 micrometre (FTIR), respectively. The crater depths and diameters were measured by mechanical stylus profilometry (Dektak 8, Veeco) [38].

3. Results

3.1. Laser ablation of amorphous PLLA.

A first series of experiments were focused on the determination of amorphous PLLA energy ablation threshold at wavelength of 532 nm. Figure 1.1 shows SEM images of single pulse craters produced in the nearly amorphous (X_c = 4%) PLLA sample by varying the pulse energy of the laser. Crater formation is observed when pulse energy is close to 25 µJ. The circular rim around the ablation zone suggests the onset of surface swelling prior to material ablation. This behaviour has been observed in other polymeric systems during laser irradiation [27]. At low pulse energy, the formation of gas bubbles in the deeper layers of the material may push the outer layers leading to surface swelling. When the pulse energy gets the ablation threshold, the gas bubble collapses producing crater formation.

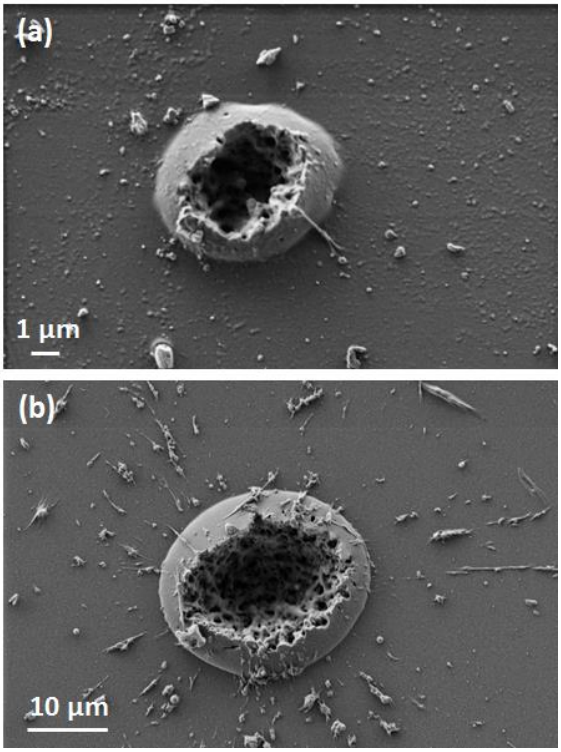

Figure 1.1. SEM images corresponding to single-shot craters at a wavelength of 532 nm for quasi-amorphous PLLA at different energies: E = 26 µJ (a); E = 51.6 µJ (b).

The diameter (D) and depth (d) of each crater was measured as a function of pulse energy (E) by SEM and profilometric evaluation. By fitting the experimental data to the equation (0.11) [39]:

$$D^2 = 2\omega_0^2 \ln\left(\frac{E}{E_{th}}\right)$$

We can obtain the spot size ω_0 (beam radius measured at 1/e^2), and the threshold energy E_{th} for crater formation. This energy is defined as the minimum energy where the onset of ablation can be observed.

As mentioned in the previous section, PLLA is a highly transparent polymer to UV-visible light. However, due to the high laser intensities achieved by picosecond pulsed laser, the transparent material could absorb the energy by nonlinear processes, such as avalanches and multiphoton absorptions. These effects are properly considered through an effective absorption coefficient that for weak absorbers is generally larger than the linear absorption coefficient [40]. According to the studies carried out by G. H. Pettit et al. [41], the effective absorption coefficient for a single-photon absorption process (α_{eff}) (at sufficiently small fluences) can be estimated from the equation (0.10):

$$d = \frac{1}{\alpha_{eff}} \ln\left(\frac{E}{E_{th}}\right)$$

However, this expression is not valid for multiphoton absorption processes. Thus, the α_{eff} values will give us information on the nature of the absorption mechanism of the polymer when picosecond pulsed with different wavelengths are considered.

Figure 1.2 (a) shows the D^2 measurements obtained by profilometry. The experimental data can be well fitted by equation (0.11). The values of the fit parameters ω_0 and E_{th} are 18 µm and 23.6 µJ, respectively. This energy value is very similar to that required for crater formation as observed by the SEM images presented in figure 1.1 (25 µJ).

Figure 1.2 (b) shows the profilometer measurements of the crater depth dependence on pulse energy. The experimental data can be well fitted by equation (0.10) in the energy range considered. Some deviations are observed at high energy values (E < 125 µJ), which have been observed by other

authors in different polymers [29-31, 42-45]. The value of the fit parameter E_{th} (≈ 3.5 μJ; α_{eff} = 0.42 μm^{-1}), is lower than the threshold observed by SEM characterisation and that obtained from the eq. (0.11) applied to the crater diameters.

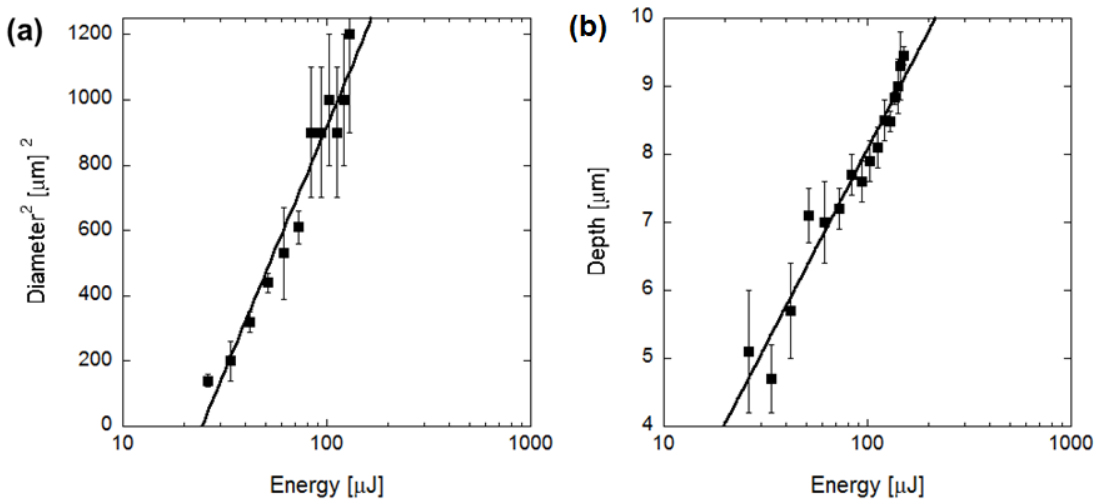

Figure 1.2. Data analysis of single pulse craters produce by 10 ps pulses at a wavelength of 532nm on amorphous PLLA. The graphs show the squared diameter of the craters measured by profilometry (a) and the etch depth per pulse (b) as a function of the pulse energy. Lines in figure 1.2 (a) and (b) indicate the fitting curves to equations (0.11) and (0.10), respectively.

In order to analyse the effect of laser wavelength on material ablation, laser irradiation experiment was conducted using a 355nm beam. Figure 3 shows the SEM images of single pulse craters produced in amorphous PLLA by varying laser pulse energy. It is important to note that the ablation mechanism at ʎ = 355 nm is different than that observed at ʎ = 532 nm (Figure 1.1). Figure 1.3 shows that the onset of ablation is observed at energies over 40 μJ and a peak of molten material appeared at the centre of the crater. The results shown that single pulse laser ablation of amorphous PLLA at this wavelength did not lead to the formation of a well-defined crater and, hence, the determination of energy threshold for ablation with one pulse was not possible.

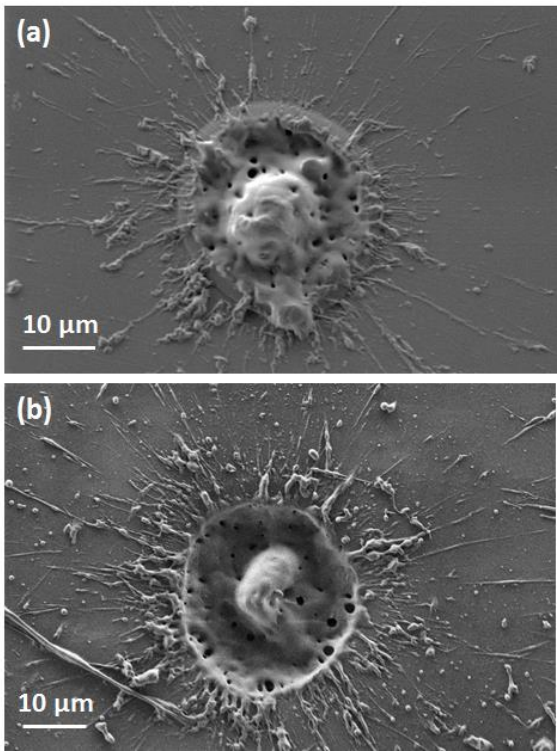

Figure 1.3. SEM images corresponding to single-shot craters at a wavelength of 355 nm for amorphous PLLA at different energies: (a) E = 42.0 µJ; (b) E = 66.7 µJ.

3.2. Laser ablation of PLLA with high degree of crystallinity

The effect of material microstructure on laser ablation behaviour was analysed considering two PLLA films with different crystallinity degrees (X_c = 33% and X_c = 49%). Figure 1.4 shows the SEM images of single pulse craters in both samples by varying the pulse energy of the laser at ƛ= 532 nm. In these cases, energy ablation threshold is smaller than that observed for amorphous PLLA. At energies of 20 µJ we do not observe any change in surface topography of amorphous PLLA, while this value leads to a crater formation in the case of crystalline samples. For PLLA of high degree of crystallinity (49%), ablation is observed at energies lower than 10 µJ. These results indicate that the energy at which crater formation is observed decreases with increasing the degree of crystallinity for semi-crystalline PLLA films.

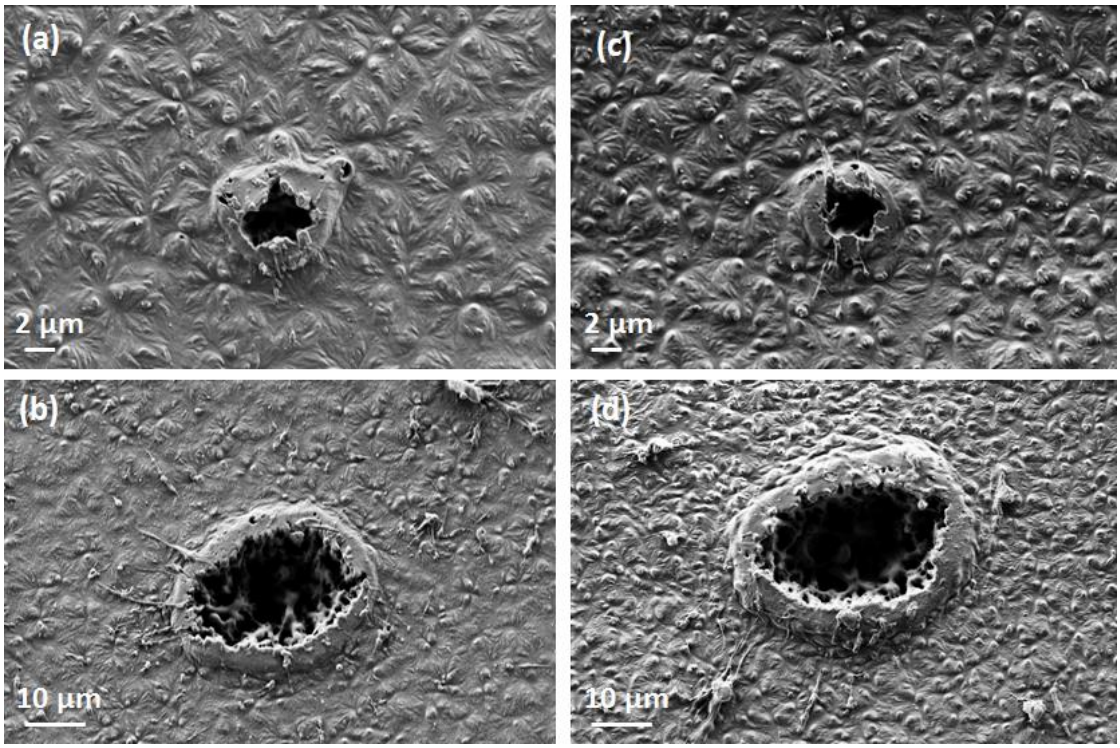

Figure 1.4. SEM images corresponding to single-shot craters at a wavelength of 532 nm for PLLA films of 33% (a, b) and 49% (c, d) crystallinity degree at different pulse energies: (a) E = 19.1 µJ, (b) E = 83.3 µJ, (c) E = 9 µJ, (d) E = 93.5 µJ.

The effect of laser wavelength on surface integrity was also analysed in the case of PLLA of high crystallinity degree (X_c = 49%). Figure 1.5 shows the SEM images of single pulse craters in this material at ʎ = 355 nm and two different energy values. Contrary to that observed in the case of amorphous PLLA, figure 1.5 shows no evidence of such a peak of molten material inside the crater. This fact allows one to measure craters diameters and depths, being able to obtain laser ablation threshold and effective absorption coefficient by fitting the experimental results to equations (0.11) and (0.10). According to the results presented in figure 1.6, for ʎ = 532 nm, lineal regime can be fitted to the data in the low (E < 59 µJ) energy region (Figure 1.6 (a)). In the case of ʎ = 355 nm, this low energy region is defined by the energy value E < 49 µJ (Figure 1.6 (b)). The fit parameter E_{th} is approximately 9 µJ for ʎ = 532 nm and 7 µJ for ʎ = 355 nm. It is important to note that, in the case of ʎ = 532 nm, this value is comparable to that obtained by fitting equation (0.10) to experimental data concerning to energy dependence of the crater depth *d* (E_{th} = 11 µJ, α_{eff} = 0.3 µm^{-1}: Figure 1.7). From this figure, it is clear that the fitting equation (0.10) encloses the experimental data generally well over the whole range of energies considered and, in the case of high crystalline PLLA, UV irradiation results in a

higher etch rate (open triangles in Figure 1.7). However, for this wavelength, the experimental data cannot be satisfactorily fitting using equation (0.10). From figures 1.4 to 1.7, it is clear that the values obtained by fitting the experimental data to equations (0.11) and (0.10) are in good agreement with the energies at which we observed surface modifications by SEM.

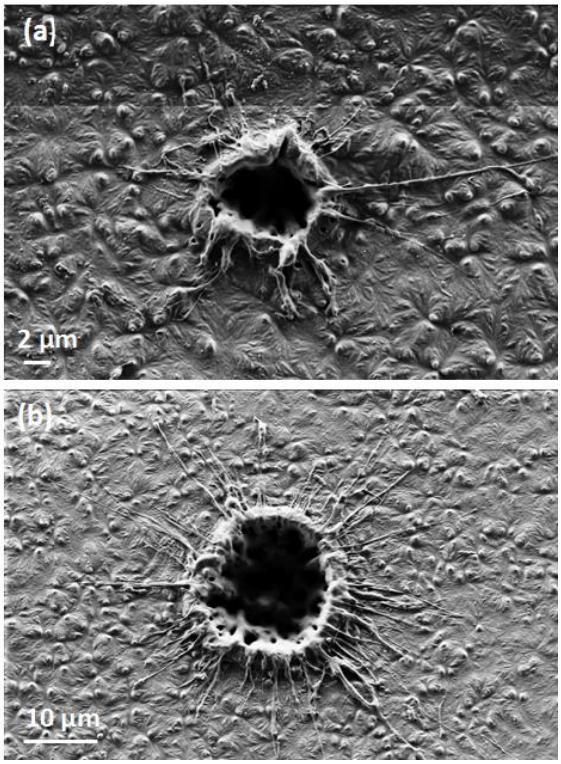

Figure 1.5. SEM images corresponding to single-shot craters at a wavelength of 355 nm for high crystalline PLLA at different energies: (a) E = 8.4 J; (b) E = 24.1 µJ.

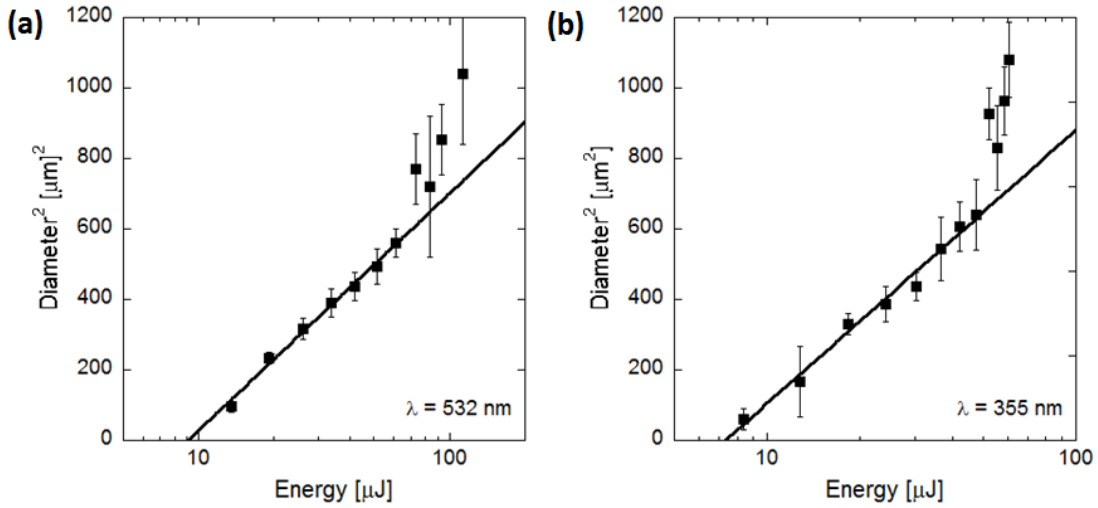

Figure 1.6. Crater square diameter as a function of the incident laser energy and wavelength (ʎ = 532 nm and 355 nm) for PLLA of high crystallinity degree (X_c = 49%). The solid lines represent the best fits according to equation (0.11).

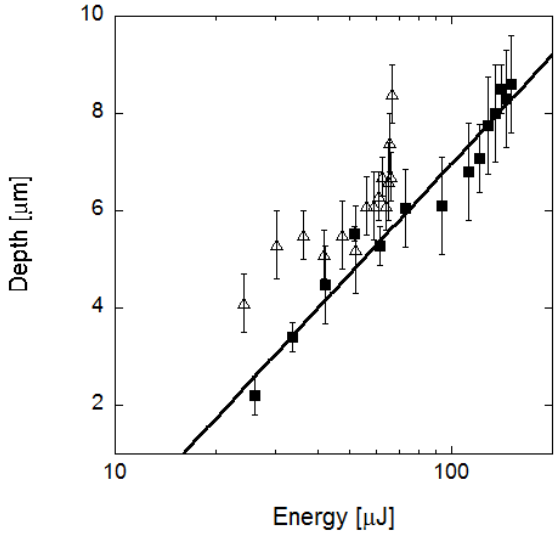

Figure 1.7: Ablation depth d as a function of the incident laser energy and wavelength for PLLA of high crystallinity degree (open triangles: ʎ= 355nm, closed squares: ʎ = 532nm). The solid line represents the best fit for the experimental data according to equation (0.10) (for ʎ = 532 nm).

3.3. Effects of pulses overlapping

In the process of groove micromachining, the sample is exposed to multiple pulses while being continuously translated at feed rate v. The effect of pulse energy and overlapping is analysed in terms of line dimensions and surface integrity by SEM analysis. Figure 1.8 shows a SEM image corresponding to grooves machined in amorphous PLLA by laser pulses at a wavelength of 355 nm and different pulse energy. Due to pulse overlapping, groove formation was observed at pulse energies (E = 2μJ) lower than those determined from the images showed in Figure 1.3. At higher pulse energies, the depth and width of the grooves became larger, improving inner surface quality (Figure 1.8 (b)). The bottom surface of the grooves is covered by micro-pores.

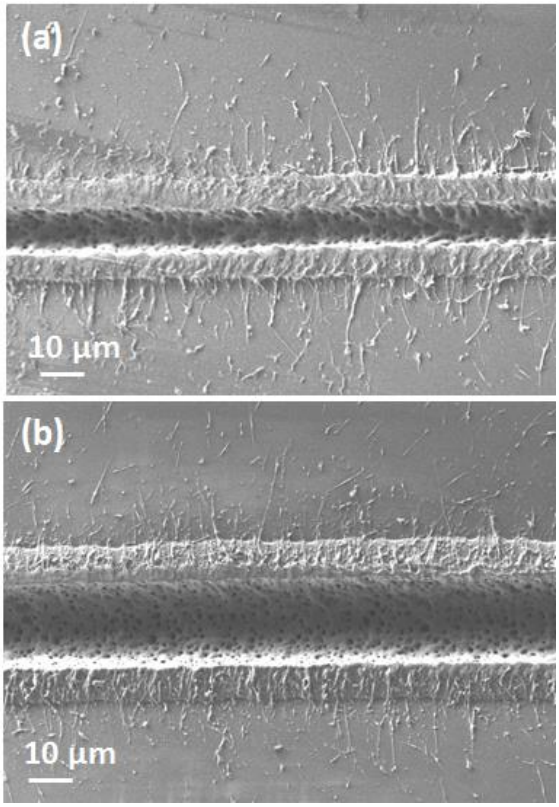

Figure 1.8. SEM images corresponding to grooves machined by laser pulse overlapping (σ_0 = 10 µm, f = 250 kHz, v = 600 mm/s) in PLLA at different pulse energy: (a) E = 6.04 µJ, (b) E = 14.44 µJ.

Figure 1.9 shows the effect of laser energy on dimensions of the groove in amorphous PLLA. It is important to note that saturation phenomena are observed at high energy values. This implies that energy values higher than a critical value (E = 7 µJ for recast layers, and E = 12 µJ for depth) do not lead to an increase in grooves depth and in the height of the recast layers.

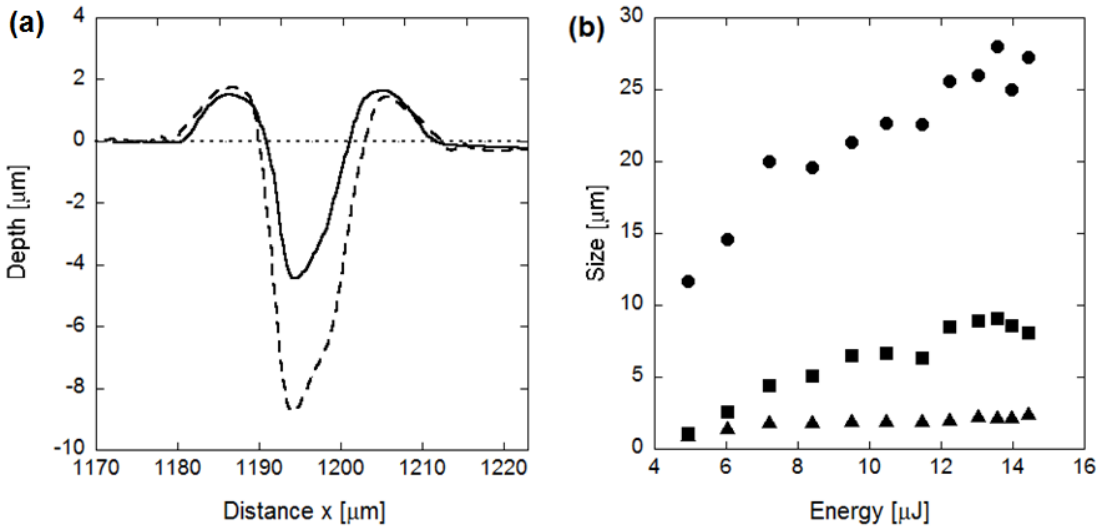

Figure 1.9. (a) Topographic profiles corresponding to the laser grooves (σ_0 = 10 μm, f = 250 kHz, v = 600 mm/s) at a wavelength of 355 nm and two different pulse energies (solid line: E = 7.2 μJ, dashed line: E = 12.2 μJ. The dotted line represents the level plane). (b) Evolution of line depth (squares), width (circles) and height of the recast layers (triangles) with increasing pulse energy.

3.4. Effect of laser irradiation on surface chemistry

As mentioned before, grooves machining by laser implies the overlapping of the laser pulses, increasing the energy deposited on the material, and, therefore, the material affectation. Grooves 17 micrometres wide and 4 micrometres deep (E = 6.5 μJ, Figure 1.9 (b)) were machined on amorphous PLLA with a period of 25 micrometres, filling an area of 40 mm x 3 mm. In these conditions the inter-groove spacing (*s*) was 8 micrometres. XPS is applied to obtain the carbon (C1s) and oxygen (O1s) spectra on the grooved area (Figure 1.10), considering a field of view of 1 mm x 20 mm, and analyse the effect of laser micromachining on the surface. Therefore, the XPS signal have the contributions from two different areas: grooves and not machined inter-groove spacing. Although this 8 μm-spacing was not under direct laser irradiation, it is otherwise modified because of the formation of recast material at grooves sides (Figure 1.9). In these conditions, the C:O ratio in the pristine (not machined) area (1.9) is higher than the stoichiometric ratio for PLLA (1.5), while the obtained C:O ratio on the grooved area is very similar to the expected value (1.56)(Table 1.1). The relative intensity of the C1s and O1s peaks, which correspond to the bonding energies of the C-O, C=O and O-C-=O functional

groups, underwent a minor but reproducible change on the grooved area respect to the pristine area (Figure 1.10). Atomic concentrations of carbon in the C-O and O-C=O functional groups are lower in the grooves, respect to the pristine area, while the atomic concentration of carbon in the C=O functional group is increased. These observed differences between pristine and grooved areas are not detected by FTIR measurements (Figure 1.11). FTIR spectra of both grooved and pristine areas show a sharp peak arising at 1748 cm^{-1} in the regime of carbonyl stretching. The appearance of this peak at lower wavenumber region than crystalline structure, and the weak shoulders arising next to the intense signals at 1177 cm^{-1} and 1085 cm^{-1}, assigned as asymmetric vibrations of C-CO-O and O-C-CO, respectively, [46] indicate that PLLA exists mainly as amorphous.

Table 1.1. C:O ratios (At%) in the pristine and grooved PLLA surfaces measured by XPS.

	Pristine area		Grooved area	
	C 1s	O 1s	C 1s	O 1s
Position	285.50	532.50	286.50	533.00
At %	65.61	34.39	60.94	39.06
C:O	1.9		1.56	

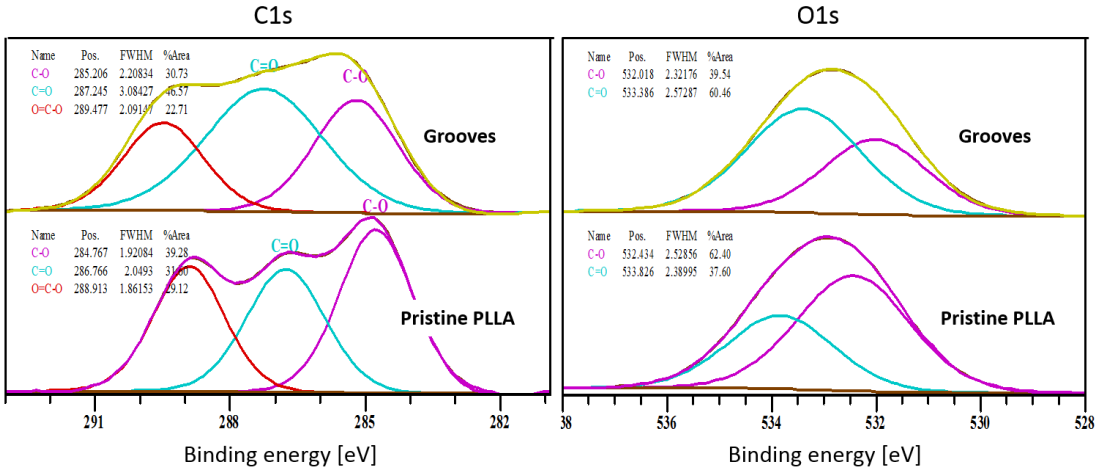

Figure 1.10. C1s and O1s spectra obtained by XPS on grooved and pristine areas of amorphous PLLA.

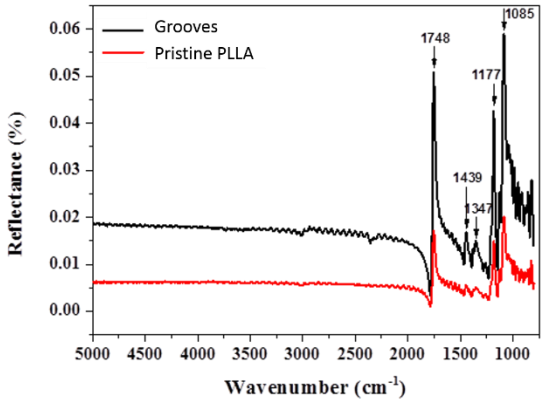

Figure 1.11. Infrared spectra of grooved and pristine areas of an amorphous PLLA film. Black and red lines represent spectra of grooved and pristine PLLA areas respectively.

3.5. Effect of laser irradiation on material structure.

In addition to surface chemistry, structural properties could be also affected as a consequence of the energy absorbed by the material under laser ablation, which, in the case of occurring via thermal effects (photothermal ablation), could produce crystallization, not only in the ablated area, but also in the surrounding material. In order to evaluate these eventual structural changes occurred on the laser ablated regions, single pulse craters produced in amorphous PLLA using the UV wavelength were considered. It is important to recall that the ablation mechanism via UV wavelength on amorphous PLLA is different than that observed at visible wavelength, showing a strong thermal behaviour characterized by a peak of molten material at the centre of the ablated crater (Figure 1.1 and 1.3). Cross-sections of non-ablated surface (pristine area) and craters were obtained by FIB and analysed by SEM (Figure 1.12). The material response to FIB is similar when considering pristine and crater areas, and not signs of crystallization (for instance, spherulite apparition) were observed on the material close to the ablated zone (Figure 1.12b-c). This is confirmed by the cross sections obtained on semi-crystalline PLLA (Figure 1.12d), where it is shown that the material response to FIB is different to that observed on amorphous PLLA.

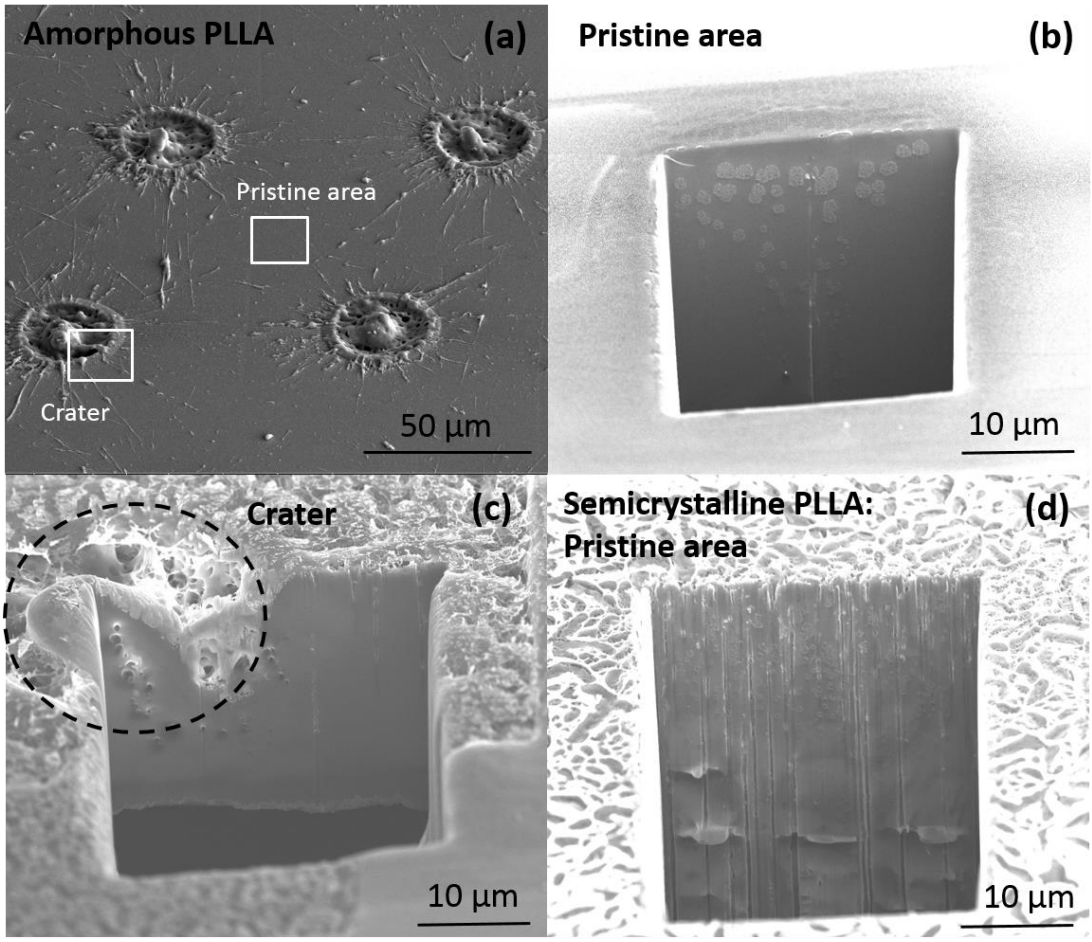

Figure 1.12. SEM images of craters produced by UV wavelength on amorphous PLLA (a), and cross sections obtained by FIB on the non-ablated area (pristine, (b)) and craters (c). These images are compared to the cross section obtained on pristine semi-crystalline PLLA film (d).

4. Discussion

As it is shown in Figure 1.2 (b), laser ablation of PLLA with 532 nm picosecond pulses is characterised by a logarithmic dependence of the etch depth per pulse on laser energy, satisfying the Lambert – Beer Law for single photon absorptions in the energy range considered. The effective absorption coefficient obtained by fitting the data to equation (0.11) is α_{eff} = 0.42 µm^{-1}. This value is significantly higher than the linear absorption coefficient obtained by means of UV – VIS spectroscopy (PLLA shows high transparency in the UV and visible range [37]) and lower than 1 µm^{-1}. According to the results presented by G. H. Pettit et al. [41] concerning to pulsed ultraviolet laser ablation of organic materials, values of the α_{eff} ≥ 1 µm^{-1} indicate significant single – photon absorption. The absorption

of laser photon leads to electronic excitation of the chromophore (C=O for PLLA), followed by intra- and intermolecular conversion to heat or bond scission. It is worth to note that single photon energy is insufficient for bond breaking (E_{bond} ≈ 8 eV for C=O) in the case of UV and visible radiation of PLLA. Thus, our results suggest that multiphoton effects play an important role in laser ablation of this polymer at both wavelengths. This result has been confirmed by theoretical models and experimental studies on ultrafast laser ablation of transparent polymers, connecting photochemical ablation by multiphoton absorption with the onset of nonlinear processes associated to the high energies achieved in the material [41, 45, 47-50]. These studies conclude that either multiphoton absorption and plume attenuation will increase the effective absorption coefficient, leading to the material ablation by a complex combination of photochemical and photothermal processes. From the experimental results presented in Figures 1.1 and 1.2, it is difficult to distinguish between photochemical and photothermal ablation mechanisms and the interplay among these processes as a function of the incident pulse energy. In general, it has been established that photothermal ablation causes high temperature, thermal degradation, melting and sublimation of the polymer, coupled with massive material ejection. The photochemical ablation process, however, is characterised by a clean cut, negligible thermal damage and ejection of gaseous fragments. Figure 1.1 and 1.3 show high – quality ablation craters for laser irradiation of amorphous PLLA with 532 nm pulses. Additionally, minimal spread of the ejected material from the crater is observed at this wavelength compared to the results obtained at ʎ = 355 nm (Figure 1.3). These results suggest that the laser ablation mechanisms of crater formation on PLLA irradiated by 355 nm and 532 nm pulses are different. These observed differences in the ablation mechanisms at two wavelengths would be related to changes in the absorption coefficient of the material and wavelength dependence of the photon energy. Figure 1.3 shows that UV single pulsed laser ablation of amorphous PLLA is characterised by a broad peak located at the centre of the crater. Various authors have observed a similar behaviour in metals and semiconductors exposed to nanosecond (ns) laser pulses [51, 52]. They correlated the final topography of the ablation crater with the hydrodynamic motion of molten material due to thermal and surface tension gradients or vapor pressure. According to molecular dynamics simulation (MDS) studies, photothermal mechanisms involved in laser ablation of polymer systems exhibit higher ablation threshold and surface temperature than that observed for photochemical (and photomechanical) processes [25]. As shown in Figure 1.1 and 1.3, the pulse energy required for UV – laser ablation of amorphous PLLA is higher than the

threshold at 532nm. These results would suggest that thermal mechanisms dominate in UV ablation of amorphous PLLA with ultrashort laser pulses. Unfortunately, for ʎ = 355 nm, determination of energy threshold for ablation and α_{eff} of PLLA with one pulse (and, hence, the photon density onto the target material) was not possible. Therefore, based on the results presented in Figures 1.1 and 1.3, it is difficult to elucidate the ablation mechanisms responsible for the differences observed between irradiation of PLLA with UV and visible laser pulses.

The analysis of the results presented in Figure 1.2 (a) indicates that the threshold energy and spot size values obtained from the fitting to the equation (0.11) (E_{th}= 24.2 μJ and σ_0 = 18 μm) were significantly higher than the energy value obtained using the Lambert – Beer law (E_{th} = 3.5 μJ) and the focal spot size at a certain pulse energy (σ_0 = 15 μm at E = 0.2 μJ). The reason for these differences in not completely understood. In previous laser ablation studies of polymers [27, 33, 53], Lambert Beer law equation was used for accurate determination of the energy threshold in the low energy regime, leading to lower energy threshold values than those required for crater formation. This result correlates well with our experimental data presented in Figures 1.1 and 1.3. The big dispersion shown by the crater depth values at low energies must be also affecting the energy threshold value obtained from the data shown in Figure 1.2 (b). Additionally, it is worth to note that the focal spot size depends on the incident pulse energy and, hence, it is difficult to establish a direct relationship between ω_0 and σ_0. A close inspection of Figure 1.2 (b) shows small deviations from the Lambert-Beer law of the etch depth per pulse at high energy values. These deviations have been already observed by other authors in a wide variety of polymer systems [29, 32, 42, 43]. Theoretical studies of UV ablation of organic materials attribute these deviations at high fluences to nonlinear effects such as chromophore saturation and multiphoton absorption processes [41]. Additionally, changes in material properties and pressure induced by material overheating at high laser fluences can preferably improve the etching rate [42].

Figures 1.1 and 1.4 show that laser irradiation with visible and UV wavelengths leads to a reduction in the pulse energy required to observe crater formation as the degree of crystallinity increases. According to the research carried out over the last few years in the field of MDS, ablation produced by ultrashort laser pulses (t<15ps) occurs in a stress confinement regime [24]. In this regime, photomechanical effects (tensile stresses) play an important role on the material removal process and

ablation is mainly produced by relaxation of a high thermoelastic pressure wave induced by laser irradiation. In this stress confinement irradiation regime, material ablation can be directly related to mechanical fractures that take place when stress exceeds the dynamic tensile strength of the material [24, 54]. In amorphous polymers, the packing heterogeneity characteristic of these systems, in terms of material microstructure, would lead to a broader distribution of the activation energy associated to their molecular dynamics [55]. Additionally, the cooperative nature of atomic motions leads to viscous flow behaviour of the system at high temperatures. These characteristics of amorphous polymers provide a better stress accommodation, and laser energy dissipation. In semi-crystalline polymers, however, cooperativity of chain motions is impeded by the higher degree of crystallinity. According to Sarasua et al. [9] the elongation at break behaviour and ductility of PLLA decreases with crystallinity. Consequently, as it is evident in Figure 1.1 and 1.4, the pulse energy required for material ejection in crystalline PLLA is lower than in the case of the amorphous one. Similar results were obtained for polymers with crystalline nanostructures and other amorphous systems such as metallic glasses [56-57]. In this scenario, photomechanical regime could be significantly higher than photothermal effects and, as it is shown in Figures 1.4 and 1.5, this regime may contribute to the material removal without forming a molten peak at the centre of the ablation crater. Although it is worth to note that the threshold energy value obtained from the fit to the Lambert – Beer Law is higher in the case of crystalline PLLA than that obtained for the amorphous one, it must be considered the big dispersion shown by the crater depth values at low energies, and it is influence on the energy threshold obtained from these data in the amorphous PLLA. This result indicates that the interplay between the mechanical and thermal properties of polycrystalline PLLA plays an important role in determination of the energy threshold value and crater morphology.

To our knowledge, only a few studies have analysed the wavelength dependence of the ablation threshold in polymers. Dumont et al. [29] observed a clear dependence of the ablation rate on the laser irradiation wavelength (from 193 to 308 nm), showing higher ablation rates for high absorption coefficients. However, the authors did not find any clear relationship between ablation threshold and absorption coefficient of the polymers studied. In addition, Raciukaitis et al. [44] found that the ablation threshold decreases gradually with increasing the effective absorption coefficient of a wide variety of polymers irradiated with picosecond pulses at two different laser wavelengths: 266 and 355 nm. They related this finding primarily to the less volume involved in the process when polymers with high

absorption coefficient are considered. Again, these results do not highlight any relationship between ablation threshold and laser wavelength. Serafetinides et al. [27] performed an experimental study focused on the ps – laser ablation process (τ = 100 ps) in three different transparent polymers subjected to radiation of wavelengths ranging from the visible to the infrared. The results of this study showed an increase in the etch rate for decreased laser wavelengths. On the other hand, several MDS studies predict an enhancement in the ablation yield when lower energy photons are used [25]. Therefore, for longer laser wavelength, a greater number of lower energy photons are absorbed and more photochemistry and material decomposition occur, which would result in a larger yield at low energy values. Although these results seem contradictory, it is important to note that the MD simulations considered a similar absorption coefficient and incident pulse energy values for both laser wavelengths, which are not the conditions under study in the Serafetinides report. Figure 1.7 shows that, when studying ablation of crystalline PLLA, as we decrease the laser wavelength from 532nm to 355 nm, the etch rate values increase over a wide range of pulse energy conditions. These results agree well with those presented by Serafetinedes et al. in different polymers. However, as already stressed above, the effective absorption coefficient of high crystalline PLLA at 355 nm is unknown. In such a situation, it becomes difficult to check the validity of the findings obtained by MDS concerning to the wavelength dependence of the etch rate in different organic materials.

Laser ablation of PLLA induced pore formation (diameter D_{pore}=500 nm – 1 µm) inside the crater and along the ablated grooves (Figure 1.8). This behaviour has been already observed in different polymer materials such as PMMA [43, 58] and PS [59]. Although its origins are not well understood, one possible explanation involves gas bubbles formation (and explosion) attributed to the chemical decomposition of the polymer during laser ablation. MDS studies show that, in the stress confinement regime, laser ablation proceeds through the void nucleation and growth, attributed to photomechanical effects [24-26]. In the thermal confinement regime, however, a severe heating followed by fast cooling is produced, and ablation involves formation of gas phase molecules and liquid droplets that might return on holes observed in the ablated zone. As it is shown in Figure 1.8, these effects became even more pronounced when using multiple overlapping laser pulses, that increase the thermal load. Paun et al. [58] observed that the pore density in PMMA zones irradiated with a femtosecond pulsed laser increases with increasing laser fluence, however, Figure 1.8 shows that both pore density and distribution inside the grooves machined on PLLA remain constant over the whole energy range

considered. The cross sections obtained by FIB of the craters produced by UV on amorphous PLLA (Figure 1.11) confirmed that this porosity must be produced by the laser ablation process, since no pores were observed in the cross-section on the non-ablated area of the film.

The C1s and O1s spectra obtained by XPS at grooves showed minor changes on the C:O ratio and the relative intensity of the C-O, O-C=O and C=O components respect to the not machined surface (Figure 1.10). The high C:O ratio measured on the not machined PLLA surface respect to the theoretical value has been already observed by other authors, which connect this finding to the sensitivity of obtained ratio to the take-off angle at which photoelectrons are recorded as well as the segregation of methyl groups at the surface [60,61]. The C:O ratio in the grooved area is very similar to the stochiometric ratio, indicating that no photo-oxidation occurred, as has been observed when femtosecond laser ablation is applied on PLA [62]. The minor changes found on the relative intensity of the above mentioned functional groups on the grooved area respect to the not modified area indicate a re-organization of these functional groups on the polymer surfaces. This could be a sign of photodecomposition, and therefore, of the photochemical nature of the ablation mechanism, at least in part. In addition, these surface changes were not observed by FTIR (Figure 1.11), indicating that only the topmost surface layer of the material (less than 10 nm) is affected by the laser and no bulk properties are modified. It is worth to note that no crystallization was detected neither by FTIR nor SEM analysis of FIB-obtained cross sections, and no structural changes were found on the material around the ablated area.

5. Conclusions.

In this chapter, we have reported experimental data corresponding to picosecond laser ablation of PLLA (surface morphology and ablation rate per pulse) as a function of laser fluence and degree of crystallinity. We conclude that multiphoton absorption mechanisms play an important role in UV and Visible laser ablation of amorphous and high crystalline PLLA: The etch depth dependence on the applied laser energy satisfied the Lambert – Beer Law with the effective absorption coefficient being less than 1 μm^{-1}. The interplay between laser material removal mechanisms involved in PLLA ablation (photochemical and photothermal) reflects some significant differences when material is irradiated with 355 and 532 nm pulses: While visible ablation leads to the formation of well-defined craters, single

pulsed UV laser ablation is characterised by a broad peak located at the centre of the crater. The hydrodynamic motion of molten material due to thermal and surface tension gradients could be correlated to this final topography of the ablation crater. Additionally, the onset of ablation is observed at pulse energies higher than those observed in the case of visible ablation. These results suggest that thermal mechanisms would dominate the UV-laser ablation of amorphous PLLA. The observed differences in the ablation mechanisms would be related to changes in the absorption coefficient of the material and wavelength dependence of the photon energy.

Laser irradiation with visible and UV wavelengths shows a reduction in the energy required for crater formation as the degree of crystallinity increases. The packing heterogeneity and larger viscous flow behaviour of amorphous PLLA could explain this reduction when laser ablation occurs in a stress confinement regime. Laser irradiation of crystalline PLLA at 355 and 532 nm shows very similar behaviour in terms of energy threshold required for crater formation. However, the etch rate increases with decreasing laser wavelength over a wide range of pulse energy conditions. These results reveal the importance of material microstructure in the ablation mechanisms that govern ultrafast laser processing of polymers. Further investigations covering MDS and theoretical studies will need to be made to establish the ablation mechanisms (and their interplay) to be consistent with the experimental results presented in this work, but these studies are far of the objectives of the present work.

In summary, the investigation shows that laser processing with picoseconds pulses is a promising technique for microstructuring biocompatible and biodegradable polymers. The machining of micro – scales features with high precision and minimal thermal impact (heat affected zone, recast layer) can be achieved on the material surface without affecting the bulk chemical or structural properties (as has been evidence by XPS and FTIR measurements), enabling high precision 3-D micromachining of scaffolds for biomedical applications.

References

[1] Seal BL, Otero TC, and Panitch A. Polymeric biomaterials for tissue and organ regeneration. Mater Sci Eng 2001; R34: 147-230.

[2] Kim MS, Hwang NS, Lee J, Kim TK, Leong K, Shamblott MJ, Gearhart J, and Elisseeff J. Musculoskeletal differentiation of cells derived from human embryonic germ cells. Stem Cells 2005; 23(1): 113-123.

[3] Wu P, Castner DG, and Grainger DW. Diagnostic devices as biomaterials: a review of nuclei acid and protein microarray surface performance issues. J Biomater Sci Polym Ed. 2008; 19(6): 725-753.

[4] Park A, and Griffith-Cima LG, J. Biomed. Mater. Res. 31, 117 (1996).

[5] Yang F, Murugan R, Ramkrishna S, Wang X, Ma YX and Wang S. fabrication of nano-structured porous PLLA scaffold intended for nerve tissue engineering. 2004; Biomaterials 25(10): 1891-900.

[6] Ma Z, Gao C, Gong Y, and Shen J. Cartilage tissue engineering PLLA scaffold with surface immobilized collagen and basic fibroblast growth factor. Biomaterials 2005; 26(11): 1253-9.

[7] Wang X, Song G, Lou T, and Peng W. Fabrication of nano-fibrous PLLA scaffold reinforced with chitosan fibers. J. Biomater Sci Polym 2009; 20(14): 1995-2002.

[8] Hu J, Sun X, Ma H, Xie C, Chen YE, and Ma PX. Porous nanofibrous PLLA scaffolds for vascular tissue engineering. Biomaterials 2010; 31(31): 7971-7.

[9] Sarasua JR, López Arraiza A, Balerdi P, and Maiza I. Crystallinity and mechanical properties of optically pure polylactides and their blends. Polym. Eng. Sci. 2005; 45(5): 745-753.

[10] Mano JF, Ribelles JLG, Alves NM, and Sánchez MS. Glass transition dynamics and structural relaxation of PLLA studied by DSC: Influence of crystallinity. Polymer 2005; 46(19) 8258-8265.

[11] Zuza E, Ugartemendia JM, Lopez A, Meaurio E, Lejardi A, and Sarasua JR. Glass transition behavior and dynamic fragility in polylactides containing mobile and rigid amorphous fractions. Polymer 2008; 49(20): 4427-4432.

[12] Freshney RI. Culture of animal cells: A manual of basic technique. Edited by Wiley-Liss 2000. New York.

[13] Ma Z, Mao Z, and Gao C. Surface modification and property analysis of biomedical polymers used for tissue engineering. Colloids Surf. B: Biointerfaces 2007; 60(2): 137-157.

[14] Hwang NS, Varghese S, and Elisseeff J. Controlled differentiation of stem cells. Adv Drug Delv Rev. 2007; 60(2): 199-214.

[15] Kilian KA, Bugarija B, Lahn BT, and Mrksich M. Geometric cues for directing the differentiation of mesenchymal stem cells. Proc Natl Acad Sci USA 2010; 107(11), 4872-4877.

[16] Hwang NS, Kim MS, Sampattavanich S, Baek JH, Zhang Z, and Elisseeff J. Effects of Three-Dimensional Culture and Growth Factors on the Chondrogenic Differentiation of Murine Embryonic Stem Cells. Stem Cells 2006; 24(2): 284-291.

[17] Liu H, and Roy K. Biomimetic Three-Dimensional Cultures Significantly Increase Hematopoitic Differentiation Efficacy of Embryonic Stem Cells. Tissue Eng. 2005; 11(1-2): 319-330.

[18] Chaubey A, Ross KJ, Leadbetter RM, and Burg KJL. Surface patterning: Tool to modulate stem cell differentiation in an adipose system. J Biomed. Mater. Res. B: Appl. Biomater. 2008; 84B(1): 70-78.

[19] Lee IC, Lee YT, Yu BY, Lai JY, and Young TH. The behaviour of mesenchymal stem cells on micrpatterned PLLA membranes. J. Biomed. Mater. Res. A. 2009; 91A(3), 929-938.

[20] Ruiz SA, and Chen CS. Microcontact printing: A toll to pattern. Soft Matter 2007; 3: 168-177.

[21] Ruiz SA, and Chen CS. Emergence of patterned stem cell differentiation within multicellular structures. Stem Cells Express 2008; 26(11): 2921-2927.

[22] Ivanov DS, and Zhigilei LV. Combined atomistic-continuum modelling of short-pulse laser melting and disintegration of metal films. Physical Review B 2003; 68(6): 064114.

[23] Lorazo P, Lewis LJ, and Meunier M. Thermodynamic pathways to melting, ablation, and solidification in absorbing solids under pulsed laser irradiation. Physical Review B 2006; 73(13): 134108.

[24] Zhigilei LV, and Garrison BJ. Microscopic mechanisms of laser ablation of organic solids in the thermal and stress confinement irradiation regimes. J. of Appl. Physics 2000; 88(3): 1281.

[25] Conforti PF, Prasad M, and Garrison BJ. Elucidating the thermal, chemical and mechanical mechanism of ultraviolet ablation in poly (methyl methacrylate) via molecular dynamics simulations. Accounts of Chemical Research 2008; 41(8): 915-924.

[26] Prasad M, Conforti PF, and Garrison BJ. Interplay between Chemical, Thermal, and Mechanical processes occurring upon laser excitation of poly (methyl methacrylate) and its role in ablation. J. Phys. Chem. C 2009; 113(27): 11491-11506.

[27] Serafetinides AA, Makropoulou MI, Skordoulis CD, and Kar AK. Ultra-short pulsed laser ablation of polymers. Appl. Surf. Sci. 2001; 180(1-2): 42-56.

[28] John SR, Langford SC, and Dickinson JT. Ablation mechanism of PTFE under 157 nm irradiation. Appl. Phys. A 2008; 92(4): 981-985.

[29] Dumont Th, Bischofberger R, Lippert T, and Wokaun A. Gravimetric and profilometric measurements of the ablation rates of photosensitive polymers at different wavelengths. Appl. Surf. Sci. 2005; 247(1-4): 115-122.

[30] Semaltianos NG, Koidis C, Pitsalidis C, Karagiannidis P, Logothetidis S, Perrie W, Liu D, Edwardson SP, Fearon F, Potter RJ, Dearden G, and Watkins KG. Picosecond laser patterning of PEDOT: PSS thin films. Synthetic Metals 2010; 161(5-6): 431-439.

[31] Ovsianikov A, Malinauskas M, Schlie S, Chichkov B, Gittard S, Narayan R, Löbler M, Sternberg K, Schmitz KP, and Haverich A. Three-dimensional laser micro- and nano-structuring of acrylated poly (ethylene glycol) materials and evaluation of their cytotoxicity for tissue engineering applications. Acta Biomaterialia 2011; 7(3): 967-974.

[32] Pfleging W, Torge M, Bruns M, Trouillet V, Welle A, and Wilson S. Laser- and UV-assisted modification of polystyrene surfaces for control of protein adsorption and cell adhesion. Appl. Surf. Sci. 2009; 255(10): 5453-5457.

[33] Pfleging W, Adamietz R, Brückner HJ, Bruns M, and Welle A. Laser-assisted modification of polymers for microfluidic, micro-optics, and cell culture applications. Proc. SPIE 6459, 2007; 645907.

[34] Rytlewski P, and Zenkiewicz M. Laser-induced surface modification of polystyrene. Appl. Surf. Sci 2009; 256(3): 857-861.

[35] Ma Z, Gao C, and Shen J. Surface modification of poly-L-lactic acid (PLLA) membrane by grafting acrylamide: and effective way to improve cytocompatibility for chondrocytes. J Biomater Sci Polym 2003; 14(1): 13-25.

[36] http://www.purac.com/

[37] Auras R, Harte B, and Selke S. An overview of polylactides as packaging materials. Macromol. Biosci. 2004; 4(9): 835-864.

[38] http://www.veeco.com/

[39] Liu JM. Simple technique for measurements of pulsed Gaussian-beam spot sizes. Optics Letters 1982; 7(5): 196-198.

[40] Kautek W, and Kruger J. Femtosecond-pulse laser microstructuring of semiconducting materials. Materials Science Forum 1995; 173-174: 17-22.

[41] Pettit GH, and Sauerbrey R. Pulsed ultraviolet laser ablation. Appl. Phys. A 1993; 56(1): 51-63.

[42] Gordon P, Balogh B, and Sinkovics B. Thermal simulation of UV laser ablation of polyimide. Microelectron. Reliab. 2007; 47(2-3): 347-353.

[43] Gómez D, and Goenaga I. On the incubation effect on two thermoplastics when irradiated with ultrashort laser pulses: Broadening effects when machining microchannels. Appl. Surf. Sci. 2006; 253(4): 2230-2236.

[44] Raciukaitis G, and Gedvilas M. Processing of polymers by UV picosecond lasers. EKSPLA Application Note No. AN0912IL02. http://ekspla.com/

[45] Sauerbrey R, and Pettit GH. Theory for the etching of organic materials by ultraviolet laser pulses. Appl. Phys. Lett. 1989; 55(5): 421-423.

[46] Meaurio E, Lopez-Rodriguez N, and Sarasua JR. Infrared spectrum of poly(L-lactide): application to crystallinity studies. Macromol 2006; 39(26): 9291-9301.

[47] Srinivasan R, Sutcliffe E, and Braren B. Ablation and etching of polymethylmethacrylate by very short (160 fs) ultraviolet (308 nm) laser pulses. Appl. Phys. Lett. 1987; 51(16): 1285-1287.

[48] Küper S and Stuke M. Ablation of polytetrafluoroethylene (Teflon) with femtosecond UV excimer laser pulses. Appl. Phys. Lett. 1989; 54(1): 4-6.

[49] Serafetinides AA, Skordoulis CD, Makropoulou MI, and Kar AK. Picosecond and subpicosecond visible laser ablation of optically transparent polymers. Appl. Surface Sci. 1998; 135(1-4): 276-284.

[50] Srinivasan R, Braren B, and Dreyfus RW. Ultraviolet laser ablation of polyimide films. J. Appl. Phys. 1987; 61(1): 372-376.

[51] Borowiec A, Tiedje HF, and Haugen HK. Wavelength dependence of the single pulse femtosecond laser ablation threshold of indium phosphide in the 400-2050 nm range. Appl. Surf. Sci. 2005; 243(1-4): 129-137.

[52] Bennett TD, Krajnovich DJ, Grigoropoulos CP, Baumgart P, and Tam AC. Maragoni Mechanism in Pulsed Laser Texturing Magnetic Disk Substrates. J. of Heat Transfer 1997; 119(3): 589-596.

[53] Obata K, Sugioka K, and Midorikawa K. F_2 Laser ablation of UV Transparent Polymer Material. J Laser Micro Nanoeng 2006; 1(1): 28-32.

[54] Dekel E, Eliezer S, Henis Z, Moshe E, Ludmirsky A, and Goldberg IB. Spallation model for the high strain rates range. J. Appl. Phys. 1998; 84(9): 4851-4859.

[55] Collective Dynamics of Nonlinear and Disordered Systems, edited by G. Radons, W. Just, P. Häussler (Springer, 2005)

[56] Quintana I, Dobrev T, Aranzabe A, Lalev G, and Dimov S. Investigation of amorphous and crystalline Ni alloys response to machining with micro-second and pico-second lasers. Appl. Surf. Sci. 2009; 255(13-14): 6641-6646.

[57] Niino H, Ihlemann J, Ono S, and Yabe A. Surface microstructure formation by ns-, ps-, and fs-laser ablation of an elastomer composite. J. Photopolym. Sci. Tech. 2000; 13(1): 167-173.

[58] Paun IA, Selimis A, Bounos G, Kecskeméti G, and Georgiou S. Nanosecond and femtosecond UV laser ablation of polymers: Influence of molecular weight. Appl. Surf. Sci.2009; 255(24): 9856-9860.

[59] Rebollar E, Bounos G, Selimis A, Castillejo M, and Georgiou S. Examination of the influence of molecular weight on polymer laser ablation: polystyrene at 248 nm. Appl. Phys. A 2008; 92: 1043-1046.

[60] Paragkumar NT, Edith D, and Six JL. Surface characteristics of PLA and PLGA films. App Surf Sci 2006; 253(5): 2758e64.

[61] Stepak BD, Antonczak AJ, Szustakiewicz K, Koziol PE, and Abramski KM. Degradation of poly(L-lactide) under KrF excimer laser treatment. Polym Degrad Stabil 2014; 110: 156-164.

[62] Jia W, Luo Y, Yu J, Liu B, Hu M, Chai L, and Wang C. Effects of high-repetition-rate femtosecond laser micromachining on the physical and chemical properties of polylactide (PLA). Opt Express 2015; 23(21): 26932-9.

Chapter 2. In vitro analysis of medical polymeric surfaces microstructured by ps-laser ablation technology: effect of pattern geometry and topographical cues on breast cancer cell proliferation.

1. Introduction

As mentioned in previous chapters, most animal cells are not viable in suspension and require to attach to a surface for surviving, growing and proliferating; in other words, they are anchorage-dependent [1]. Recent reports have shown that cell behaviour is strongly dependent on the surface properties of the substrate material, such as the topology, the charge, the degree of hydrophobicity or hydrophilicity and other mechanical or chemical properties [2-7]. Thus, by changing the physicochemical properties of the substrate, cell-material interactions can be modified and hence influence cell adhesion, migration and proliferation. Among the biomaterial properties that affect cell behaviour, the substrate mechanics has a particular strong effect upon cell fate [8-10]. Cells in vivo are subjected to mechanical forces (i.e. tensile or compressive) through the extracellular matrix (ECM). Under these conditions, the cellular cytoskeleton suffers stress changes that affect cellular shape. These morphological changes may affect the direction and accumulation of cells at a proper site or even influence cell phenotype [11-13]. Some of the cellular processes that can be controlled by physical interactions between cells and their ECM or microenvironment (growth, differentiation, motility, apoptosis) are critical for cancer development [14-16]. Several researchers have observed that cancer epithelial cells revert to normal behaviour (healthy cells) when they are in contact with the ECM of an embryonic tissue [17-19]. In this context, surface microstructuring and micromanufacturing techniques can be a useful tool for the investigation of the influence of the cell microenvironment in the behaviour of cancer cells and tumour growth.

As previously highlighted, surface modification by laser technologies is a promising technique for scaffold microstructuring. Liu et al. [20] applied for the first time the ultra-short pulsed laser technique for this purpose. They used a femtosecond pulsed laser to obtain microstructured collagen substrates (holes, grooves and grids), and analysed the growth, adhesion and viability of human fibroblast and mesenchymal stem cells from rat bone marrow on the patterns. Only five subsequent reports have applied laser ablation by femtosecond laser for the 3D microstructuring of biocompatible materials for cell seeding [21-25]. The purpose of the experiments performed in this chapter is to evaluate the picosecond pulsed laser ablation technology (much faster than femtosecond pulsed laser ablation technology) applied to the fabrication of three-dimensional

scaffolds aimed for cell engineering. To the best of our knowledge, no other reports exist on the application of picoseconds pulsed laser ablation in the study of the effect of topographical cues on cell proliferation. We examined the effect of the laser-created topography on cell behaviour by observing proliferation and adhesion of breast cancer cells on different laser structures on poly-L-lactide (PLLA) [26,27] and polystyrene (PS, a biocompatible polymer frequently used in the fabrication of devices for cell culture applications) [28]. It is worth noting that PLLA has been investigated for many years as scaffold for tissue engineering [29-34] showing morphological, mechanical and degradation properties that make this material very suitable for such purpose. Likewise, we examined the influence of the topography in cell morphology when cells were cultured in confined environments.

2. Materials and Methods

2.1. Materials

Poly-L-lactide (PLLA) was supplied by Purac Biochem (The Netherlands) [35]. PLLA pellets were dried at 40˚C for 24 h and dissolved in chloroform at a concentration of 2 wt%. PLLA films were prepared by casting the PLLA solution on glass Petri dishes. After preparation, the films were dried at least 24 h at 60˚C to ensure complete evaporation of the solvent. Under these conditions, films of 50 μm thickness were obtained. The degree of crystallinity of these films was 4% as measured by differential scanning calorimetry. Polystyrene (PS) Petri dishes for cell culture were manufactured by SARSTEDT (Germany).

2.2. Surface microstructuring technique

Surface microstructuring of polymer samples was carried out by means of a ps-laser system. A detailed description of the characteristics of this laser system can be found in previous section (Introduction and Chapter 1). By means of pulse overlapping different trenches can be fabricated. Trench width and depth were controlled by selecting an appropriate energy (E), frequency (f) and pulse distance (d_p). By using a galvanometric scanner and appropriate control strategies, any

desired topography and geometry can be generated on the workpiece. The optimization of the microstructuring process for PLLA was described in chapter 1. Flat PLLA substrates (Ra = 240 nm, water contact angle of 70˚ ± 5˚) and PS Petri dishes (Ra = 20 nm, water contact angle of 80˚ ± 5˚) were laser-irradiated by UV wavelength (355 nm) applying an energy of 0.9 µJ at a frequency of 100 kHz, and 5 µm of pulse distance. These laser parameters are different from those applied in Chapter 1 to obtain grooves on amorphous PLLA (Figures 1.8 and 1.9), since, in this case, the aim is to increase the surface roughness without generating well-defined grooves. Therefore, after the treatment, the average surface roughness (Ra) increased, leading to values of 700 nm and 500 nm for PLLA and PS Petri dishes, respectively (Figure 2.1) and both material surfaces become slightly more hydrophobic (water contact angles of 90˚ ± 5˚). Microgrooves of different width (*w*) and depth (d) were obtained on PS Petri dishes. Laser-micromachining of PS to generate well-defined microgrooves implied the application of pulse energies (from 1 µJ to 12 µJ) and pulse distance (d_p= 2 µm) similar to those applied on PLLA, but at a frequency lower (*f* = 100 kHz) than that applied on chapter 1. Microgrooves were also produced on PLLA by applying an energy of 6 µJ at a frequency of 250 kHz, and a pulse distance of 2.4 µm (Figure 1.9). Squared micro-compartments of 500 µm of width and 40 µm deep were fabricated by overlapping grooves with energy of 0.5 µJ, at a frequency of 250 kHz, and 2 µm of distance between grooves. Dimensions (*w* and d) of the different laser-generated topographies were measured by a mechanical stylus profilometer (Dektak 8, Veeco) [36]. According to DIN EN ISO 4288:1998, samples profiles of 4 mm length were considered in the measurement of the average surface roughness (Ra).

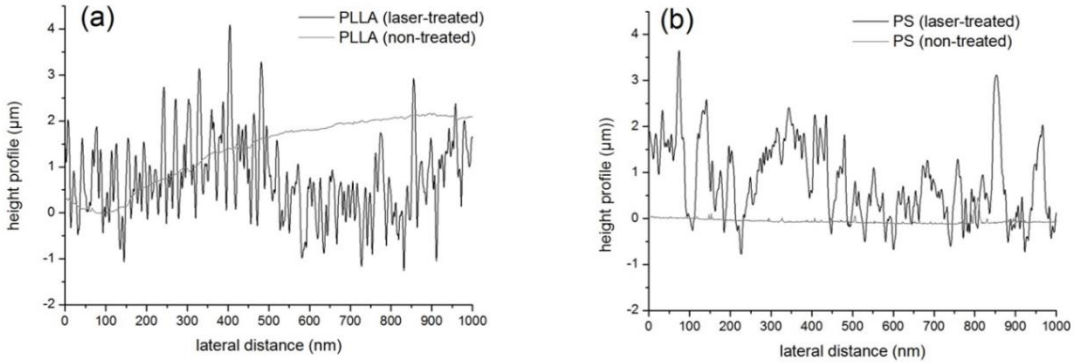

Figure 2.1. Surface profiles of PLLA substrates (a) and PS Petri dishes (b) before and after laser treatment.

2.3. Cell culture

For evaluation of the compatibility and the influence of laser microstructured materials on cell behaviour we used MCF-7 cells and MDA-MB-231 cells. The MCF-7 cell line is a model of estrogen receptor (ER)-positive breast cancer, which accounts for about 70% of breast tumours. MDA-MB-231 cells are ER-negative breast cancer cells. Both cell lines were genetically modified to express the fluorescent GFP protein (GFP MCF-7 [37]), and cultured in Dulbecco's modified Eagle's medium (DMEM, Sigma) supplemented with 9% Fetal Bovine Serum (Sigma-Aldrich Co. USA), 2% L-glutamine, and 0.5% penicillin/streptomycin (Gibco-RBL Life Technologies, Paisley, UK). Prior to cell culture, PLLA films were placed in Petri dishes, which were first disinfected with 70% ethanol and then UV-sterilized for 30 minutes. Drops of cell suspension at a concentration of 150 cells/µL were deposited on the patterned substrates in cell culture medium by means of a micro-pipette. After cell seeding, the samples were kept in the cell incubator at 37˚C and 5% CO_2 and the media was changed three-times a week. Cell proliferation was observed as a function of time with an inverted fluorescence microscope equipped with a cell incubator (Carl Zeiss Cell Axio Observer, Germany [38]). The visualization of the stained cells on PS and PLLA substrates was impaired in some cases by the light scattered by the laser-treated regions due to the increase in surface roughness produced by this technology.

2.4. Statistics

Fluorescence microscopy images were processed using ImageJ software to obtain the fraction of area covered with cells, and single cell or cell cluster sizes from at least three selected areas of 1344 x1024 pixels. Cell counting was carried out on at least ten different areas of the substrate of 1280 x1024 pixels. All data were expressed as means ± standard deviation. Statistical analysis was carried out using the Student's t-test and the values are considered significantly different when $p<0.05$.

3. Results

3.1 Effect of roughness on cell proliferation

Surface microstructuring by laser irradiation modifies the initial surface roughness of the substrate. Therefore, we first analysed the effect of that surface roughness modification on cell adhesion and proliferation. Amorphous PLLA substrates and PS Petri dishes were laser-irradiated on half of their total area. Figure 2.2 shows MCF-7 cells cultured on laser-treated and non-treated PS (Figure 2.2a), and PLLA (Figure 2.2b-c), after two incubation days. The results did not show a significant preference for cells to adhere and proliferate on laser-treated areas compared to non-treated areas on both PS and PLLA. Figure 2.2d shows the percentage of area covered by cells for each type of substrate. This chart represents the average value of the fraction of area covered by cells, which was calculated from several images of different zones of the substrate for the same period. The values obtained on laser-treated and non-treated zones were very similar in the case of PLLA (approximately around (65 ± 10) % of area covered by cells). For PS, only slight differences were observed when non-treated and treated areas were considered ((70 ± 10) % on non-treated PS and (55 ± 10) % on treated PS). Therefore, laser irradiation did not significantly affect cell adhesion and proliferation of the cells (according to Student's t-test).

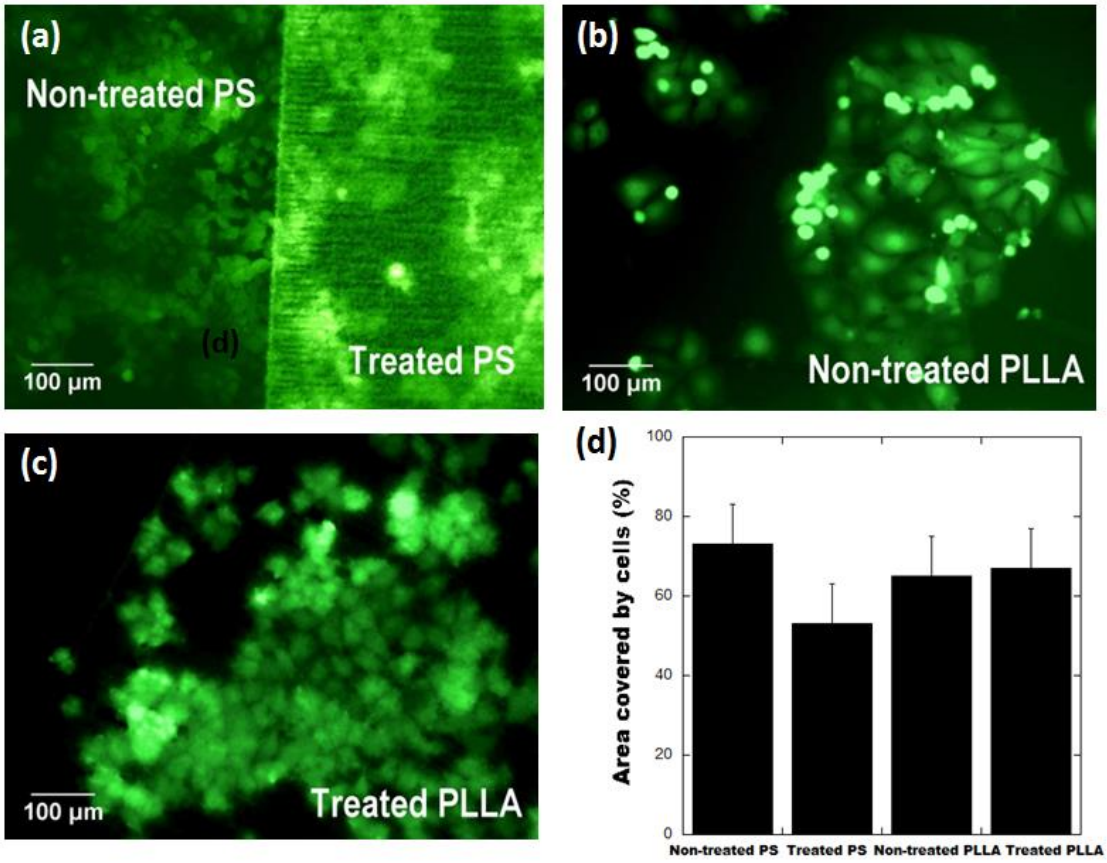

Figure 2.2. Fluorescence microscopy images of MCF-7 cells proliferating on non-treated and treated PS Petri dishes (a) and films of PLLA (b, c) after two days of incubation. (d) Bar-chart of the fraction of area covered by cells on treated and non-treated zones of PS and PLLA substrates. According to the Student's t-test there were no significant differences. Images were treated by ImageJ to highlight cell morphology (green colour).

3.2. Effect of substrate topography on cell proliferation and orientation

3.2.1. MFC-7 cells: low-invasive cells.

In order to analyse the effect of a defined topography on cell proliferation and morphology, an array of parallel grooves of variable width, depth and inter-groove spacing (*s*) was patterned in both substrate materials. Figure 2.3a-e shows MCF-7 cell clusters growing on non-patterned and laser-patterned PS after twelve days of incubation. On non-patterned PS, cell clusters underwent isotropic growth, leading to circular-shaped clusters (Figure 2.3a). On patterned PS, however, cell clusters underwent a noticeable elongation along the groove direction and the growth was thus

anisotropic leading to elliptical-shaped clusters. The effect of pattern geometry and density over the cell cluster growth and orientation is shown in Figure 2.3b-e. The ratio of the major (parallel to groove direction, a) and minor (perpendicular to groove direction, b) axes of the elliptical-shaped clusters is represented (Figure 2.3f) and it will be referred to as shape ratio (a/b) from now on (Figure 2.3g). The laser ablation technique applied for groove generation does not allow us to distinguish between the effects of groove width and depth separately, since an increase of the laser energy leads to the simultaneous increase of groove width and depth. In these experiments, the w:d ratio of the grooves increased in a 40%, while w increased in more than 200%: therefore, we considered w as the groove representative parameter and represented the cell cluster shape for a range of w:s ratios. This representation quantifies the cell cluster elongation along the grooves. On non-patterned PS the cell cluster shape was approximately round, thus the shape ratio approaches 1. On patterned PS, the shape ratio was larger, reaching a maximum for the 15 µm-wide grooves and 6 µm-spacing. When the values of the width and the spacing increase the cell cluster elongation is still evident. According to these results, the effect of surface topography on cell cluster elongation becomes more evident when pattern density increases, and parallel grooves with widths comparable to the cell size (20 ± 5) µm are considered.

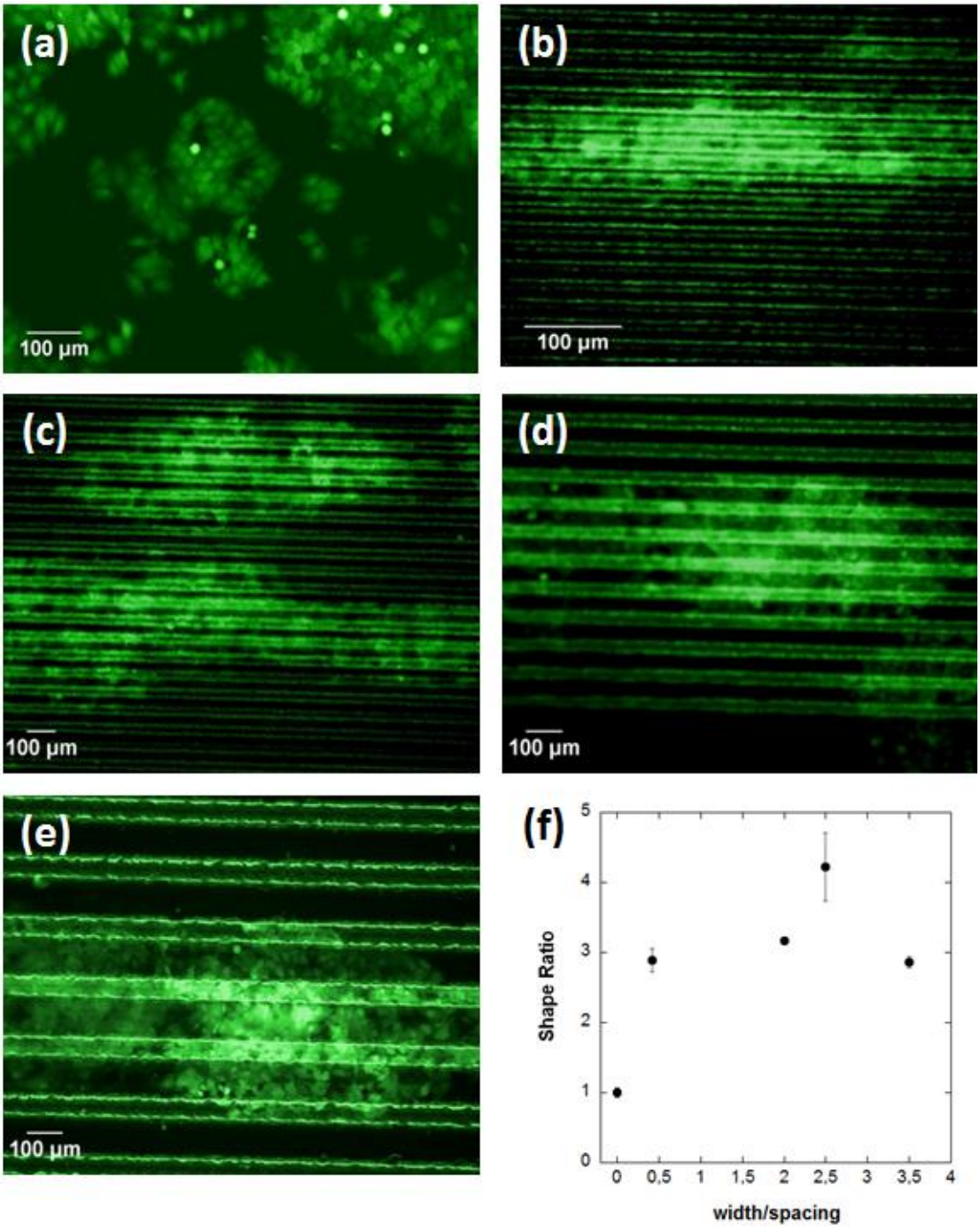
(a)
100 µm
(b)
100 µm
(c)
100 µm
(d)
100 µm
(e)
100 µm
(f)
Shape Ratio
width/spacing
0
1
2
3
4
5
0
0,5
1
1,5
2
2,5
3
3,5
4

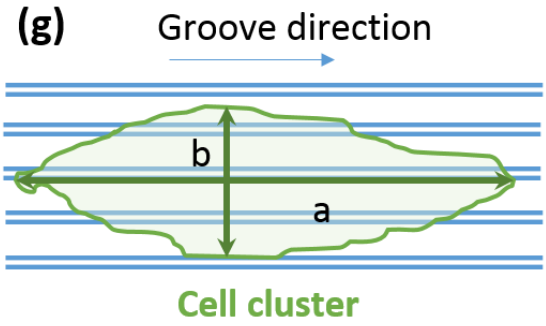
(g)
Groove direction
b
a
Cell cluster

Figure 2.3. Fluorescence microscopy images of MCF-7 cells proliferation on non-patterned PS (a) and patterned PS with grooves of variable w, s and d: (b) w = 15 µm, s = 6 µm, d = 3 µm; (c) w = 35 µm, s = 10 µm, d = 5 µm; (d) w = 40 µm, s = 20 µm, d = 6 µm; (e) w = 50 µm, s = 120 µm, d = 10 µm. (f) Representation of the shape ratio of the elliptical cell clusters growing over lines of different widths and spacing in comparison to the circular cell clusters growing in non-patterned PS. Images were treated by ImageJ to highlight cell morphology (green colour).

Figure 2.4 shows the time evolution of cell proliferation on patterned PS substrates considering the pattern configuration that induces a maximum shape ratio in cell clusters (w = 15 µm, s = 6 µm) with different directions. After three days, 87% of the cells that adhered to the substrate proliferated along the grooves. Figure 2.4a shows that some cells were more fluorescent than others, which could likely be due to changes on cell shape induced by the topography or it may represent cells at different stages of the cell cycle. We observed that cell clusters remained elongated along the grooves after 12 or even 14 days of incubation (Figure 2.4d-f). When cell population was very high, nearby cell clusters merged and the elongation effect was suppressed (Figure 2.4e). However, the shape ratio of the cell clusters remained approximately constant over the whole incubation period (Figure 2.4g).

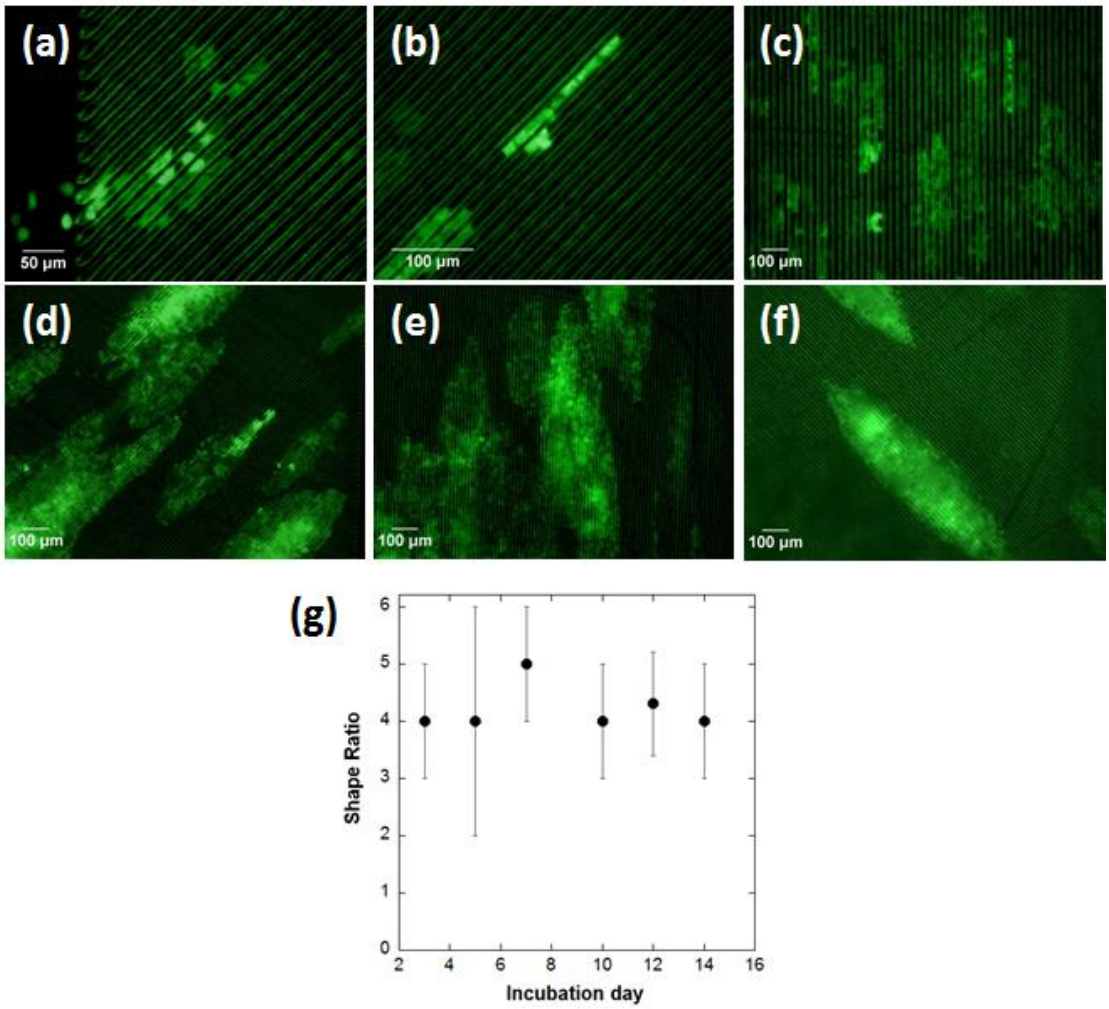

Figure 2.4. Fluorescence microscopy images of MCF-7 cells proliferating over patterned PS for 3 (a), 5 (b), and (c), 12 (d) and (e), and 14 (f) incubation days. (g) Shape ratio of the elliptical cell clusters growing for two weeks over grooves of different direction like a function of incubation time. According to the Student's t-test there were no significant differences. Images were treated by ImageJ to highlight cell morphology (green colour)

Time-lapse micrographs such as those represented in Figure 2.4a-f can be used to estimate the growth rate of cell clusters on patterned surfaces. As shown in Figure 2.4a, on non-treated PS, cell clusters grew almost isotropically. Growth speed of cell clusters was estimated by measuring the radial axis of circular cell clusters and the major and minor axes of elliptical cell clusters on non-patterned and patterned PS, respectively, for different time lapses. Measurement of circular-cluster size on non-patterned PS revealed an average radial growth speed of (7 ± 0.7) µm h^{-1}. On patterned PS, however, cell clusters grew at a rate of (2.5 ± 0.5) µm h^{-1} along the laser grooves, and at rate of (1 ± 0.4) µm h^{-1} along the perpendicular direction. Cell proliferation is hindered when

compared to the rate on non-patterned PS. Figure 2.5 shows a cell cluster over a non-patterned area of PS that has reached the patterned area after 2.5 incubation days. As highlighted before, when a cell cluster reaches the grooves, it tends to align along the groove direction, showing an elongated shape.

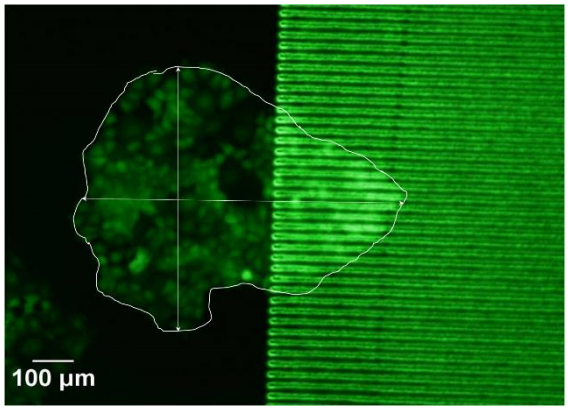

Figure 2.5. Fluorescence microscopy image of a cell cluster on PS growing homogeneously and reaching the patterned area. Images were treated by ImageJ to highlight cell morphology (green colour).

Next, the effect of surface topography on cellular proliferation for PLLA substrates was examined (Figure 2.6) considering the same pattern configuration applied on PS to maximize the shape ratio of the elliptical cell clusters. Cells proliferating on grooves 15 µm wide showed a similar cluster elongation as that observed in PS substrates (Figure 2.6a-c). Most of the cells spread within the grooves, suggesting a strong effect of the topography on cell morphology. As in the case of PS, the shape ratio of the cell clusters remained approximately constant on PLLA (Figure 2.6d). MCF-7 clusters showed anisotropic growth and thus, cell cluster elongation was also clearly noticeable on patterned PLLA.

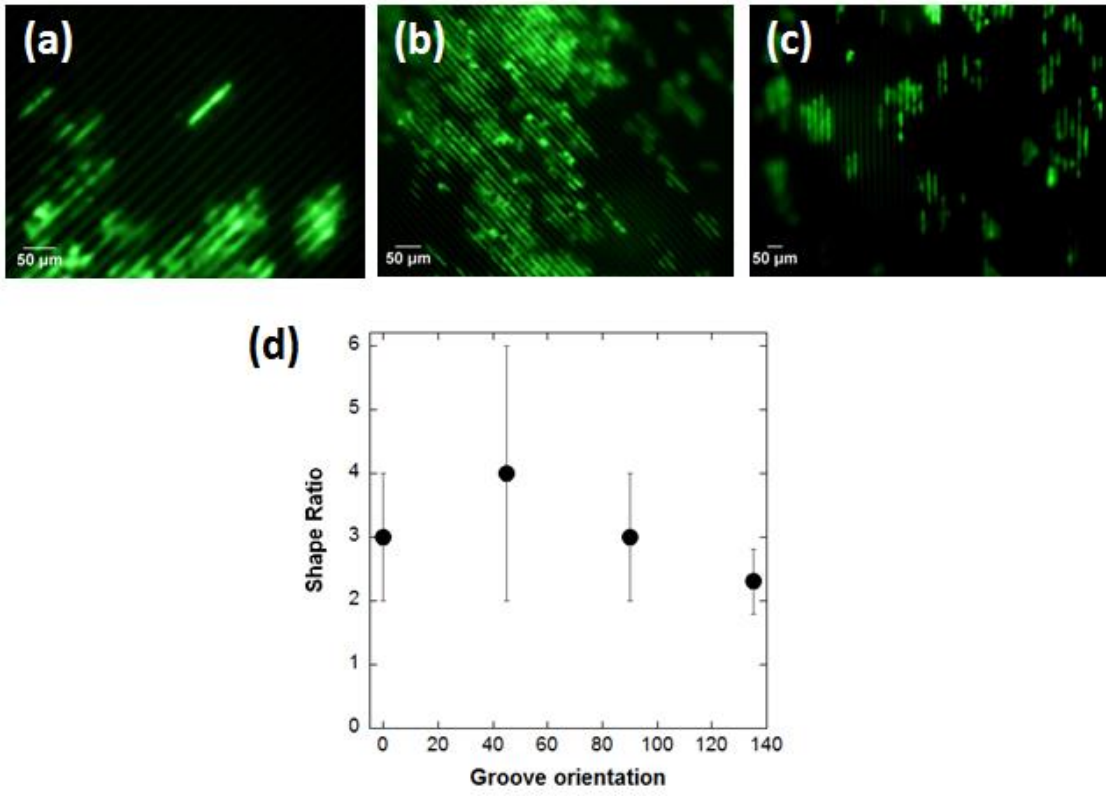

Figure 2.6. Fluorescence microscopy images of MCF-7 cells proliferating after 5 incubation days on patterned PLLA (w = 15 µm, d = 3 µm, s = 6 µm) at different directions (a-c). Shape ratio of the elliptical cell clusters growing for 5 incubation days on lines of different direction like a function of groove direction (d). Images were treated by ImageJ to highlight cell morphology (green colour).

3.2.2. MDA-MB-231 cells: high-invasive cells.

Proliferation and orientation of MDA-MB-231 cells (more invasive than MCF-7 cells) on patterned PS petri dishes was also examined for comparison of ER-negative and ER-positive breast cancer (MCF-7 cells) to determine whether patterns affect in the same way the growth of both breast cancer types. Figure 2.7a-b show that unlike the MCF-7 line, these cells did not proliferate in clusters and orientation along groove direction occurred in this case at cellular level. Figure 2.7c shows SEM images of MDA-MB-231 cells fixed on non-patterned and patterned PS: on non-patterned PS, cells showed randomly spread over the surface, however, on patterned PS cells (white arrows) were elongated and confined inside grooves and in the inter-groove spacing, where the groove edges formed by the recast material act as a barrier for the cells. White particles, which were likely remains from the growth medium, were observed all over the surface. Approximately (81 ± 7) % of cells were elongated along the groove direction, both inside and outside grooves (Figure 2.7d).

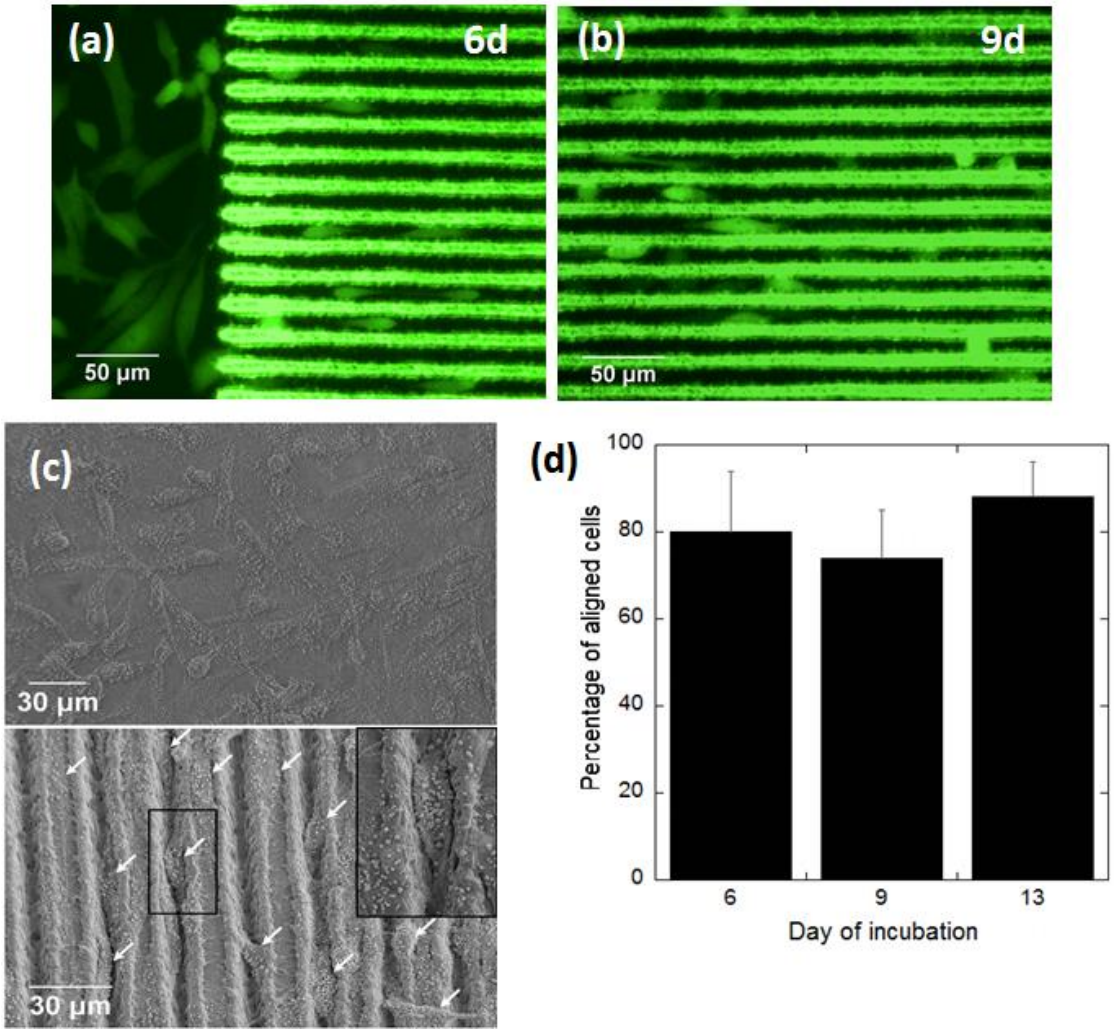

*Figure 2.7. Fluorescence microscopy images of GFP-MDA-MB-231 cells proliferating after 6 (a), and 9 (b) incubation days on patterned PS Petri dishes (w = 15 µm, d = 3 µm, s = 6 µm). SEM images of cells proliferating on non-patterned and patterned PS after 13 incubation days (c). Percentage of cells aligned on non-patterned and patterned PS after 9 incubation days (d) *** Significance level: p < 0.001 according to Student's t-test. Images were treated by ImageJ to highlight cell morphology (green colour).*

3.3. Effect of three-dimensional (3D) structures on cell proliferation and confinement

In order to analyse the impact that confinement has on cancer cells proliferation, MCF-7 cells were cultured on PS with laser-machined microcompartments of area 500 μm^2 and depth 40 µm linked by a channel 100 µm wide (Figure 2.8a). Cell proliferation was periodically monitored inside the compartments during two weeks (Figure 2.8b-f). In this time period, cells remained confined within the compartment for eleven days, until the compartment was completely filled (100% confluence). Between the eleventh and the thirteenth days of incubation individual cells could be observed around the compartment (Figure 2.8f, white arrows): since cells were only seeded in the compartments, the observed cells must have escaped from inside the compartment.

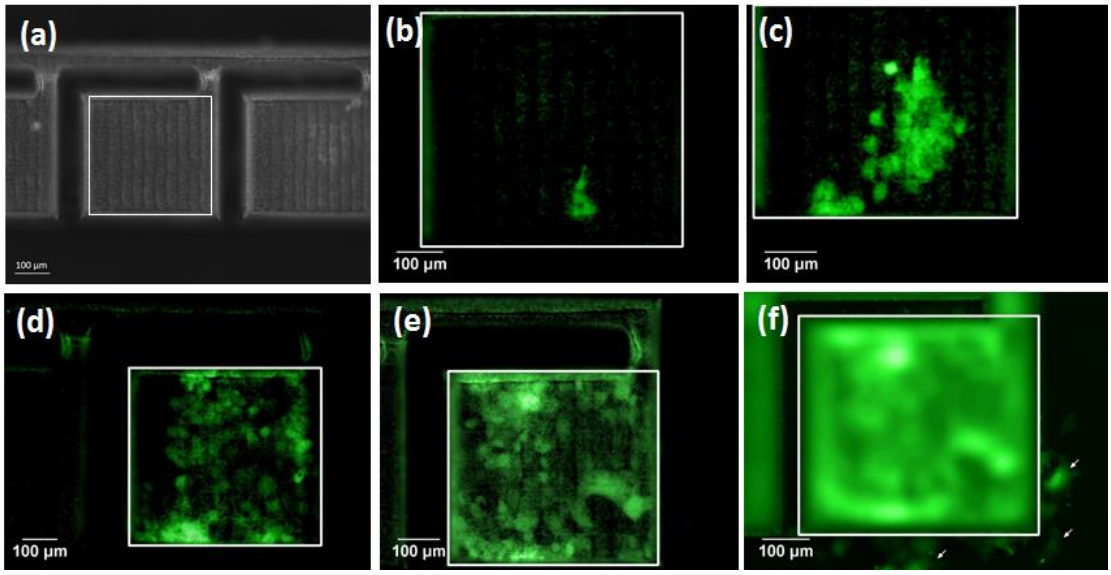

Figure 2.8. Images obtained by fluorescence microscopy of MCF-7 cells adhered to the bottom of a square compartment (a) at 3 (b), 7 (c), 11 (d) and 13 (e, f) incubation days. The photograph (e) shows the bottom of the square compartment in focus, and photograph (f) shows cells outside the square (focus on the plane outside the square) (white arrows). Images (b-f) were treated by ImageJ to highlight cell morphology (green colour).

4. Discussion

As reported in Section 3, the surface roughness modification induced by the laser treatment on PS and PLLA substrates did not show any alteration on cellular proliferation of breast cancer MCF-7 cells. Hence, picosecond pulsed laser machining can be used to produce different topographies for cell seeding without any apparent side effect over cell morphology and proliferation. According to these results, modification of the surface roughness by means of ultra-short pulsed laser would not suppose a drawback in terms of cell culture applications. Contrary to these findings, Pfleging et al. [3] reported that in the case of L929 cells proliferating on PS, cell adhesion was affected by laser irradiation (Excimer laser, 193 nm), finding an optimal range of laser energies at which cell adhesion was improved by changing the surface chemical properties of the material. In our case, the wettability of the surface is similar before and after laser irradiation, and no further chemical changes seem to be induced by the laser on the surface.

When growing on PS and PLLA patterned substrates by picosecond pulsed laser irradiation, MCF-7 cell proliferation on high density patterns of parallel grooves of single-cell width (15 µm wide, 3 µm deep) occurs preferentially along the grooves. Therefore, anisotropic expansion of cell clusters along the groove direction was directly related to changes on surface topography by laser machining. This phenomenon is called “contact guidance effect” when single cells are considered [39]. Our findings agree well with the orientation phenomena observed by many previous researchers for a variety of cell types and substrates [5, 12, 40-48], although cell response seems to be dependent on cell type. It is worth noting that the elongation effect observed in the present work for MCF-7 cells is linked to cell clusters (contact guidance effect occurred at supra-cellular scale), instead of single cells as it is observed for MDA-MB-231 cells. In addition, our experiments confirm that physical constraints play an important role in cell expansion: Cell clusters grow easier and faster along the grooves, where cells do not find physical barriers. Cells proliferating perpendicularly to the groove direction, however, must overcome edges of nearly 1 µm and depths of 3 µm (higher than the laser-induced roughness on treated surfaces), leading to a substantial slowdown of the cell replication rate along that direction. To the best of our knowledge, this is the first reported evidence of such phenomenon. But, certainly related, it is the work of Irimia et al. [49], who found that motility of human cancer cells (MDA-MB-

231) is enhanced along microchannels with cross-sections comparable to the cell size. Hence, cell confinement not only favours motility of more invasive cancer cells (MDA-MB-231), but according to our findings it also promotes cell proliferation along microchannels of less invasive breast cancer cells (MCF-7).

The effect of physical confinement on MCF-7 cell proliferation was explored in a square area of approximately 500 μm^2 and depth of about 40 µm. We found that cell clusters on non-patterned PS grew at 7 µm h^{-1} in all directions. Assuming that the cell cluster inside the square grows at this velocity, it would reach the edge in two to three days. However, we found that the cell cluster stayed for eleven days inside the 40 µm deep box. The presence of cells outside the compartments after this period indicates that cell proliferation was not restricted by the edges. Hence, these cells could overcome the 40 µm barrier, suggesting a high adaptability to topographical features. According to this, other authors [50-52] have presented similar findings, reporting the ability of high invasive MDA-MB-231 breast cancer cells in adapting their shape to the sidewalls of physical micro-features regardless of their form (star or circular-shaped).

5. Conclusions

In this chapter, we have applied ultra-short laser technology to produce microstructured surfaces on PS and PLLA that influence on breast cancer cell elongation or confinement. Contact guidance effect on a supracellular scale is observed when MCF-7 cells proliferate on groove-patterned substrates, while contact guidance effect on a cellular scale is observed when MDA-MB-231 cells are considered. MCF-7 cell growth is slowed down both on patterns and in the squared compartments, in which time of cell confinement increases from 3 to 11 days compared to the unconstrained case (non-patterned substrate). These findings show that laser micromachining with ultra-short laser pulses is a very suitable tool to create different 3D microstructures and, thus, analyse the effect of the cell microenvironment on the behaviour of cancer cells and tumour growth *in vitro*. Furthermore, our observations confirm that further examination of the potential applications of microstructuring by laser technologies in biomedicine is warranted.

References

[1] Melzak KA, Moreno-Flores S, Vivanco MdM, and Toca-Herrera JL. Mechanical Cues for Cell Culture. Handbook on Biofunctional Surfaces. Ed. W Knoll, Pan Stanford Publishing 2013; 25: 865-897.

[2] Walboomers XF, Croes HJE, Ginsel LA, and Jansen JA. Growth behavior of fibroblasts on microgrooved polystyrene. Biomaterials 1998; 19(20): 1861-1868.

[3] Pfleging W, Bruns M, Welle A, and Wilson S. Laser-assisted modification of polystyrene surfaces for cell culture applications. Appl Surf Sci 2007; 253(23): 9177–9184.

[4] Ito Y. Surface micropatterning to regulate cell functions. Biomaterials 1999; 20(23-24): 2333-2342.

[5] Liliensiek SJ, Campbell S, Nealey PF, and Murphy CJ. The scale of substratum topographic features modulates proliferation of corneal epithelial cells and corneal fibroblasts. J Biomed Mater Res A 2006; 79(1): 185-192.

[6] Dike LE, Chen CS, Mrksich M, Tien J, Whitesides GM, and Ingber DE. Geometric control of switching between growth, apoptosis, and differentiation during angiogenesis using micropatterned substrates. In vitro Cell Dev Biol Anim 1999; 35(8): 441-448.

[7] Guan Y and Kisaalita W. Cell adhesion and locomotion on microwell-structured glass substrates. Coll Surf B: Biointer 2011; 84(1): 35-43.

[8] Chen CS, Tan J, and Tien J. Mechanotransduction at cell-matrix and cell-cell contacts. Annu. Rev. Biomed. Eng. 2004; 6: 275-302.

[9] Ghosh K and Ingber DE. Micromechanical control of cell and tissue development: Implications for tissue engineering. Adv Drug Deliv Rev 2007; 59(13): 1306-1318.

[10] Galbraith CG and Sheetz MP. Forces on adhesive contacts affect cell function. Curr Opin Cell Biol 1998; 10(5): 566-571.

[11] Kumar G, Chen B, Co CC, and Ho CC. Differential migration and proliferation of geometrical ensembles of cell clusters. Exp Cell Res 2011; 317(10): 1340-1352.

[12] Matsuzaka K, Walboomers XF, Ruijter JE, and Jansen JA. The effect of poly-L-lactic acid with parallel surface micro groove on osteoblast-like cells in vitro. Biomaterials 1999; 20(14): 1293-1301.

[13] Kilian KA, Bugarija B, Lahn BT, and Mrksich M. Geometric cues for directing the differentiation of mesenchymal stem cells. Proc Nat l Acad Sci USA 2010; 107(11): 4872-4877.

[14] Paszek MJ, Zahir N, Johnson KR, Lakins JN, Rozanberg GI, Gefen A, Reinhart-King CA, Margulies SS, Dembo M, Boettiger D, Hammer DA, and Weaver VM. Tensional homeostasis and the malignant phenotype. Cancer Cell 2005; 8(3): 241-254.

[15] Huang S and Ingber DE. Cell tension, matrix mechanics, and cancer development. Cancer Cell 2005; 8(3): 175-176.

[16] Suresh S. Biomechanics and biophysics of cancer cells. Acta Materialia 2007; 55(12): 3989-4014.

[17] Petersen OW, Rønnov-Jessen L, Howlett AR, and Bissell MJ. Interaction with basement membrane serves to rapidly distinguish growth and differentiation pattern of normal and malignant human breast epithelial cells. Proc Natl Acad Sci U.S.A. 1992; 89(19): 9064-9068.

[18] Hendrix MJC, Seftor EA, Seftor REB, Kasemeier-Kulesa J, Kulesa PM, and Postovit LM. Reprogramming metastatic tumour cells with embryonic microenvironments. Nat Rev Cancer 2007; 7: 246-255.

[19] Ingber DE. Can cancer be reversed by engineering the tumor microenvironment? Semin Cancer Biol 2008; 18(5): 356-364.

[20] Liu Y, Sun S, Singha S, Cho MR, and Gordon RJ. 3D femtosecond laser patterning of collagen for directed cell attachment. Biomaterials 2005; 26(22): 4597-4605.

[21] Yeong WY, Yu H, Lim KP, Ng KLG, Boey YCF, Subbu VS, and Tan LP. Multiscale topological guidance for cell alignment via direct laser writing on biodegradable polymer. Tissue Eng Part C: Methods 2010; 16(5): 1011–21.

[22] Lee CH, Lim YC, Farson DF, Powell HM, and Lannutti JJ. Vascular Wall Engineering Via Femtosecond Laser Ablation: Scaffolds with Self-Containing Smooth Muscle Cell Populations. Ann Biomed Eng 2011; 39: 3031-3041.

[23] Lee BLP, Jeon H, Wang A, Yan Z, Yu J, Grigoropoulos C, and Li S. Femtosecond laser ablation enhances cell infiltration into three-dimensional electrospun scaffolds. Acta Biomaterialia 2012; 8(7): 2648-2658.

[24] Li H, Wen F, Wong YS, Boey FYC, Subbu VS, Leong DT, Ng KW, Ng GKL, and Tan LP. Direct laser machining-induced topographic pattern promotes up-regulation of myogenic markers in human mesenchymal stem cells. Acta Biomaterialia 2012, 8(2): 531–539.

[25] Li H, Wong YS, Wen F, Ng KW, Ng GKL, Subbu SV,Boey FYC and Tan LP. Human Mesenchymal Stem-Cell Behaviour On Direct Laser Micropatterned Electrospun Scaffolds with Hierarchical Structures. Macomol Biosci 2013; 13(3): 299-310.

[26] Virgilio N, Sarazin P, and Favis BD. Towards ultraporous poly($_L$-lactide) scaffolds from quaternary immiscible polymer blends. Biomaterials 2010; 31(22): 5719-5728.

[27] Yang F, Murugan R, Ramkrishna S, Wang X, Ma YX, and Wang S. Fabrication of nano-structured porous PLLA scaffold intended for nerve tissue engineering. Biomaterials 2004; 25(19): 1891-1900.

[28] Rytlewski P, and Zenkiewicz M. Laser-induced surface modification of polystyrene. Appl Surf Sci 2009; 256(3): 857-861.

[29] Ma Z, Gao C, Gong Y, and Shen J. Cartilage tissue engineering PLLA scaffold with surface inmobilized collagen and basic fibroblast growth factor. Biomaterials 2005; 26(11): 1253-1259.

[30] Wang X, Song G, Lou T, and Peng W. Fabrication of Nano-fibrous PLLA Scaffold Reinforced with Chitosan Fibers. J. Biomater Sci Polym Ed 2009; 20(14): 1995-2002.

[31] Hu J, Sun X, Ma H, Xie C, Chen YE, and Ma PX. Porous nanofibrous PLLA scaffolds for vascular tissue engineering. Biomaterials 2010; 31(31): 7971-7977.

[32] Nuutinen JP, Clerc C, Reinikainen R, and Törmälä P. Mechanical properties and in vitro degradation of bioabsorbable self-expanding braided stents. J Biomater Sci Edn 2003; 14 (3): 255-266.

[33] Sarasua JR, López Arraiza A, Balerdi P, and Maiza I. Crystallinity and mechanical properties of optically pure polylactides and their blends. Polym Eng Sci 2005; 45(5): 745-753.

[34] Park A and Cima LG. In vitro cell response to differences in poly-L-lactide crystallinity. J Biomed Mater Res 1996; 31(1): 17-30.

[35] http://www.purac.com/

[36] http://www.veeco.com

[37] Simões BM, Piva M, Iriondo O, Comaills V, López-Ruiz JA, Zabalza I, Mieza JA, Acinas O, and Vivanco MdM. Effects of estrogen on the proportion of stem cells in the breast. Breast Cancer Res Treat 2011; 129(1): 23-25.

[38] http://www.zeiss.es/

[39] Bremus-Koebberling EA, and Gillner A. Laser structuring and modification of surfaces for chemical and medical micro components. Proc SPIE 2003; 5063: 217-222.

[40] Teixeira AI, Abrams GA, Bertics PJ, Murphy CJ, and Nealey PF. Epithelial contact guidance on well-defined micro- and nanostructured substrates. J Cell Sci 2003; 116: 1881-1892.

[41] Yim EKF, Reano RM, Pang SW, Yee AF, Chen CS, and Leong KW. Nanopattern-induced changes in morphology and motility of smooth muscle cells. Biomaterials 2005; 26(26): 5405-5413.

[42] Bettinger CJ, Orrick B, Misra A, Langer R, and Borenstein JT. Microfabrication of poly (glycerol-sebacate) for contact guidance applications. Biomaterials 2006; 27(12): 2558-2565.

[43] Yao L, Wang S, Cui W, Sherlock R, O'Connell C, Damodaran G, Gorman A, Windebank A, and Pandit A. Effect of functionalized micropatterned PLGA on guided neurite growth. Acta Biomaterialia 2009; 5(2): 580-588.

[44] Pelaez-Vargas A, Gallego-Perez D, Magallanes-Perdomo M, Fernandes MH, Hansford DJ, De Aza AH, Pena P, and Monteiro FJ. Isotropic micropatterned silica coatings on zirconia induce guided cell growth for dental implants. Dental Materials 2011; 27(6): 581-589.

[45] Holthaus MG, Stolle J, Treccani L, and Rezwan K. Orientation of human osteoblasts on hydroxyapatite-based microchannels. Acta Biomaterialia 2012; 8(1): 394-403.

[46] Cañas N, Kamperman M, Völker B, Kroner E, McMeeking RM, and Arzt E. Effect of nano- and micro-roughness on adhesion of bioinspired micropatterned surfaces. Acta Biomaterialia 2012; 8(1): 282-288.

[47] Von Recum AF and Van Kooten TG. The influence of micro-topography on cellular response and the implications for silicone implants. J Biomater Sci Polym Ed. 1996; 7(2): 181-198.

[48] Nikkhah M, Edalat F, Manoucheri S, and Khademhosseini A. Engineering microscale topographies to control the cell-substrate interface. Biomaterials 2012; 33(21): 5230-5246.

[49] Irimia D and Toner M. Spontaneous migration of cancer cells under conditions of mechanical confinement. Integr Biol 2009; 1(8-9): 506-512.

[50] Nikkhah M, Strobl JS, De Vita R, and Agah M. The cytoeskeletal organization of breast carcinoma and fibroblast cells inside three dimensional (3-D) isotropic silicon microstructures. Biomaterials 2010; 31(16): 4552-4561.

[51] Nikkhah M, Strobl JS, and Agah M. Attachment and response of human fibroblast and breast cancer cells to three-dimensional silicon microstructures of different geometries. Biomed Microdev 2009; 11: 429-441.

[52] Nikkhah M, Strobl JS, and Agah M. Development of a three-dimensional (3-D) silicon micro-array for cell capturing. Sensors, 2010 IEEE; 1609-1612.

Chapter 3. In vitro analysis of laser-microstructured PLLA surfaces via seeding human mesenchymal stem cells: effect of topographical cues on cell differentiation.

1. Introduction

Adult stem cells are the main source for developing future new strategies in regenerative medicine, cell-based therapy, and tissue engineering [1-3]. Proliferation and differentiation of stem cells *in vivo* are regulated by their microenvironment, known as niche, which comprises both cellular components and interacting signals between them [4, 5, 6]. These niches, in addition to other functions, provide stem cells with physical anchors (by means of adhesion molecules) and regulate the molecular factors that control cell number and fate [5]. Some of these factors are influenced by cell shape, cytoskeletal tension and contractility [7, 8]. In this regard, the design of biomaterials with architectures that mimic natural cell microenvironments might be a powerful tool to better understand and manipulate cell function as a strategy for future cell-based therapies. Among the biomaterial properties that affect cell behaviour, surface topography has shown a great potential to control cell shape and location [9]. Several researchers have observed that microscale and nanoscale topographies in the form of pillars, grooves, pits or pores can induce the differentiation of human mesenchymal stem cells (MSCs) to a certain cell lineage [10, 11, 12]. In this context, surface microstructuring technologies play an important role in the manufacturing of functionalized 3D scaffolds, resembling the cellular three-dimensional networks and the structural organization of human tissues [13, 14].

As have been seen in chapter 2, pulsed-laser-based technology is a promising approach for the fabrication of scaffolds to guide the spatial distribution of living cells. In 2005 Liu and collaborators applied for the first time an ultra-short pulsed laser for this purpose [15], which reflects the novelty of this strategy. Last years have witnessed the application of the femtosecond-pulsed laser technology to create 3D microstructures on biocompatible materials for cell culture [16-21]. In these studies, channels were created to control different aspects of cell behaviour on biopolymers. Lee et al [17] observed that channels fabricated inside electro spun scaffolds made of polycaprolactone favour the formation of vascular walls in that they promote the adhesion of smooth muscle cells on the channel walls. Other authors employed a similar strategy to increase the infiltration of cells and nutrients [18]. Channels carved on a biopolymer film have also been employed to induce cell alignment and promote myogenic differentiation of MSCs [19] although the authors did not obtain conclusive results at this respect. In spite of the high-quality structures

that a femtosecond pulsed laser is able to generate, it has though technical limitations, such as the low processing speed and the low ablation rate that makes it difficult to implement in industry, where both power scaling and versatility are required. In contrast, picosecond pulsed lasers are easier to implement in industrial processes due to their better cost-effectiveness, versatility and reliability. Consequently, the presence of these lasers has noticeably increased in the industrial market during the last years. Surprisingly it has been scarcely used for scaffold fabrication [22, 23]: previous to our work only Schlie and collaborators have applied the picosecond laser micromachining technology (PLM) on silicon substrates to test cell compatibility [22], while we employed this technology on biocompatible polymers to create microstructures that modulate the morphology and proliferation of breast cancer cells (chapter 2) [23]. In this chapter, we examined the effects that carved micropatterns created by PLM on substrates made on Poly-L-Lactide (PLLA) may have on human MSCs and their differentiation into adipocytes and osteoblasts.

2. Materials and Methods

2.1 Materials

PLLA was supplied by Biomer (Biomer Krailling, Germany). PLLA sheets of approximately 300 µm in thickness and a degree of crystallinity of 4% (measured by differential scanning calorimetry) were obtained by thermoforming. Under these conditions, the PLLA film is hydrophobic (contact angle = 70° ± 5°) with a surface free energy of 38.18 mJ/m^2 in air at 23ºC [24]. Cell culture dishes were fabricated by sealing Nylon rings onto PLLA sheets with a biocompatible silicone (Picodent Twinsil, Picodent GmbH, Germany) (Figure 3.1).

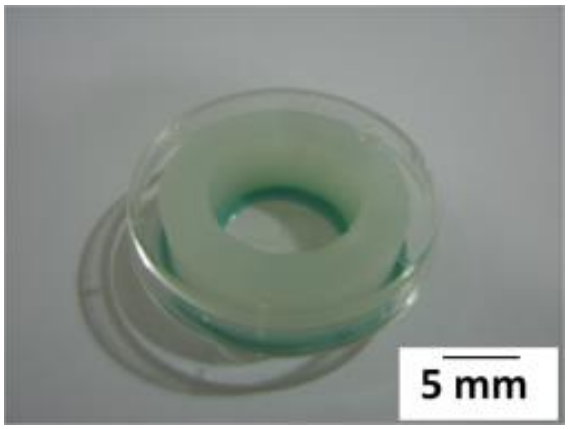

Figure 3.1. A typical PLLA-bottom Petri dish used in this study. The thermoformed PLLA sheet (approximately 300 µm thick) is sealed to a Nylon ring to create a PLLA-bottomed container appropriate for 2D tissue culture.

2.2 Surface microstructuring technique

Surface microstructuring of the PLLA films was carried out with a picosecond-pulse laser system. A detailed description of the experimental set-up and the optimization of the microstructuring process for PLLA was described in previous chapters [25]. To analyse the effect of surface roughness on cell activity, flat PLLA substrates (FLAT PLLA) of Ra = 240 nm (Ra, average surface roughness) were laser-irradiated with the same parameters applied in Chapter 2 (ʎ = 355 nm, E = 0.9 µJ, *f* = 100 kHz, d_p = 5 µm). After this treatment, Ra increased to 700 nm (ROUGH PLLA, Figure 3.2a). To evaluate the effect of surface patterning on the cellular behaviour, parallel grooves (*w* = 10 µm, d = 4 µm) (figure 3.2b) were obtained by applying same parameters than those applied in Chapter 2 for groove generation (ʎ = 355 nm, *f* = 250 kHz, d_p = 2.4 µm). In this case, considering thermal-formed sheets (obtained from PLLA supplied by BIOMER) instead of films obtained by casting from solution (obtained from PLLA supplied by Purac), the application of a low pulse energy (E = 2.3 µJ) allowed us to produced narrow grooves on the PLLA substrates, which reflects the laser ablation dependence on the material properties and processing. These groove dimensions matched to human mesenchymal stem cell size (10-12 µm in diameter). The inter-groove spacing was set to 15 µm (GROOVES 1) and 25 µm (GROOVES 2). In order to analyse the effect of geometry on stem cell differentiation, 3D microcavities were fabricated in

different geometrical shapes, such as circles and rectangles (figures 3.2c-d), with same parameters (ʎ, *f* and d_p) and an energy of 1 µJ. The diameter or side of these geometries is about 200 µm. To ensure cell confinement, the depth of these microcavities was set to 40 µm, approximately 8 times as high as a cell height. Width and depth of the microcavities and grooves were measured by a mechanical stylus profilometer (Dektak 8, Veeco, USA). Ra was calculated from 4 mm long surface profiles, according to DIN EN ISO 4288:1998.

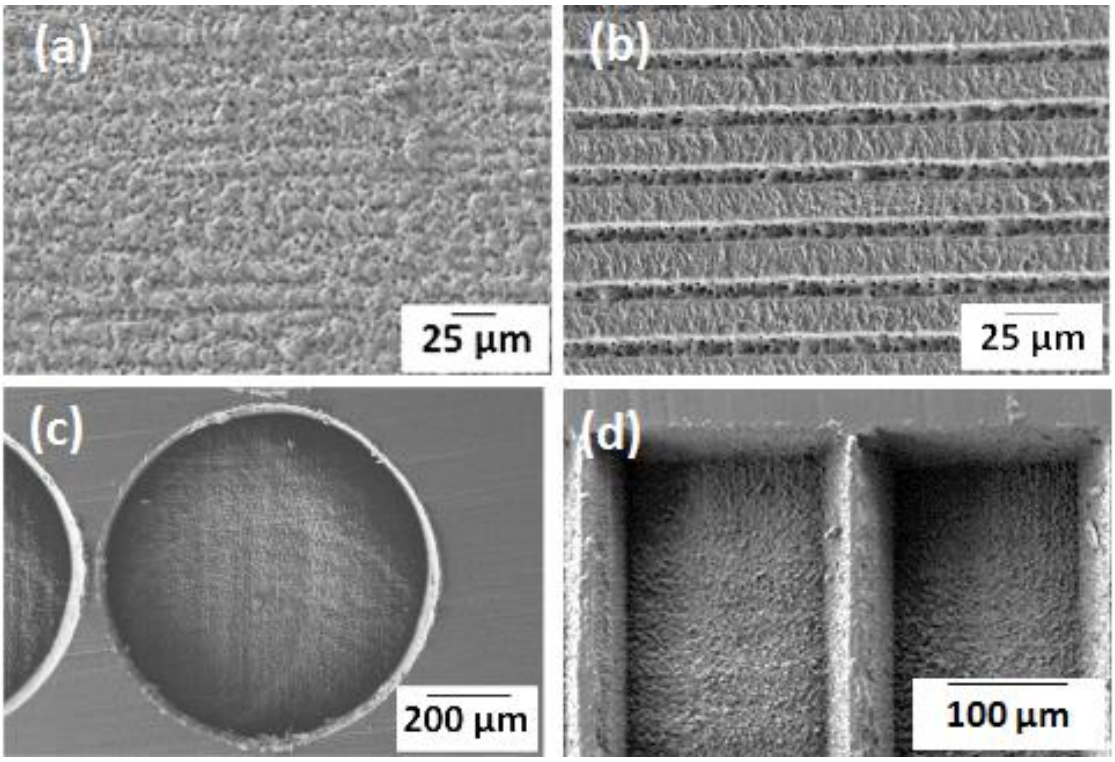

Figure 3.2. SEM images of PLM-treated PLLA: laser-irradiated ("rough") PLLA (a); grooves with *w* = 10 µm, d = 4 µm, and *s* = 15 µm *(b); circular (c) and rectangular (d) microcavities.*

2.3 Cell culture

Human MSCs from bone marrow were provided by Promocell (Germany). Prior to cell culture, all PLLA surfaces were cleaned gentle with 70% ethanol and UV-sterilized for 30 minutes. Cells were cultured on the surfaces in growth medium (Promocell) and were maintained at 37˚C and 5% CO_2.

Cell proliferation was measured on all the PLLA surfaces (FLAT PLLA, ROUGH PLLA, GROOVES 1, GROOVES 2) by means of a MTT assay at 4 different cultivation times: 1, 4, 7 and 14 days. The plated cell density was 20000 cells/cm^2. These experiments were done in triplicate on 3 surfaces of each type. Glass coverslips were used as control.

Cell morphology was examined on all the PLLA surfaces by means of immunofluorescence microscopy applying two different staining methods: in one hand, cells were stained with NeuroDio, a green-fluorescent cytoplasmic membrane stain (Promokine, Germany) before seeding. On the other hand, cells were fixed and stained for DAPI (cell nuclei, blue), phalloidin (cell cytoplasm, red), and vinculin (focal adhesions, green). Cell density was 1000 cells/cm^2 for both staining methods. These experiments were performed in triplicate for every type of surface. Cell morphology was observed at three different cultivation times.

In order to study cell differentiation, MSCs were seeded on PLLA dishes at higher densities, 30000 cells/cm^2, to attain 100% confluence after 24 hours in culture. The growth medium was then replaced with a differentiation-induction medium, which contained a 1:1 mix of adipogenic and osteogenic induction media (Promocell). Cells were incubated in this medium for 2 weeks. The induction medium was changed every three days. After two weeks, cells were fixed in 4% formaldehyde for 5 minutes at room temperature and stained immediately after with Fast Blue RR Salt/Napthol solution (Sigma-Aldrich, Germany) and Oil Red O solution (Sigma-Aldrich, Germany) according to the manufacturer´s instructions. The first staining agent tags alkaline phosphatase activity (AP staining), an early indicator of cells that undergo osteogenesis, while the second tags the deposits of fat or lipid vacuoles characteristic of adipogenesis. Cells were visualized with an inverted microscope in bright field and fluorescence modes (Nikon Eclipse TE-2000-S, 6V30W halogen lamp, Bright field (BF) and GFP filter, Japan).

2.4. Data analysis

Optical micrographs were analysed with the image analysis freeware Image J (http://imagej.nih.gov/ij/). Image brightness and contrast were adjusted to optimize the visualization of single cells from a strongly light-scattering background. In order to quantify cell alignment on grooves, in terms of cell cytoplasm, cells oriented along groove direction were

counted out of 11-23 images of as many different sample locations taken after a specific number of days in culture. Round cells or cells oriented perpendicularly to groove direction were counted as non-oriented. Alignment of cell nucleus was quantified by ImageJ, using images of 5 different areas for each type of substrate and incubation period. Each cell nucleus was marked and an ellipse was fitted to it to measure the orientation angle of each cell nucleus. The location and number of clusters of lipid vacuoles inside and outside of grooves were obtained from images such as those shown in the inset of the figure 12 taken after two weeks in culture and at 10 different sample locations. All data were expressed as means ± standard deviation. Statistical analysis was carried out using the Student's *t*-test and the values were considered significantly different when $p<0.05$.

3. Results

3.1. Effect of surface topography on undifferentiated MSCs

As described in the material and methods section, cell proliferation was examined on 4 different types of surfaces: FLAT PLLA, ROUGH PLLA, and two different groove-configurations (GROOVES 1 and GROOVES 2) based on grooves with the same dimensions but different inter-groove spacing. Figure 3.3 shows the relative cell growth on these surfaces as a function of the cultivation time compared to cell growth on glass coverslips (Figure 3.3.a) and FLAT PLLA (Figure 3.3.b) at 1 day of incubation. As we observe in this figure, MSC growth is significantly slow on this material compared to glass coverslips, although there is a noticeable increase of cell growth in time, and there are no significant differences between the different surfaces.

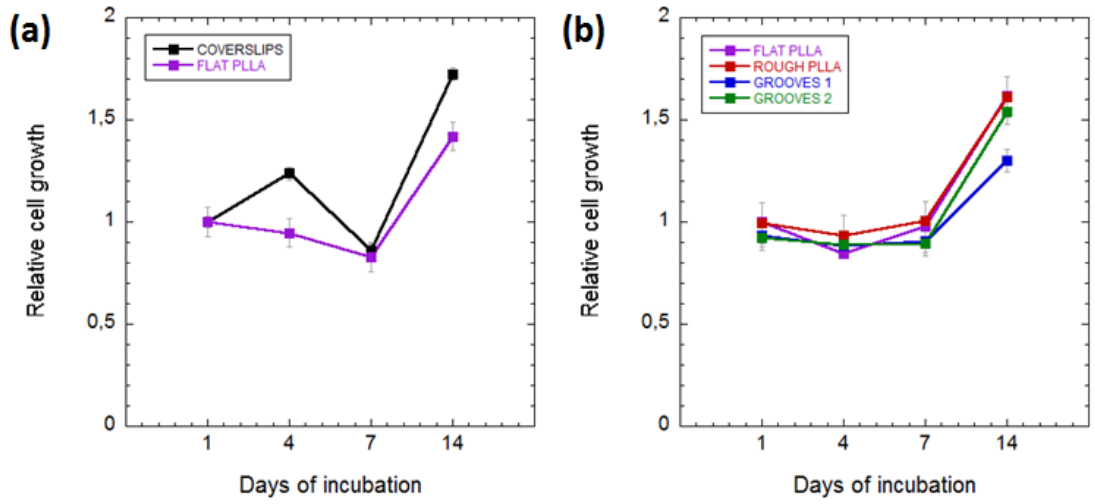

Figure 3.3. hMSC proliferation on non-patterned PLLA (FLAT PLLA) compared to cell proliferation on glass coverslips (a); and on 3 different types of surfaces: PLLA treated by laser to increase the surface roughness (ROUGH PLLA), and PLLA patterned by grooves of w = 10 μm, d = 4 μm and s = 15 μm (GROOVES 1) and 25 μm (GROOVES 2) compared to FLAT PLLA (b).

The PLM fabrication of grooves on PLLA produces two major transformations on the material surface: *depressions* caused by material removal by the laser pulses and *protrusions* of recast material at the groove ends and edges (Figure 3.4). The depth of the depression and the pile of recast material are particularly prominent at the end of the trench as figures 3.4a and 3.4b show. Here, protrusions can be 226% higher than at any other location along the trench. This phenomenon is ever present in the laser manufacturing technology and it is a consequence of the *first-pulse effect* [26]. The highly intense first laser pulse that initiates the micromachining process produces a particularly strong effect on the material.

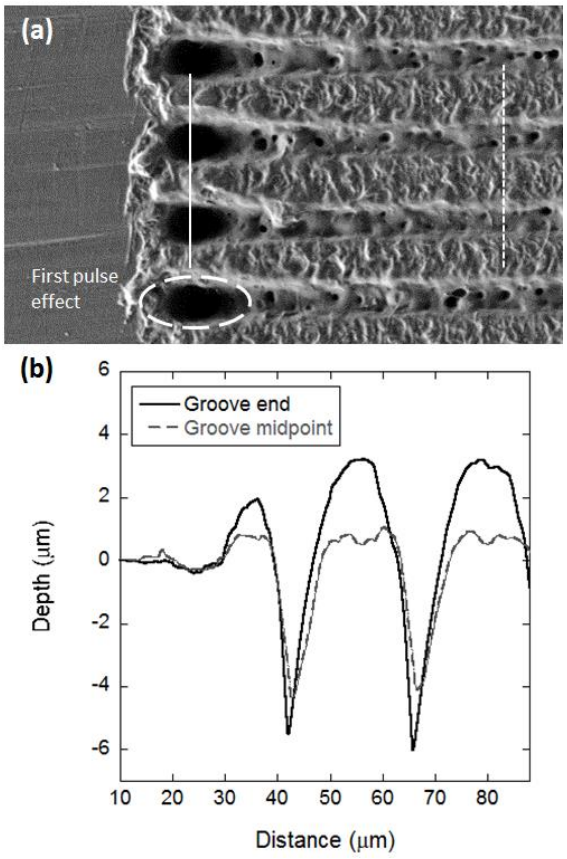

Figure 3.4. SEM image of grooves created by PLM (a); line profiles across the grooves; at the end of the trenches (continuous line) and at the trenches´ midpoint (dashed line) (b)

To examine the cell behaviour of undifferentiated hMSCs on patterned PLLA, the centre of the PLLA-bottomed dish was divided into 2x2 micro sized squares, three of which were filled with parallel grooves each at different orientations (0°, 45°, and 90°). A fourth square was left unpatterned as control (FLAT PLLA). In each row, the patterned squares were separated by a 200 µm-wide stripe of flat PLLA. Figure 3.5 shows MSCs on FLAT PLLA (Figure 3.5a-c) and on grooves of different orientation (Figure 3.5d-i) after 1, 8 and 22 days of culture and at low cell confluency. As occurred in the experiments reported in chapter 2, the visualization of the stained cells on the PLLA sheets was impaired in some cases by the translucent thick PLLA sheet and the light scattered by the laser-treated regions. Despite this fact, it was possible to observe that on FLAT PLLA and after one day in culture, MSCs adopt a variety of shapes, resulting in a mixed population of rounded and elongated cells, the latter oriented in non–specific directions. In contrast, on patterned PLLA MSCs with elongated shapes predominate already after 1 day in culture. The direction of these elongated cells matched the groove orientation as shown in Figure 3.5g-i, which clearly shows the influence of substrate topography on the early alignment of cells.

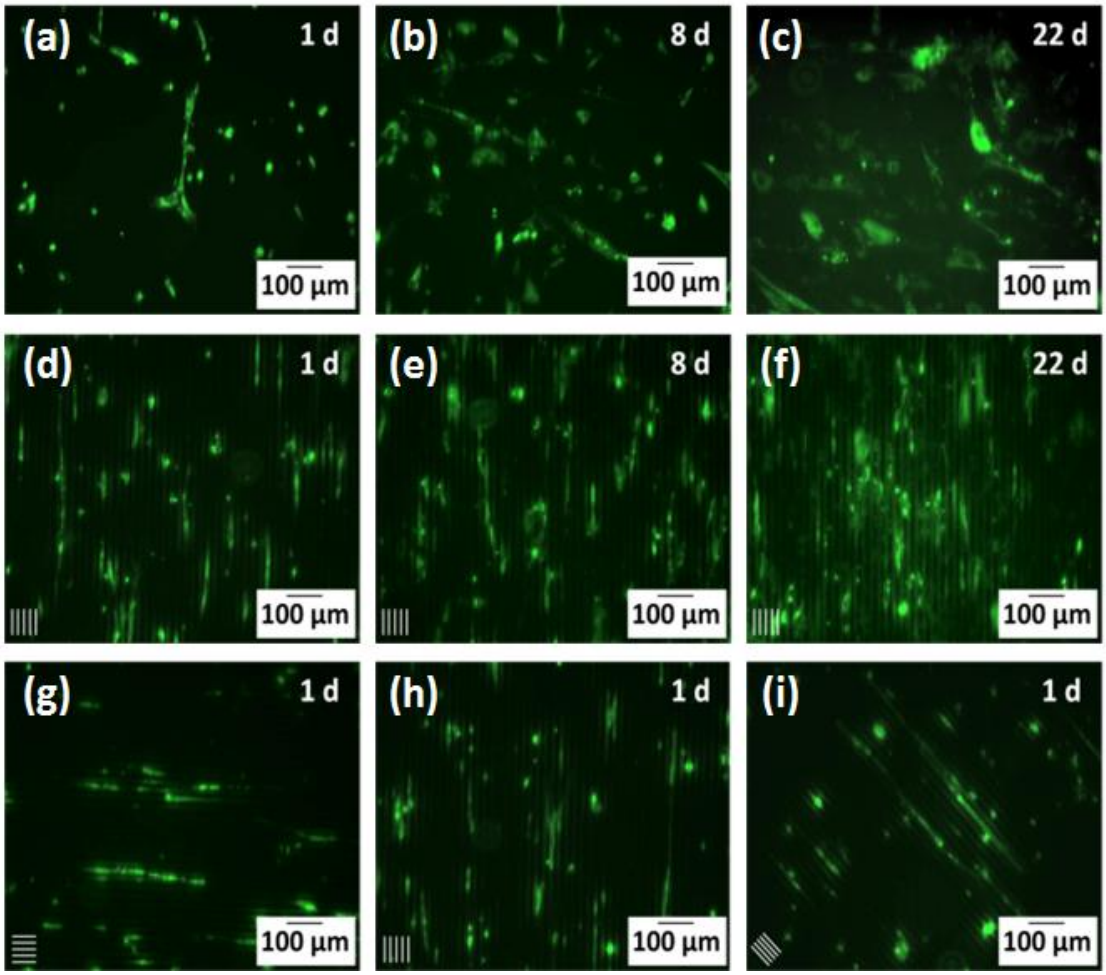

Figure 3.5. Fluorescence microscopy images of MSCs cultured on patterned PLLA. MSCs on flat PLLA (a-c), and MSCs on vertical grooves as a function of time (d-f). Images (g-i) show cells on grooves oriented at different directions after one day in culture. The white lines at the lower left corner of the images depict the orientation of the grooves.

Figure 3.6 represents the number of oriented cells (considering the cell cytoplasm) normalized to the total cell number (in percentage) as a function of the orientation angle and time in culture: The effect of cell patterning is clearly shown in this diagram when low cell confluence was considered. Polar graphs for 1 and 8 days in culture show that, on flat surfaces (circle-shaped dots), dots representing the number of oriented cells at a certain angle are inside the first circumferential division (cell number below 20%): this means that on flat surfaces there were few cells oriented at different angles. On PLLA grooves with different directions (square-, diamond- and triangle-shaped dots), however, the number of oriented cells for a certain angle was clearly high (from 40 to 80%) and only few cells were oriented at a different angle (cell number below 20%). The histogram show that, after 22 days, cell alignment on FLAT PLLA increased, but this effect was

produced by the high cell confluency found at higher incubation times: cells tend to align parallel to one another and form bundles in a random orientation, most likely to maximize cell-cell interactions. On PLLA grooves cell alignment was induced and controlled by the surface and remained constant at a value of 70 ± 10% even at high cell confluence.

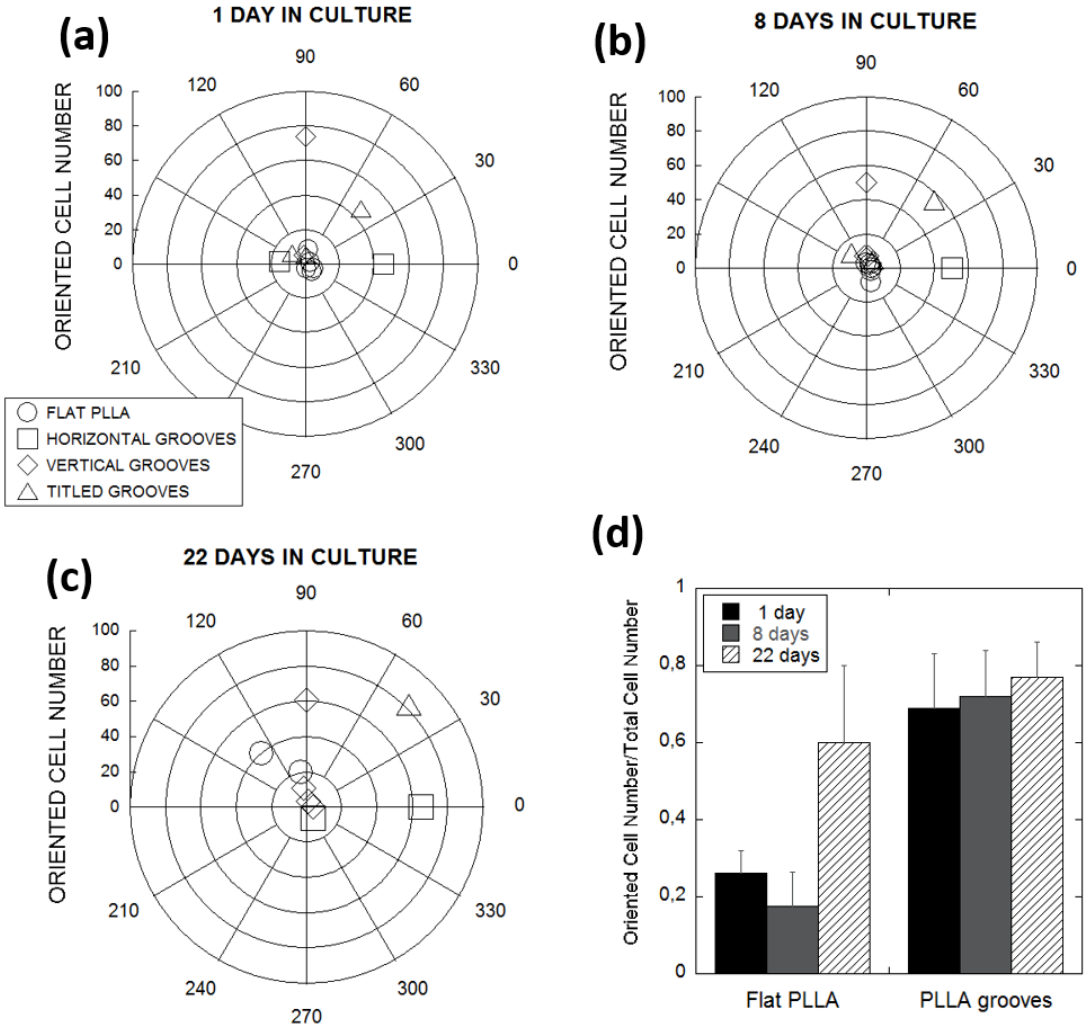

Figure 3.6. Polar diagrams showing the number of oriented cells (in terms of cytoplasm) as a function of the pattern orientation angle after 1 (a), 8 (b) and 22 (c) days in culture. Dot size indicates the error (about 5%). (d) Number of oriented cells normalized to the total number of cells as they appear in the fluorescence images as a function of time.

Figure 3.7 shows representative images of cell morphology obtained by immunofluorescence confocal microscopy on 4 different PLLA surfaces (FLAT PLLA, ROUGH PLLA, GROOVES 1 and GROOVES 2) using cover slips as control. It is worth to note that Confocal microscopy allows to

avoid most of the light scattered by the laser-regions and therefore obtain good quality images of cells on patterns, although grooves are still appreciable. These images show that cell proliferation and adhesion was qualitatively lower in the PLLA surfaces compared to standard glass cover slips. A closer look at the cell morphology confirmed cell alignment along the groove-patterned surfaces.

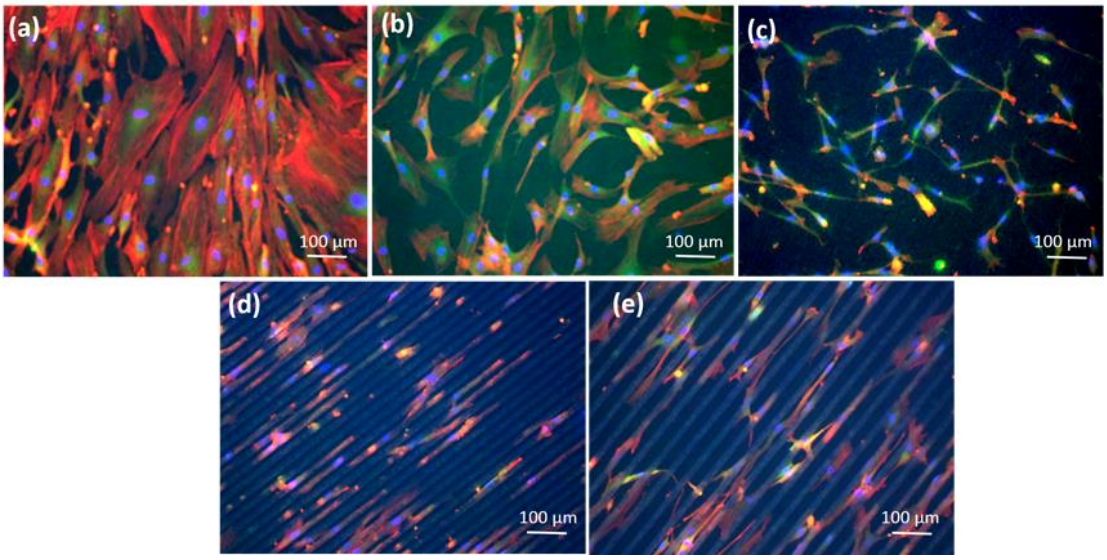

Figure 3.7. Representative images of MSCs obtained by immunofluorescence microscopy on the 4 different PLLA surfaces compared to cover slips after 14 days in culture: (a) MSCs on cover slips; (b) MSCs on FLAT PLLA; (c) MSCs on ROUGH PLLA; (d) MSCs on GROOVES 1; (e) MSCs on GROOVES 2.

The effect of substrate topography on cell nuclei orientation is shown in Figures 3.8 and 3.9. Figure 3.8 shows the polar graphs representing the angle at which each cell nuclei were oriented on every surface (measured by ImageJ) after 3 different cultivation times (1, 7 and 14 cultivation days). All these graphs show that the cell guidance effect clearly affected cell nuclei when groove-patterned PLLA surfaces are considered compared to the flat and rough PLLA surfaces. The polar graphs show cell nuclei with a wide range of orientation angles when cells grew on flat and rough PLLA surfaces, while cells growing on the groove-patterned PLLA surfaces showed nuclei with a noticeable trend to orientate along a preferred direction.

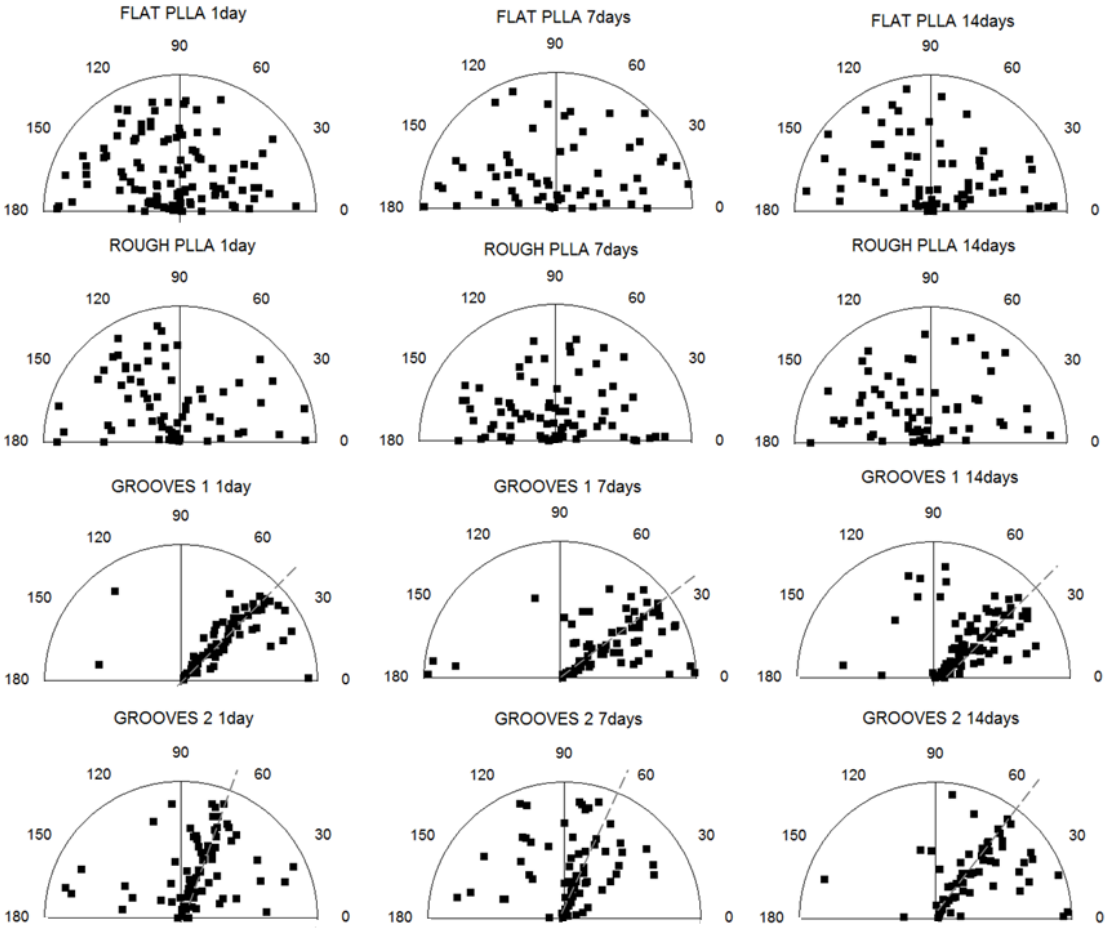

Figure 3.8. Polar graphs showing the angle of orientation of the cell nuclei on the 4 different PLLA surfaces (FLAT PLLA, ROUGH PLLA, GROOVES 1 and GROOVES 2) after 1, 7 and 14 cultivation days. Each spot represents one cell nucleus. The dashed line highlights the main trend found on the groove-patterned surfaces.

Figure 3.9 shows the histograms representing how much the nuclei deviates from the main trend on GROOVES 1 and 2 surface at the same 3 different cultivation times. The histograms show that about 75% of the cell nuclei were oriented with a deviation angle minor of 20º on the groove-patterned surface, when a groove configuration of 15 micrometres of inter-groove spacing was applied, and approximately 60% of the nuclei were oriented in the same range of deviation angle, when grooves of 25 micrometres of inter-groove spacing were considered. Moreover, cell nuclei on grooves with a minor inter-groove spacing (s = 15 µm) were all aligned inside the laser-created channels (approximately (85 ± 5)%) and few nuclei were observed to be in the spacing between them ((15 ± 5)%); however, when we increased the inter-groove spacing (s = 25 µm), cells showed

again aligned, but, in this case, many cell nuclei were found to attach at the spacing between grooves ((46 ± 5)%).

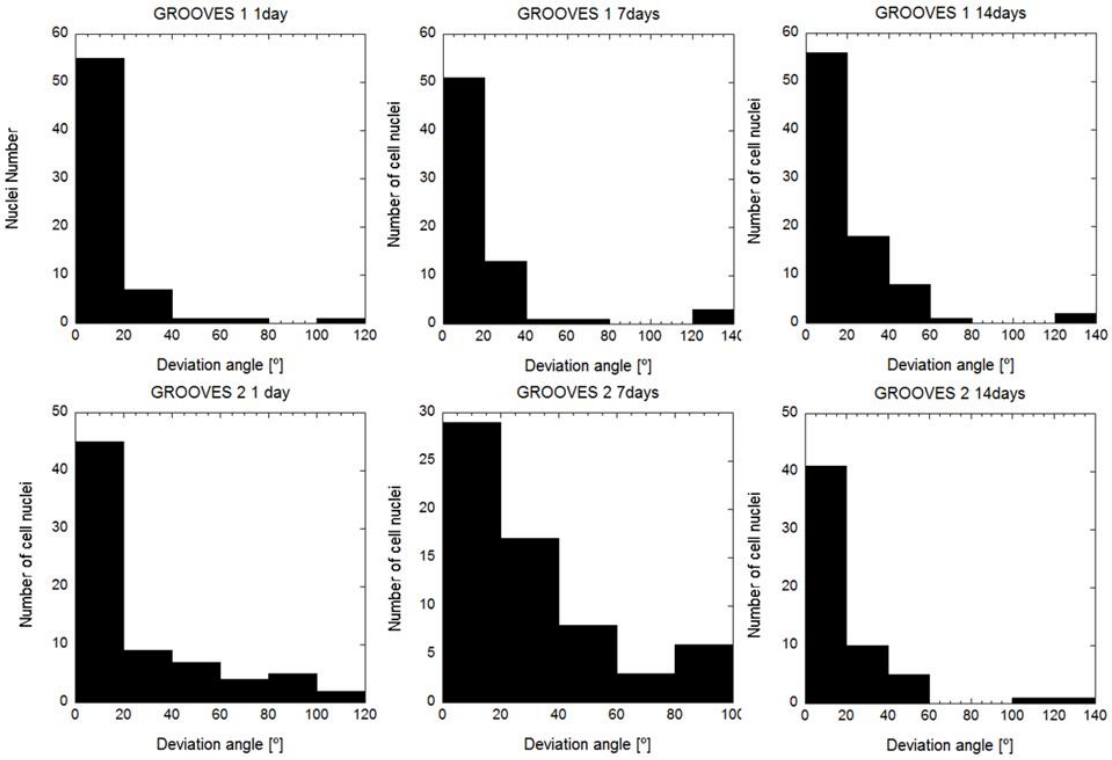

Figure 3.9. Histograms representing the deviation angle of cell nuclei respect to the trend angle on the patterned-PLLA surfaces (GROOVES 1 and GROOVES 2) after 1, 7 and 14 cultivation days.

As shown in figures 3.5-9, contact guidance of MSCs on grooves occurs within the patterned squares, however, in the regions between squares, and within the first 24 h in culture, cells spread across the gap, extending between groove endpoints of neighbouring squares, as shown in figure 3.10a, or between endpoints and groove edges, as shown in figure 3.10b. According to the images of figure 3.10, single cells develop filopodia-like extensions between topological protrusions that are at least 200 µm apart.

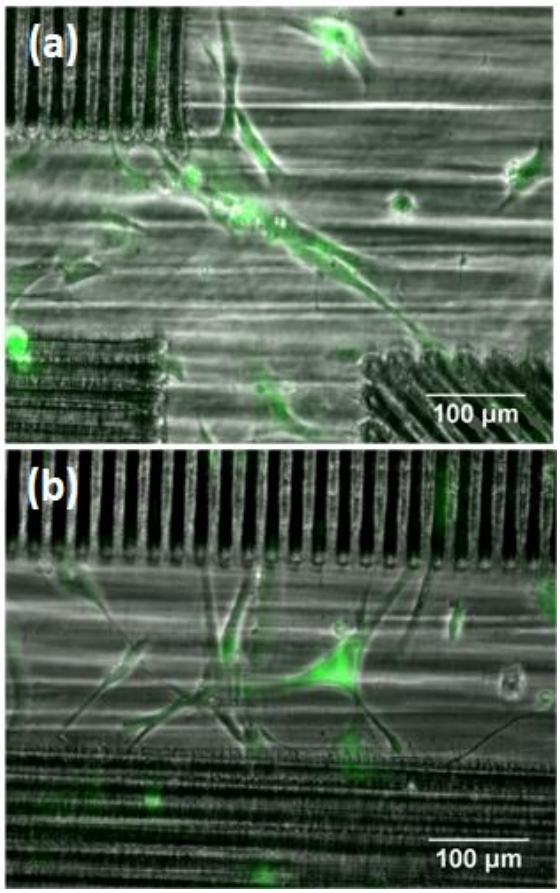

Figure 3.10. Human MSCs adhered on flat PLLA in between PLM-patterned squares after 24h in culture. Cells spreading from one groove endpoint to another of the second-nearest neighbour square (a) and from groove endpoints to groove edge of a first-nearest neighbour square (b). Images were treated by ImageJ to highlight cell morphology (green colour).

3.2. Effect of surface topography on differentiated human MSCs

In-vitro differentiation of MSCs is most efficient when it is induced at high cell confluency (i.e.90%) [27]. Under these conditions, it has been shown that cell-cell interactions may be more relevant than cell-substrate interactions to determine the shape and orientation of MSCs [27]. Nevertheless, the presence of topological barriers and cavities may alter the behaviour of differentiated MSCs (i.e., adipocytes and osteoblasts) as we will show in this section.

Adipocytes and osteoblasts descend from a MSC precursor. Adipocytes are round to allow maximal lipid storage in the adipose tissue, while osteoblasts tend to spread to facilitate matrix deposition activity. After 14 days of adipogenic differentiation, the distribution of lipid vacuoles cultured on FLAT and ROUGH PLLA was examined. In both cases, the clusters of lipid vacuoles are quasi globular and their distribution is not affected by substrate roughness (Figure 3.11a-b). Similarly, AP staining suggests that osteoblast distribution is unaffected. However, the lipid vacuoles appear to line the edge separating regions of different roughness (Figure 3.11c). A similar behaviour is observed on the edges of the microcavities, where cells confront a topological barrier of approximately 40 μm in height (Figures 3.11d-e). Lipid vacuoles close to the edge of these cavities line the borderline regardless of the shape and size of the microcavity, which in this case is much larger than a single cell. On grooved-patterned PLLA, the distribution of the lipid vacuoles on the surface differs (Figures 3.12a-c): Lipid vacuoles arrange in strings both inside and in between the grooves, however, they were more likely to be found inside the grooves (67 ± 11 %) than outside (29 ± 13 %) (Figure 3.12d). In contrast, osteoblasts did not show any noticeable predefined orientation on the patterned surface.

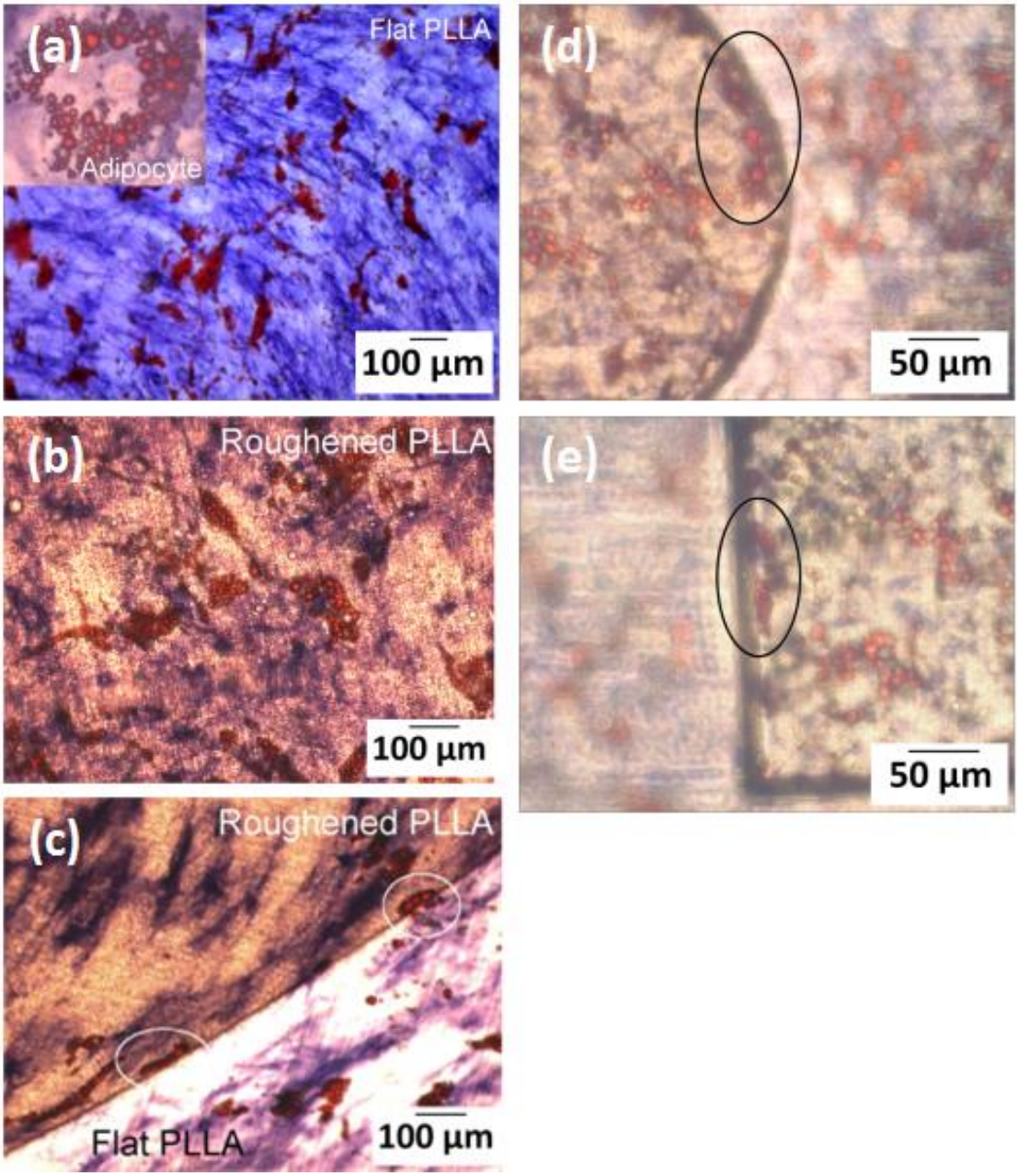

Figure 3.11. Bright field (BF) images of MSCs differentiated into adipocytes (presence of lipid vacuoles in red) and osteoblasts (AP staining in blue) on FLAT PLLA (a), ROUGH PLLA (b,c), and in microcavities (d, e). In figures c-e strings of lipid vacuoles lining the walls of the microcavities are outlined.

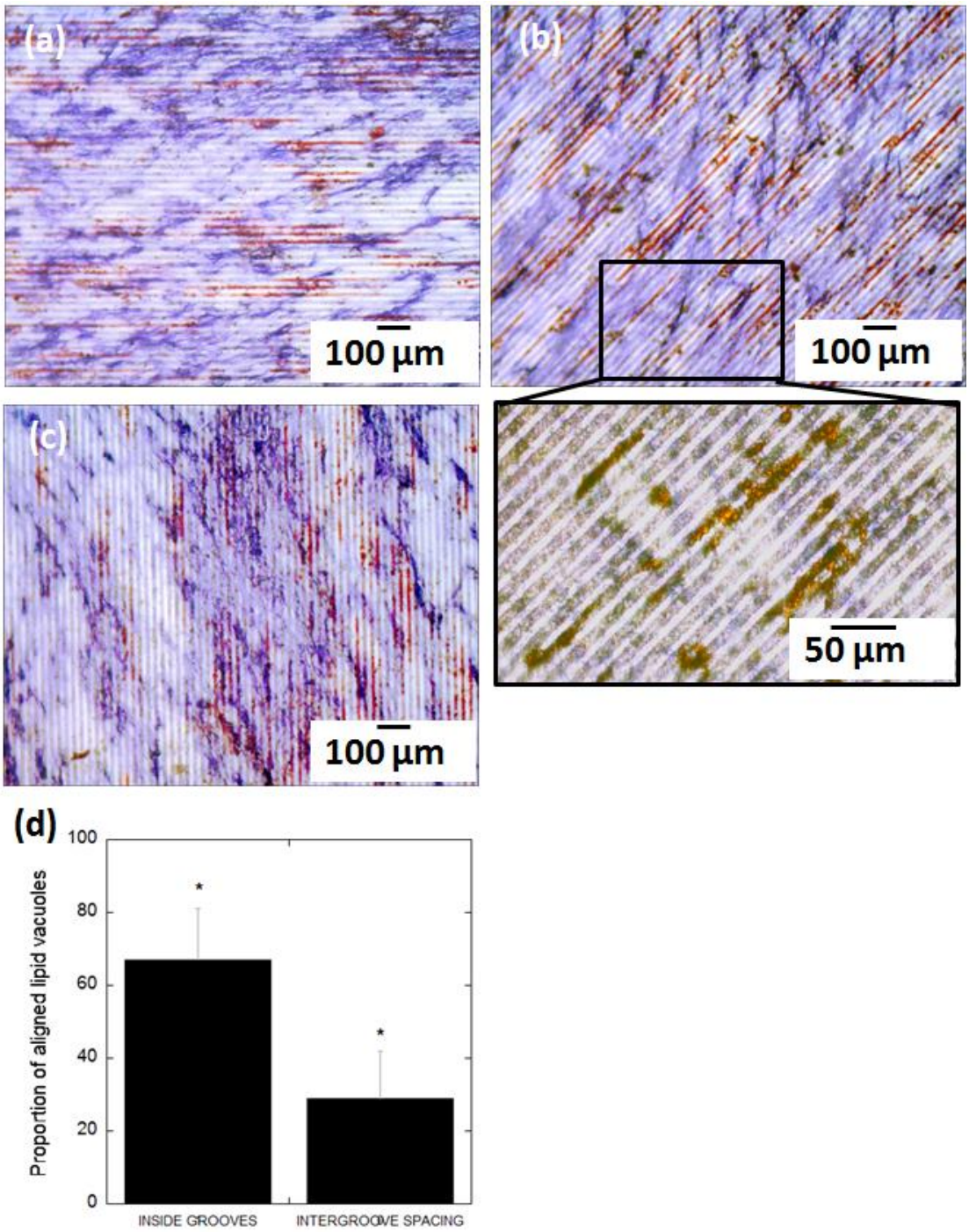

*Figure 3.12. BF images of MSCs differentiated into adipocytes (presence of lipid vacuoles in red) and osteoblasts (AP staining in blue) on GROOVES after 14 days in culture (a-c). (d) Ratio of clusters of lipid vacuoles confined in the grooves and on the inter-groove spacing (*significance level according to the Student t-Test: $p<0.005$).*

4. Discussion

In this research, we have examined the effects that PLLA substrates modified by picosecond pulsed laser ablation have on MSC shape, and differentiation into adipocytes and osteoblasts. MSCs cultured on patterned PLLA showed the characteristic contact guidance effect [27], both in terms of cell cytoplasm and cell nucleus, already after 24 h in culture and throughout a period of 22 days. These results agree with previous reports on stem cell alignment along micro- and nano-grooved-patterned substrates [28-31, 20]. Cell nuclei alignment is promoted on grooves with minor inter-groove spacing respect to the further apart grooves, with an increment of approximately 25%. A minor inter-groove spacing also increase the percentage of cell nuclei confined inside the grooves: 85% of cell nuclei were found attached to the inner surface of the grooves for s = 15 µm, while 54% of cell nuclei were attached in the spacings between grooves for s = 25 µm. One possible explanation for this behaviour could be in the slight change undergone by the topographical profile of the inter-groove spacing when increasing this (Figure 3.13): for an inter-groove spacing of 15 µm, the surface between grooves is formed by the merger of the recast material deposited at both sides of each groove, leading to a spacing surface approximately flat; however, for an inter-groove spacing of 25 µm, the groove ridges formed by the recast material at both sides if each groove distance from each other, leading to the formation of a shallow channel between the grooves, which is wide enough to have the same effect of the “proper” grooves and promote cell nuclei confinement. In addition, the protrusions generated by the laser ablation technique at grooves´ ends and grooves´ edges provides convenient anchorage points for MSC and can potentially control their adhesion and shape. Hamilton and collaborators observed a similar phenomenon in osteoblasts proliferating on boxes and pillars [32], which they called gap guidance, a type of contact guidance for cell alignment that is associated to discontinuous topographical edges. Our results on microgrooves show that these microstructures influence MSCs in two ways: on the one hand, grooves influence cell orientation, since cells adapted their shape to groove width (in terms of cell cytoplasm) and orientation (both cell cytoplasm and nucleus), and the maximal effect was observed at the first stages of MSCs proliferation; on the other hand, grooves´ edges promote cell adherence and provide guidance. These effects appear to resemble the influence of stem cell niches *in vivo* [5], which makes PLM a convenient technique to create *in vivo*-like cellular environments.

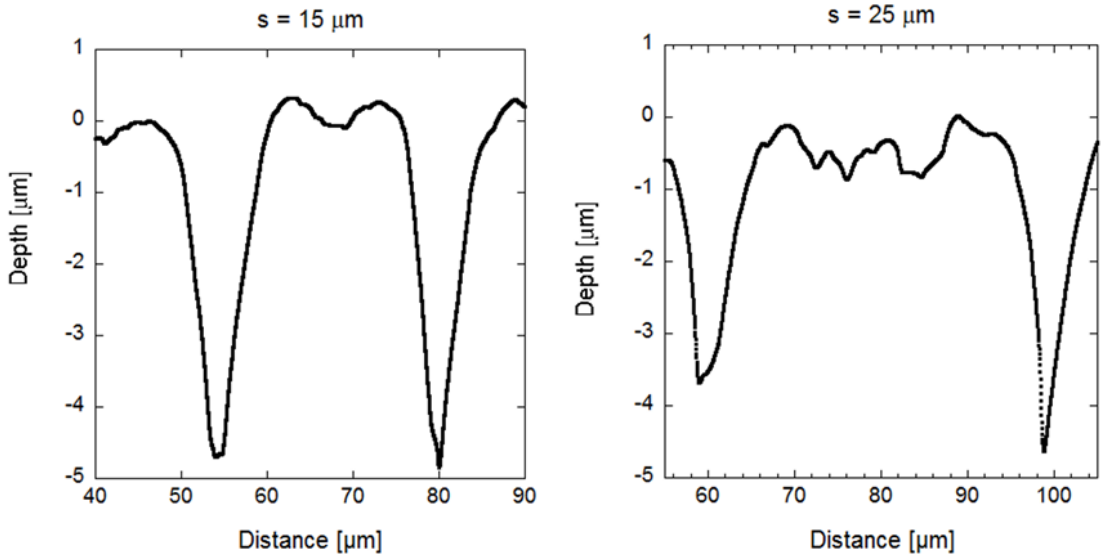

Figure 3.13. Topographical profile measured by profilometry of the laser-created grooves for an inter-groove spacing of 15 and 25 µm.

In terms of MSCs differentiation, Figure 3.12 showed that adipocytes, in contrast to osteoblasts, are highly sensitive to topographical features. Lipid vacuoles in adipocytes cultured on patterned PLLA align in strings along the grooves. Similarly, the distribution of lipid vacuoles was affected by the presence of topological edges, such as the borderline between flat and rough PLLA, as well as the walls of microcavities. The images of adipocytes on non-modified substrates suggest that the adipocyte shape is defined by the distribution of the lipid vacuoles. According to this, it can be expected that when lipid vacuoles arrange in lines of beads alongside the grooves, the adipocyte bodies may as well be aligned with these grooves (Figure 3.14). To the best of our knowledge, this is the first observation of adipocyte compliance to exclusively topological cues in the micrometre scale. Kim et al. [33] reported on preadipocyte alignment, in terms of cell cytoplasm, on nanometric-grooves fabricated on polyurethane acrylate surfaces treated by oxygen plasma (to make the surface hydrophilic) and coated by fibronectin to increase cell adhesions; however, they did not observe the confinement and alignment of the lipid vacuoles inside the grooves, and the shape of the adipocytes looked very similar on the nanogrooves respect to the control (non-patterned) surface (adipocytes showed circular distribution of lipid vacuoles around the cell nucleus). Our finding reveals that surface topography alone can control adipocyte morphology. Mature adipocytes release a big variety of factors that play a fundamental role in the regulation of many important functions of the body [34]. The expression of these factors

is, in many cases, controlled by adipocyte size and location [35, 36]. In this context, adipocytes should be able to change their morphology in order to store the optimum amount of fat and to perform properly their physiological functions [37]. Therefore, it is likely that, according to the results presented in our study, surface topography could also affect the expression of these factors as it influences adipocyte morphology. Hence, PLM of surfaces may greatly contribute to nano- and regenerative medicine, since surface topography could be tailored to treat diseases related to the dysfunctional expression of those factors. In addition, specially designed scaffolds can be employed to promote adipocyte adhesion and direct the formation of adipose tissue for repairing soft tissue defects [38], or for implantation of artificial organs that require fat tissue regeneration into a predefined geometry, such as ear or larynx [39, 40].

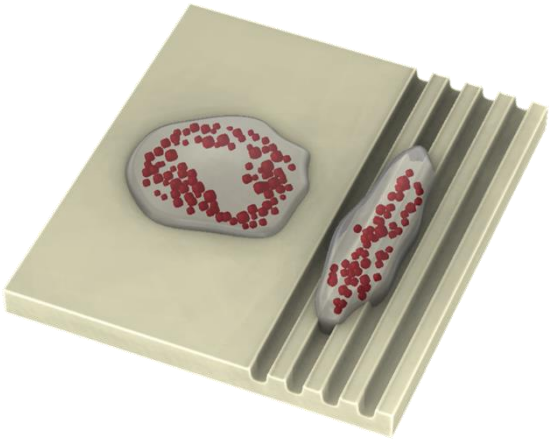

Figure 3.14. Adipocytes on a flat substrate and on grooves according to the experimental observations.

Several authors have reported on the effect of the pattern geometry on cell differentiation into a certain lineage based on biochemical cues, as it is the case of surfaces patterned with agents that induce or hinder cell adhesion [7, 41-44]. In these studies, chemical restrictions were imposed on stem cells, which induce mechanical force gradients at the pattern edges that lead to differentiation into a particular cell type. In our research, where cells were confined by purely physical means, no significant differences were found between the distribution of differentiated cells inside and outside the microcavities. In addition, according to our findings, cells did not differentiate into a particular cell type at the edges of microcavities, contrary to the reported results on chemically confined cells. Only the distribution and orientation of the lipid vacuoles were affected by these edges (as shown in Figure 3.6).

5. Conclusions

Although further investigation is required to elucidate underlying molecular mechanisms, the present study shows that substrate topography at the micrometre scale affects the morphology and orientation of human mesenchymal stem cells and adipocytes without the interplay of biochemical factors. Laser-generated microstructures induce contact guidance of human mesenchymal stem cells, favouring cell organization and directing cell anchorage. In addition, in terms of MSCs induced differentiation, adipocytes, contrary to osteoblasts, are influenced by the substrate topography, in that the cellular distribution of lipid vacuoles aligns along topological edges and confining barriers. In view of these results, PLM represents a potential tool for providing 3D microenvironments mimicking *in vivo* stem cell niches and promoting cell organization. Although both physical and chemical surface modifications are likely required to control cell differentiation and induce cell fate, this work shows the impact of surface topography on the biocompatibility and functionality of biomaterials that can be used as scaffolds in tissue engineering and/or *in vitro* studies about MSCs behavior under specific physical constraints.

References

[1] Chen Y, Shao JZ, Xiang LX, Dong XJ, and Zhang GR. Mesenchymal stem cells: a promising candidate in regenerative medicine. Int J Biochem and Cell Biol 2008; 40: 815-820.

[2] Wu P, Castner DG, and Grainger DWJ. Diagnostic devices as biomaterials: a review of nuclei acid and protein microarray surface performance issues. J Biomater Sci Polym Ed 2008; 19: 725-753.

[3] Ghosh K and Ingber DE. Micromechanical control of cell and tissue development: Implications for tissue engineering. Adv Drug Deliv Rev 2007; 59: 1306-1318.

[4] Marx V. Where stem cells call home. Nat Methods 2013; 10(2): 111-115.

[5] Peerani R, and Zandstra PW. Enabling stem cell therapies through synthetic stem cell-niche engineering. J Clin Invest 2010; 120: 60-70.

[6] Prewitz MC, Seib FP, von Bonin M, Friedrichs J, Stiβel A, Niehage C, Müller K, Anastassiadis K, Waskow C, Hoflack B, Bornhäuser M, and Werner C. Tightly anchored tissue-mimetic matrices as instructive stem cell microenvironment. Nat Methods 2013; 10(8): 788-794.

[7] Kilian KA, Bugarija B, Lahn BT, and Mrksich M. Geometric cues for directing the differentiation of mesenchymal stem cells. Proc Nat l Acad Sci USA 2010; 107(11): 4872-4877.

[8] Kolind K, Leong KW, Besenbacher F, and Foss M. Guidance of stem cell fate on 2D patterned surfaces. Biomater 2012; 33: 6626-6633.

[9] Ross AM, Jiang Z, Bastmeyer M, and Lahann J. Physical aspects of cell culture substrates: topography, roughness, and elasticity. Small 2012; 8(3): 336-355.

[10] Béduer A, Vieu C, Arnauduc F, Sol JC, Loubinoux I, and Vaysse L. Engineering of adult human neural stem cells differentiation through surface micropatterning. Biomater 2012; 33: 504-514.

[11] Khang D, Choi J, Im YM, Kim YJ, Jang JH, Kang SS, Nam TH, Song J, and Park JW. Role of subnano-, nano-, and submicron-surface features on osteoblast differentiation of bone marrow mesenchymal stem cells. Biomater 2012; 33: 5997-6007.

[12] Kumar G, Tison CK, Chatterjee K, Pine PS, McDaniel JH, Salit ML, Young MF, and Simon CG Jr. The determination of stem cell fate by 3D scaffold structures through the control of cell shape. Biomater 2011; 32: 9188-9196.

[13] Liu H and Roy K. Biomimetic Three-Dimensional Cultures Significantly Increase Hematopoietic Differentiation Efficacy of Embryonic Stem Cells. Tissue Eng A 2005; 11: 319-330.

[14] Morimoto Y and Takeuchi S. Three-dimensional cell culture based on microfluidic techniques to mimic living tissues. Biomater Sci 2013; 1(3): 257-264.

[15] Liu Y, Sun S, Singha S, Cho MR, and Gordon RJ. 3D femtosecond laser patterning of collagen for directed cell attachment. Biomaterials 2005; 26: 4597-4605.

[16] Yeong WY, Yu H, Lim KP, Ng KLG, Boey YCF, Subbu VS, and Tan LP. Multiscale topological guidance for cell alignment via direct laser writing on biodegradable polymer. Tissue Eng C: Methods 2010; 16: 1011–21.

[17] Lee CH, Lim YC, Farson DF, Powell HM, and Lannutti J. Vascular Wall Engineering Via Femtosecond Laser Ablation: Scaffolds with Self-Containing Smooth Muscle Cell Populations. Ann Biomed Eng 2011; 39: 3031-3041.

[18] Li-Ping Lee B, Jeon H, Wang A, Yan Z, Yu J, Grigoropoulos C, and Li S. Femtosecond laser ablation enhances cell infiltration into three-dimensional electrospun scaffolds. Acta Biomater 2012; 8: 2648-2658.

[19] Li H, Wen F, Wong YS, Boey FY, Subbu VS, Tai Leong D, Woei Ng K, Ka Lai Ng G, and Tan LP. Direct laser machining-induced topographic pattern promotes up-regulation of myogenic markers in human mesenchymal stem cells. Acta Biomater 2012; 8: 531–539.

[20] Li H, Wong YS, Wen F, Ng KW, Ng GK, Venkatraman SS, Boey FY, and Tan LP. Human Mesenchymal Stem-Cell Behaviour on Direct Laser Micropatterned

Electrospun Scaffolds with Hierarchical Structures. Macromol Biosci 2013; 13: 299-310.

[21] Rusen L, Cazan M, Mustaciosu C, Filipescu M, Sandel S, Zamfirescu M, Dinca V, and Dinescu M. Tailored topography control of biopolymer surfaces by ultrafast lasers for cell-substrate studies. Appl Surf Sci 2014; 302: 256-261.

[22] Schlie S, Fadeeva E, Koroleva A, and Chichkov BN. Laser-engineered topography: correlation between structure dimensions and cell control. J Mater Sci: mater Med 2012; 23: 2813-2819.

[23] Ortiz R, Moreno-Flores S, Quintana I, Vivanco MdM, Sarasua JR, and Toca-Herrera JL. Ultrafast laser microprocessing of medical polymers for cell engineering applications. Mat Sci Eng C 2014; 37: 241-250.

[24] Neuendorf RE, Saiz E, Tomsia AP, and Ritchie RO. Adhesion between biodegradable polymers and hydroxyapatite: Relevance to synthetic bone-like materials and tissue engineering scaffolds. Acta Biomater 2008; 4: 1288-1296.

[25] Ortiz R, Quintana I, Etxarri J, Lejardi A, and Sarasua JR. Picosecond laser ablation of poly-L-lactide: Effect of crystallinity on the material response. J Appl Phys 2011; 110: 094902.

[26] Vuchkov NK. UV copper ion laser in Ne-Cubr pulse-longitudinal discharge. In Advances in laser and optics research vol. 2. Ed. William T. Arkin, Nova Science Publishers, Inc. 2002. 1-34.

[27] McBeath R, Pirone DM, Nelson CM, Bhadriraju K, and Chen CS. Cell shape, cytoskeletal tension, and RhoA regulate stem cell lineage commitment. Dev Cell 2004; 6: 483-495.

[28] Fadeeva E, Deiwick A, Chichkov B, and Schlie-Wolter S. Impact of laser-structured biomaterial interfaces on guided cell responses. Interface Focus 2014; 4: 20130048.

[29] Kantawong F, Burgess KEV, Jayawardena K, Hart A, Riehle MO, Oreffo RO, Dalby MJ, and Burchmore R. Effects of a surface topography composite with puerariae radix on human STRO-1-positive stem cells. Acta Biomater 2010; 6: 3694–3703.

[30] Yim EKF, Darling EM, Kulangara K, Guilak F, and Leong KM. Nanotopography-induced changes in focal adhesions, cytoskeletal organization, and mechanical properties of human mesenchymal stem cells. Biomater 2010; 31: 1299–1306.

[31] Kantawong F, Burchmore R, Wilkinson CDW, Oreffo ROC, and Dalby MJ. Differential in-gel electrophoresis (DIGE) analysis of human bone marrow osteoprogenitor cell contact guidance. Acta Biomater 2009; 5: 1137-1146.

[32] Hamilton DW, Wong KS, and Brunette DM. Microfabricated discontinuous-edge surface topographies influence osteoblast adhesion, migration, cytoskeletal organization, and proliferation and enhance matrix and mineral deposition in vitro. Calcif Tissue Int 2006; 78: 314–325.

[33] Kim MS, Kim AY, Jang KJ, Kim JH, Kim JB, and Suh KY. Effect of nanogroove geometry on adipogenic differentiation. Nanotech 2011; 22: 494017.

[34] Ali AT, Hochfeld WE, Myburgh R, and Pepper MS. Adipocyte and adipogenesis. Eur J Cell Biol 2013; 92: 229-236.

[35] Bahceci M, Gokalp D, Bahceci S, Tuzcu A, Atmaca S, and Arikan S. The correlation between adiposity and adiponectin, tumor necrosis factor –a, interleukin-6 and high sensitivity C-reactive protein. Is adipocyte size associated with inflammation in adults? J Endocrinol Invest 2007; 30: 210-214.

[36] Meyer LK, Ciaraldi TP, Henry RR, Wittgrove AC, and Phillips SA. Adipose tissue depot and cell size dependency of adiponectin synthesis and secretion in human obesity. Adipocyte 2013; 2(4): 217–226.

[37] Carraway KL, and Carraway CAC. Membrane-cytoskeleton interaction in animal cells. Biochim Biophys Acta 1989; 988: 147-171.

[38] Casadei A, Epis R, Ferroni L, Tocco I, Gardin C, Bressan E, Sivolella S, Vindigni V, Pinton P, Mucci G, and Zavan B. Review article: Adipose tissue regeneration: a state of the art. J Biomed Biotechnol 2012; 2012: 462543.

[39] Baiguera S, Gonfiotti A, Jaus M, Comin CE, Paglierani M, Gaudio C, Bianco A, Ribatti D, and Macchiarini P. Development of bioengineered human larynx. Biomater 2011; 32: 4433-4442.

[40] Lee JS, Hong JM, Jung JW, Shim JH, Oh JH, and Cho DW. 3D printing of composite tissue with complex shape applied to ear regeneration. Biofabrication 2014; 6: 024103.

[41] Ruiz SA and Chen CS. Emergence of patterned stem cell differentiation within multicellular structures. Stem Cells 2008; 26(11): 2921-2927.

[42] Peng R, Yao X, and Ding J. Effect of cell anisotropy on differentiation of stem cells on micropatterned surfaces through the controlled single cell adhesion. Biomater 2011; 32: 8048-8057.

[43] Goubko CA and Cao X. Patterning multiple cell types in co-cultures: A review. Mater Sci Eng C 2009; 29: 1855-1868.

[44] Song Wei, Lu H, Kawazoe N, and Chen G. Adipogenic differentiation of individual mesenchymal stem cell on different geometric micropatterns. Langmuir 2011; 27(19): 6155-6162.

Final remarks

The investigation developed in this thesis work proves that laser processing with picosecond pulses is a more than promising technique for micro-structuring of biocompatible and biodegradable polymers for cell and tissue engineering applications. This conclusion is supported by the following findings:

- ✓ Micromachining by picosecond laser pulses enabled to create micro-scale features with high precision (spot sizes around 10 µm) and minimal thermal impact (recast material and HAZ) by means of an effective ablation process on a transparent and biodegradable polymer (PLLA). Surface quality can be optimised by selecting the appropriate laser wavelength to tip the balance between the two main material removal mechanisms involved in PLLA ablation (photothermal and photochemical) in favour of that most desirable to occur, photochemical ablation, which transforms the polymer into gaseous products, diminishing the deposition of ablation products and leading to clean micro-structured surfaces with no need of post-processing steps. Surface quality it is also influenced by the materials properties, specifically by material microstructure (degree of crystallinity): the interplay between photothermal and photochemical ablation mechanisms can be tuned by modifying the degree of crystallinity of the material, so that photochemical ablation plays a leading role in material removal and clean and precise microstructures are generated. Moreover, laser micromachining is applied on the material surface minimising the changes produced on the surface chemistry to a nanometric surface layer (less than 10 nm), and without affecting material microstructure. Therefore, bulk properties remain intact. Generally, picosecond lasers enable to reach high mechanizing speeds leading to faster processing than other microfabrication technologies, which make it highly convenient for processing and manufacturing of large and complex 3D plastic components, like those required for scaffold fabrication. Laser micro-processing offers many advantages compared to the other existing surface modification technologies, such as versatility in terms of materials to be processed (almost any material) and geometries to be generated, the fact of being a single-step and contactless method, the easy adaptation of the process for micropatterning of tubular or

more complex sample shapes, and an easy scaling up by means of micropatterning of metal moulds for manufacturing of plastic components series.

- ✓ The micro-scale structures that can be tuned via ps-laser ablation technology had a significant influence on cell-material interactions that govern cellular behaviour. In particular, in this thesis work, the surface micro-structures proposed have demonstrated their ability to:
    - Modulate the proliferation of breast cancer cells, which could be a key issue in the study of tumour growth *in vitro*.
    - Modulate morphology and elongation of mesenchymal stem cells, and organization and confinement of lipid vacuoles inside the adipocytes, which shows a great potential for the design of polymeric scaffolds with a customized regenerative function.
    - Modulate elongation and improve adhesion of endothelial cells, which has a major impact on the acceleration of the endothelium regeneration in medical applications such as minimally invasive treatment of coronary artery disease via cardiovascular stents.

In addition, it is worth highlighting that all these cellular behaviours were controlled only by physical/topological mechanisms at the micro-scale, without the interplay of chemical factors, and therefore, without modification of the chemical surface properties. This would enable to control independently both physical and chemical surface properties of scaffolds to get a versatile surface properties “palette” which could be customized to each biomedical application.

Additional information

The findings of the study performed during this thesis have been disseminated through publications in scientific journals and participations in international conferences via lectures, which are cited below.

Publications:

- Ortiz R, Quintana I, Etxarri J, Lejardi A, and Sarasua JR. Picosecond laser ablation of poly-L-lactide: Effect of crystallinity on the material response. J Appl Phys 2011; 110: 094902.
- Ortiz R, Moreno-Flores S, Quintana I, Vivanco MdM, Sarasua JR and Toca-Herrera JL. Ultra-fast laser microprocessing of medical polymers for cell engineering applications. Mater Sci Eng C 2014; 37: 241-250.
- Ortiz R, Moreno-Flores S, Quintana I, Vivanco MdM, Sarasua JR, and Toca-Herrera JL. Topological cues to anchor stem cells, control adipocyte morphology, and improve cell adherence. Surf Coat Technol 2017. In progress.
- Pacharra S, Ortiz R, McMahon S, Wang W, Salber J, and Quintana I. Surface patterning of a novel PEG-functionalised Poly-L-lactide polymer to improve its biocompatibility: Applications to Bioresorbable Vascular Stents (BVS). J Biomed Mat Res A 2017. In progress.

Lectures in international conferences:

- Ortiz R, Quintana I, Moreno-Flores S, Toca-Herrera JL, Etxarri J, Lejardi A, Sarasua JR, and Vivanco MdM. Ultra-fast laser microprocessing of medical polymers for cell engineering applications. European Symposium on Biomaterials and Related Areas. April 13-14, 2011. Jena, Germany.
- Ortiz R, Moreno-Flores S, Quintana I, and Toca-Herrera JL. Surface modification of poly-L-lactide by picosecond laser irradiation: Effect of substrate topography on morphology and differentiation of human Mesenchymal Stem Cells. World Conference on Regenerative Medicine. October 23-25, 2013. Leipzig, Germany.
- Quintana I. Bioresorbable Systems: The role of surface functionalization. 27th European Conference on Biomaterials. August 31-September 3, 2015. Cracow, Poland.

In addition to the aforementioned publications, the work performed during this thesis has allow for participation in the next European Project:

Reinforced Bioresorbable Biomaterials for Therapeutic Drug Eluting Stents (ReBioStent, https://rebiostent.eu/) funded by the European Union Seventh Framework Program (FP7/2007-2013) under grant agreement nº604251-ReBioStent.